AD-A007 913

SOVIET MATERIAL ON INTERNAL WAVE
EFFECTS, NO. 3, APRIL 1975

Stuart G. Hibben, et al

Informatics, Incorporated

Prepared for:

Defense Advanced Research Projects Agency
Navy Foreign Language Service

April 1975

SECURITY CLASSIFICATION OF THIS PAGE (When Data Entered)

REPORT DOCUMENTATION PAGE	READ INSTRUCTIONS BEFORE COMPLETING FORM

1. REPORT NUMBER	2. GOVT ACCESSION NO.	3. RECIPIENT'S CATALOG NUMBER
		AD·A007 913

4. TITLE (and Subtitle)	5. TYPE OF REPORT & PERIOD COVERED
Soviet Material on Internal Wave Effects No. 3, April, 1975	Scientific . . . Interim
	6. PERFORMING ORG. REPORT NUMBER

7. AUTHOR(s)	8. CONTRACT OR GRANT NUMBER(s)
Stuart G. Hibben, John Kourilo, B. L. Shresta, M. Ness	N00600-75-C-0018

9. PERFORMING ORGANIZATION NAME AND ADDRESS	10. PROGRAM ELEMENT, PROJECT, TASK AREA & WORK UNIT NUMBERS
Informatics Inc. 6000 Executive Boulevard Rockville, Maryland 20852	DARPA Order No. 2790 Program Code No. L13003

11. CONTROLLING OFFICE NAME AND ADDRESS	12. REPORT DATE
Defense Advance Research Projects Agency/TAO 1400 Wilson Boulevard Arlington, Virginia 22209	April, 1975
	13. NUMBER OF PAGES /3/

14. MONITORING AGENCY NAME & ADDRESS(if different from Controlling Office)	15. SECURITY CLASS. (of this report)
U. S. Navy Foreign Language Service 4301 Suitland Road, Bldg. 5 Washington, D. C. 20390	UNCLASSIFIED
	15a. DECLASSIFICATION/DOWNGRADING SCHEDULE

16. DISTRIBUTION STATEMENT (of this Report)

Approved for public release; distribution unlimited.

17. DISTRIBUTION STATEMENT (of the abstract entered in Block 20, if different from Report)

18. SUPPLEMENTARY NOTES

Scientific . . . Interim

19. KEY WORDS (Continue on reverse side if necessary and identify by block number)

Internal Waves
Capillary Waves
Surface Signature
Turbulent Flow
Ocean Microstructure

20. ABSTRACT (Continue on reverse side if necessary and identify by block number)

This the the third collection of abstracts of recent Soviet articles on generation and detection of internal waves. It is based on items listed in the third Bibliography of Soviet Material on Internal Waves, published January 27, 1975 and covering material received from April through December, 1974.

The abstracts are divided into internal effects, and surface effects comprising active and passive measurement of wave states. An author index is appended.
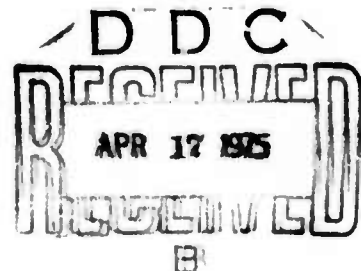
PRICES SUBJECT TO CHANGE

DD FORM 1473   EDITION OF 1 NOV 65 IS OBSOLETE

SOVIET MATERIAL
ON
INTERNAL WAVE EFFECTS

No. 3, April, 1975

Sponsored by

Defense Advanced
Research Projects Agency

DARPA Order No. 2790

DDC
RECEIVED
APR 17 1975
RECEIVED
B

Informatics inc
Systems and Services Company
6000 Executive Boulevard
Rockville, Maryland 20852
(301) 770-3000 Telex 89-521

ia

INTRODUCTION

This is the third collection of abstracts of recent Soviet articles on generation and detection of internal waves. It is based on items listed in the third Bibliography of Soviet Material on Internal Waves, published January 27, 1975 and covering material received from April through December, 1974.

The abstracts are divided into internal effects, and surface effects comprising active and passive measurement of wave states. An author index is appended.

TABLE OF CONTENTS

1. Internal Effects

Belyayev, V. S., A. S. Monin, and V. T. Paka. **Experimental measurements of deep sea turbulence.** FAiO, no. 5, 1974, 533-542.

Results of a study of oceanic turbulence are described, as well as the method and turbulimeter employed. The experiments were conducted in the Indian Ocean during the 7th cruise of the R/V Dmitriy Mendeleyev in January-April 1972.

Pulsations in electrical conductivity were measured by a quick-response probe under conditions of standard vertical sounding or tethered "free" fall to a depth of 1200 m. The "sigma" probe used was designed by V. T. Paka (Fig. 1). The electric resistivity of the water
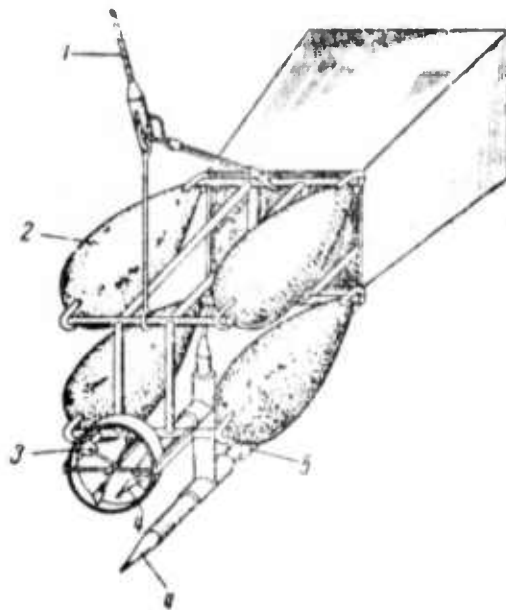

Fig. 1. Sigma Turbulimeter.

1- Electrical cable; 2- weights or frame with a box-like stabilizer; 3- current meter; 4- sensors of electrical conductivity; 5- hydrostatic pressure indicator.

column between the electrodes of the sensor (4) is connected to a high-frequency oscillatory circuit, modulating the signal amplitude. Amplitude modulation is linear over the range 0.02-0.06 ohm^{-1} cm^{-1}. Noise level at the output is equivalent to a temperature fluctuation of 10^{-4} °C. The relative speed of the instrument package is measured by a current meter (3).

The average electrical conductivity $\bar{\sigma}$, relative probe speed V, and electrical conductivity fluctuations σ' measured between the lower boundary of the thermocline ($\sim$250 m) and a depth of 800 m are shown in Fig. 2. The figure indicates that large fluctuations of electrical conductivity
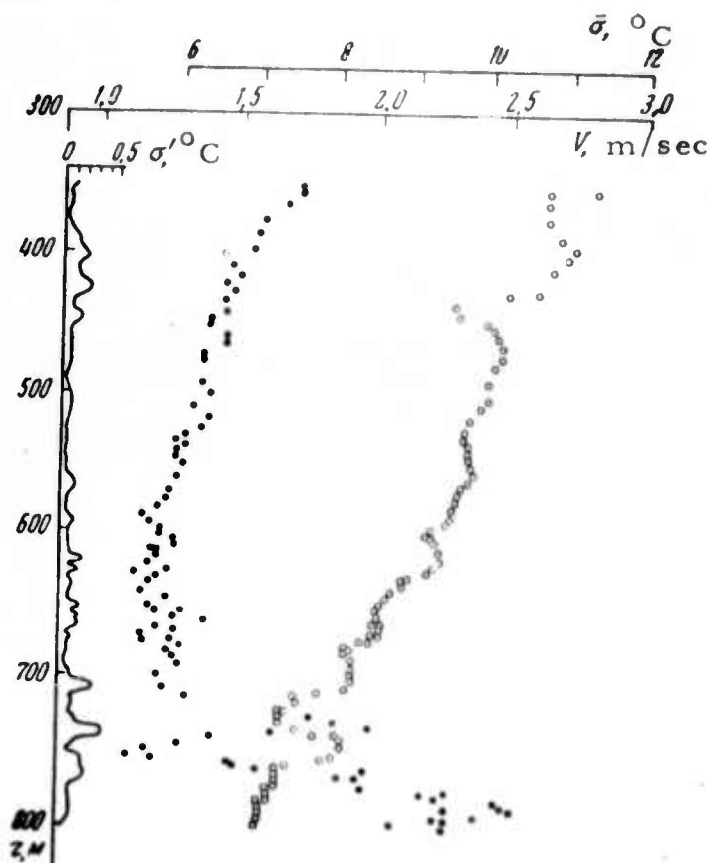

Fig. 2. Vertical distribution of $\bar{\sigma}$ (open circles),
V (solid circles); and σ' (solid line).

-2-

are associated with large vertical gradients of the average electrical conductivity and with the relative speed of the probe.

The vertical distribution of average electrical conductivity, obtained by vertical sounding to a depth of 1250 m, (at 10^O59N; 55^O40E) is shown in Fig. 3. Conductivity fluctuations were observed during
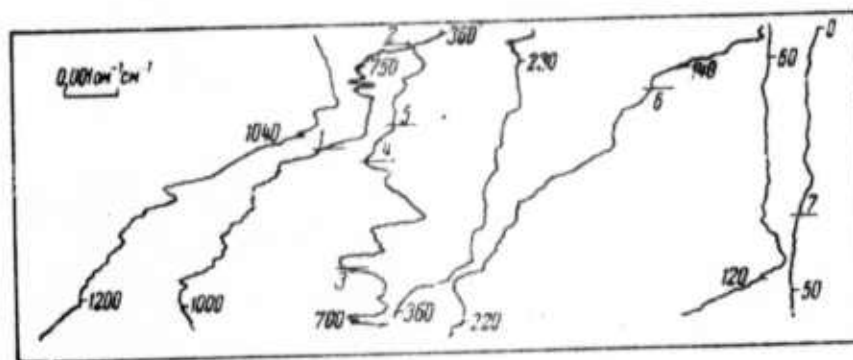
Fig. 3. Record of average electrical conductivity during probe descent.

9 minute intervals at seven levels (indicated by single numbers in Fig. 3). Variations of the average electrical conductivity, mean square fluctuations of electrical conductivity, and depth of the probe during 9 minute-intervals are shown in Fig. 4.

Spectral densities $E^{(\sigma)}(k)$ of fluctuations σ' observed during 9 minutes intervals are shown in Fig. 5.

Energy spectra k $E^{(\sigma)}(k)$ of fluctuations σ' increase with a drop in k more quickly in the high frequency range, and slower in the low frequency range. At smaller depths, they tend to have maxima at the frequency of ship roll.
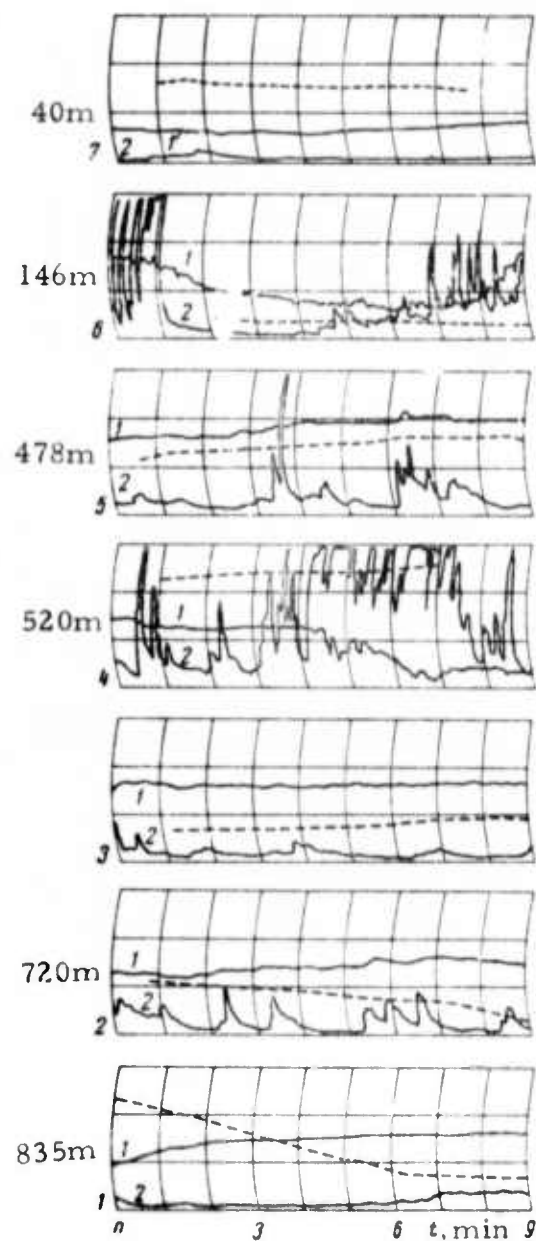
Fig. 4. Variations of $\bar{\sigma}(1)$, $(\bar{\sigma}')^2$ (2), and probe depth (dashed line) during observations of electrical conductivity fluctuations.
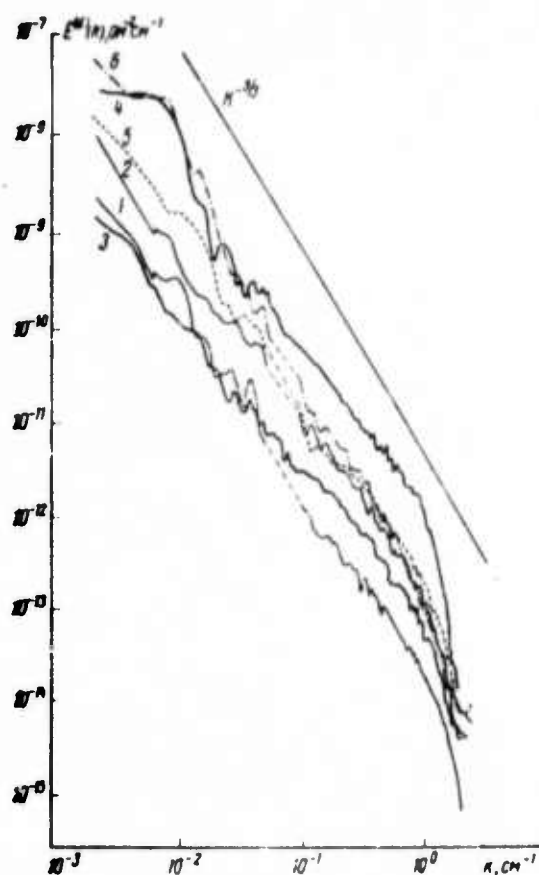
Fig. 5. Spectral densities of electrical
conductivity fluctuations (1- 835m; 2- 720m;
4- 520m; 5- 478m; 6- 146m)

Dissipation spectra $k^2 E^{(\sigma)}(k)$ of fluctuations are shown in
Fig. 6. At all levels except 146m, they display maxima at $10^{-1} cm^{-1} < k < 2\ cm^{-1}$.
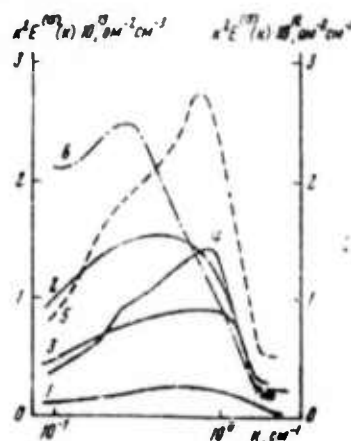
Fig. 6. Smoothed dissipation spectra of electrical
conductivity fluctuations. (1- 835m; 2- 720m; 4-
520m; 5- 478m; 6- 146m).

At smaller depths, $k^2 E^{(\sigma)}(k)$ curves also have pronounced maxima at the frequency of ship roll.

Turbulence intermittence was observed at all measured levels (see Fig. 4). It was proposed to use the running structural function $D(\tau_n)$ of fluctuation σ' as a criterion for turbulence intermittence (Fig. 7).
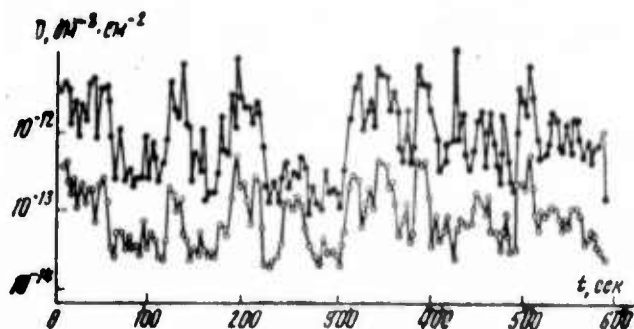
Fig. 7. Running structural function of electrical conductivity fluctuations at 720 m for 1 cm shift (open circle) and 30 cm (solid circles).

The periodicity displayed in the variations of $D(\tau_n)$ (~ 80 sec periods) is thought to be associated with the passage of internal wave packets. Turbulence intermittence was manifested in the histograms of σ' values as well (Fig. 8).
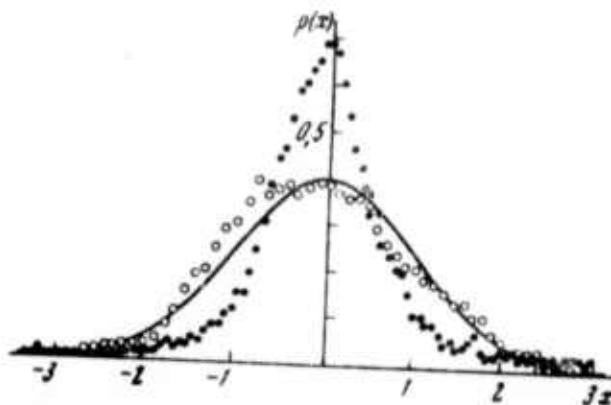
Fig. 8. Histograms of electrical conductivity fluctuations at a depth of 720 m with time separation of 5 min.

Belyayev, V. S., R. V. Ozmidov, and M. L.
Pyzhevich. Empirical laws for one-dimensional
spectral density distributions of velocity and
electrical conductivity pulsations in the ocean.
Okeanologiya, no. 5, 1974, 802-805.

This covers the same exercise of the foregoing paper,
reviewing measurements of pulsations in flow velocity and electrical
conductivity performed in the Atlantic Ocean during the 9th cruise of the
R/V Academician Kurchatov and in the Indian Ocean during the 7th cruise
of the R/V Dmitriy Mendeleyev. Experiments were conducted both in
the region of equatorial currents and in a relatively quiet region, both under
instrument towing and vertical sounding conditions. The vertical structures
of temperature and salinity in the uppermost oceanic layer differed in
the two areas of experiments. The data on oceanic turbulence were analyzed
without accounting for background hydrometeorological conditions.

Spectral densites $E_1(k)$ of pulsations of the longitudinal
velocity component u' at depths of 20-213 m for $k = 4.6 \times 10^{-2} - 5.9 \times 10^{0}$ cm^{-1}
are shown in Fig. 1 for both the Kurchatov and Mendeleyev; spectral densities
of pulsations of electrical conductivity σ' at depths of 23-217 m for
$k = 6.9 \times 10^{-2} - 6.1$ cm^{-1} are shown in Fig. 2 for the Mendeleyev.

Histograms and empirical integral functions of $\lg E_1(k)$ distribution
for u' and σ' are shown in Fig. 3, a and b respectively.

Statistical parameters of $\lg E_1(k)$ distributions are given in
the table.

Fig. 1. Family of smoothed $E_1(k)$ curves of velocity pulsations in the ocean.
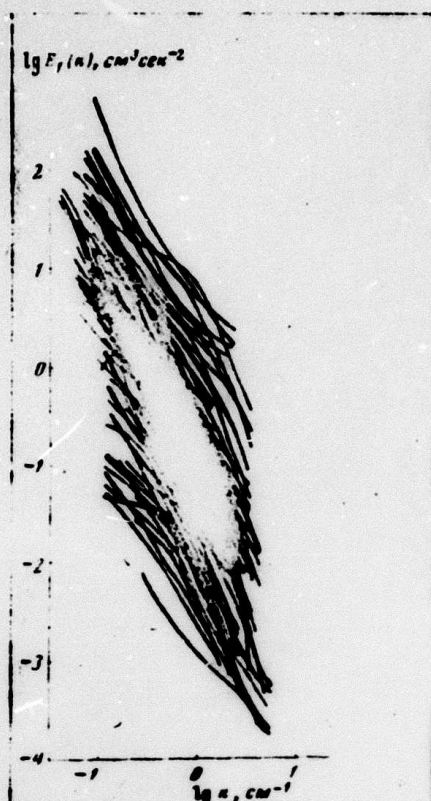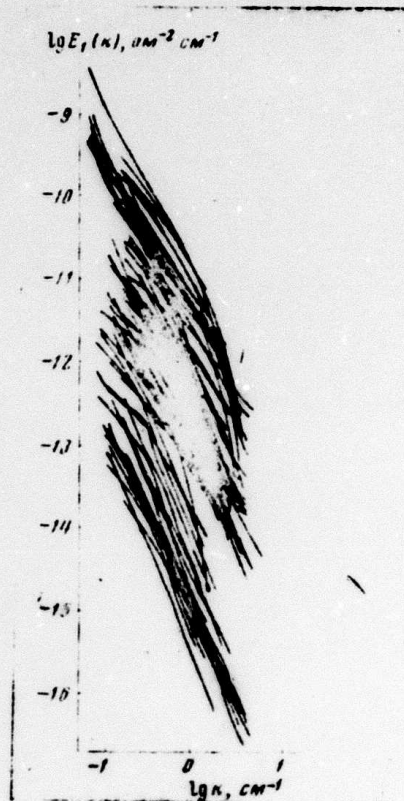

Fig. 2. Family of smoothed $E_1(k)$ curves of electrical conductivity pulsations in the ocean.
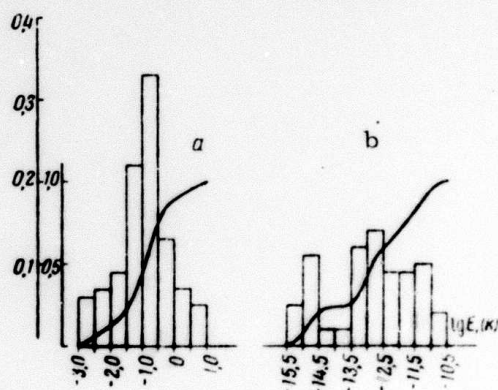
Fig. 3. Histograms and empirical integral function of $\lg E_1(k)$ distribution for current velocity pulsations (a) and electrical conductivity pulsations (b) in the ocean at $k = 1\ \text{cm}^{-1}$. (left vertical scale corresponds to histograms)

Parameters of $\lg E_1(k)$ distributions for current
velocity pulsations and electrical conductivity pulsations

	m_1	D	S	A	E	D(A)	D(E)
u'	-0.94	0.64	0.80	-0.09	0.01	0.06	0.20
σ'	-12.87	1.72	1.31	-0.35	-0.92	0.07	0.25

The probability that $\lg E_1(k)$ has a normal distribution,
evaluated using Kolmogorov's criterion, was found to be 70% for current
velocity pulsations, but only 7% for electrical conductivity pulsations.

Bezuglov, V. A., G. Ya. Vasilevskis, and
Yu. A. Shcherbina. Effect of flow deformation on
turbulent diffusion of dye. IN: Tr. 18-y Nauch.
konf. Mosk. fiz.-tekhn. in-t, 1972. Ser.
Aeromekhanika. Protsessy upr. Dolgoprudnyy,
1973, 25-30. (RZhMekh, 4/74, #4B1047).
(Translation)

Results are presented of an experimental study on the effect
of turbulent flow deformation, in a pipe with the Venturi-type nozzle, upon
the relative rms value of pulsations of passive dye concentration near the
axis of pipe, $c'/< c> = \left[< (c/ < c> - 1)^2>\right]^{1/2}$, and upon the density of probability
distribution of these pulsations. It is shown that in a smooth pipe, the ratio
$c'/< c>$ near the axis can be represented with sufficient accuracy by a
parabolic function. Behind the nozzle, this ratio is "compressed" proportionally
to the ratio between the pipe diameter and nozzle section, while at the axis
the ratio $c'/< c>$ is somewhat decreased. The latter is explained as being
caused by an intermittence decrease owing to flow deformation.

Belyayev, V. S., A. S. Monin, R. V. Osmidov, and V. T. Paka. Experimental study of small-scale turbulence in the ocean. FAIO, no. 9, 1974, 959-975.

This article details the methods and instrumentation used in complex measurements made since 1969 during four expeditions organized by the Shirshov Institute of Oceanography. The 2nd, 5th, and 7th cruises of the R/V Dmitriy Mendeleyev and the 9th cruise of the R/V Akademik Kurchatov were conducted in the framework of a broad program of research on small-scale fluctuations of hydrophysical fields in ocean test areas.

The data collected in two test areas (Fig. 1) on the 7th cruise
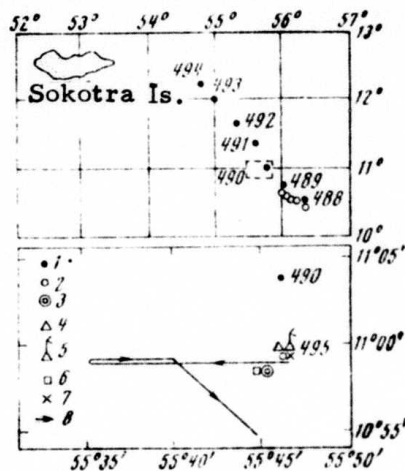
Fig. 1. Test area and type of measurements:

1- hydrological series, bathythermogram, probing with the AIST-STD meter and acoustic ocean current meter; 2- probing with same meters as in 1; 3- multiple probings with AIST; 4- buoy station using moorings with current meters and photothermographs; 5- radio buoy for thermistor chain; 6- measurement with a sigma deep-sea probe; 7- bathythermogram; and 8- towing tacks with turbulimeters. The dashed rectangle is shown in the lower figure to a large scale.

of the Dmitriy Mendeleyev (Indian Ocean in 1972) are presented as an attempt to correlate small-scale fluctuations of hydrophysical fields with background hydrological conditions. Apparently, differences in shape and absolute value of statistical characteristics of small-scale oceanic turbulence measured in the two test ares (Fig. 2 and 3) can be

Fig. 2. Spectral density of current velocity fluctuations in test area A. Observation depth (m): 1a, 1b- 100; 2- 105; 3a, 3b- 115; 4- 120; and 5- 187.

correlated with the difference in averaged background hydrological factors including large-scale fluctuations in the same two areas (Fig. 4 and 5).
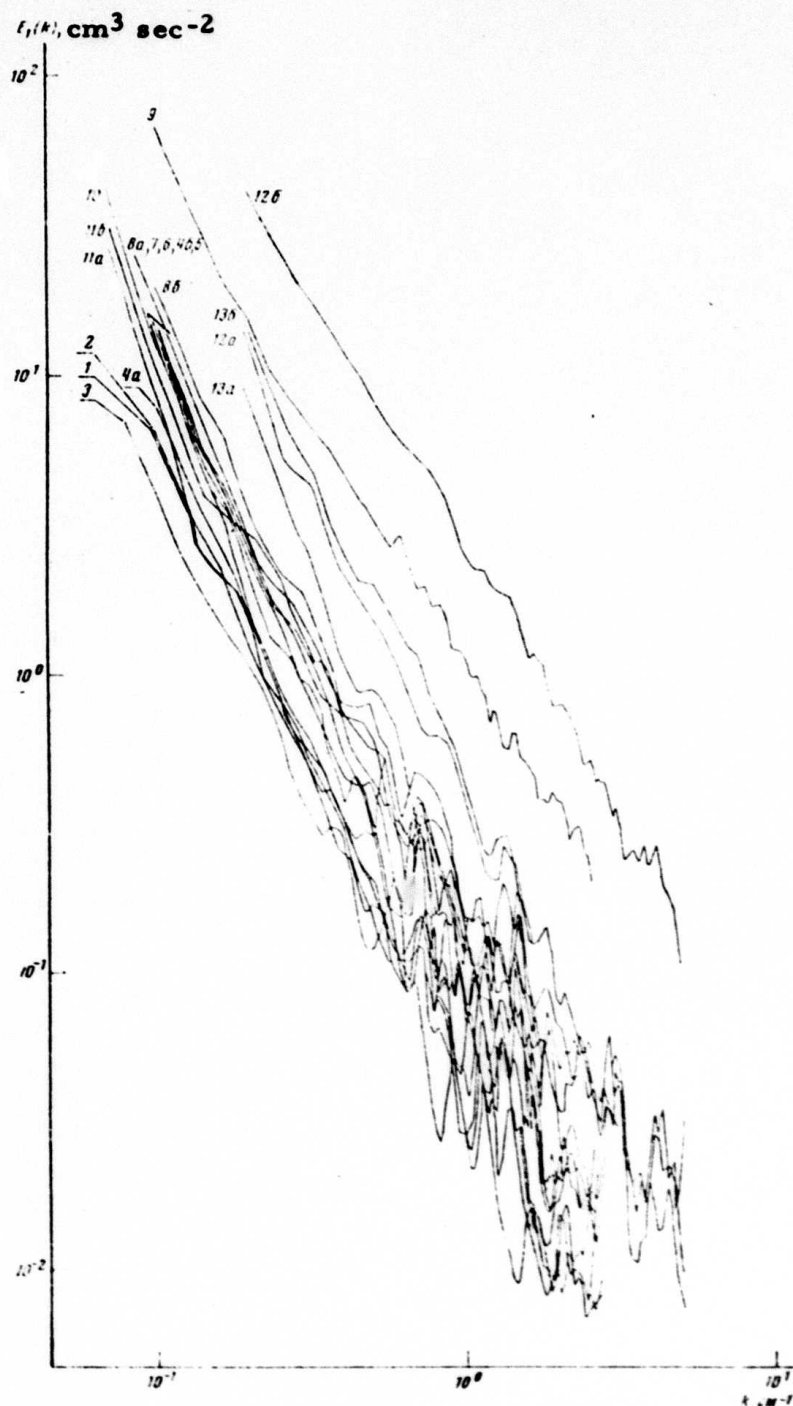
Fig. 3. Spectral density of current velocity
fluctuations in test area B. Observation depth
(m): 1- 20; 2- 37; 3- 55; 4a and 4b- 77; 5- 94;
6- 103; 7- 127; 8a and 8b- 138; 9- 157; 10- 160;
11a and 11b- 168; 12a and 12b- 195; 13a and 13b- 213.
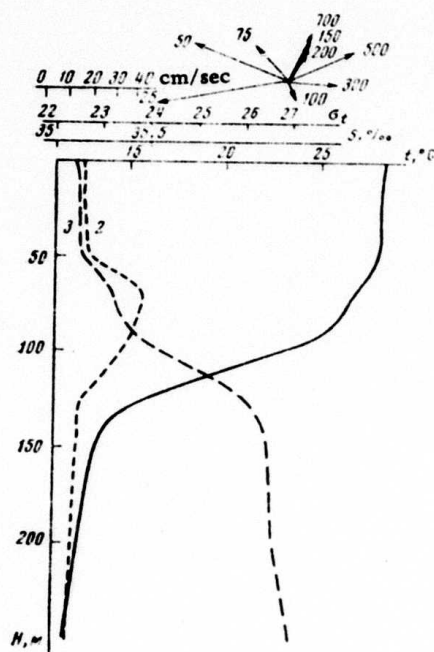
Fig. 4
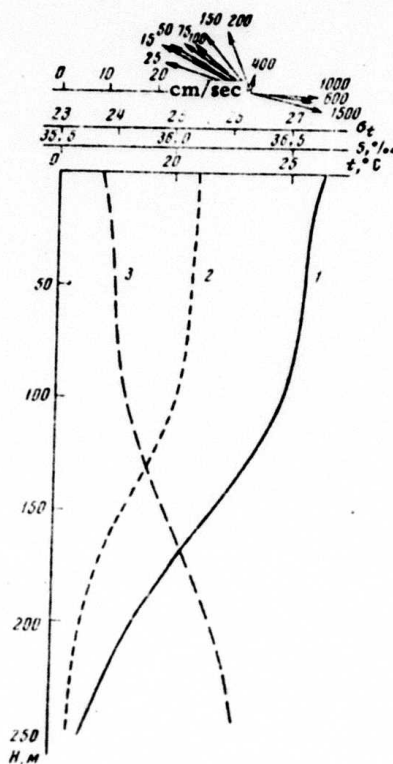
Fig. 5

Fig. 4 and 5. Vertical temperature (1), salinity
(2), and density (3) profiles and vertical distribution
of current vectors in test areas A (Fig. 4) and B
(Fig. 5) from standard hydrological data and buoy
station data.

However, the difference noted between a pair of spectral curves obtained
at the same (Fig. 3, curves 12a and 12b) or nearly the same (Fig. 2, curves
3 and 4) depth levels in a given test area cannot be explained on the basis of
averaged background conditions, including large scale fluctuations. Further-
more the mesoscale background data measured with special instruments
(e. g., Fig. 6 and 7) are difficult to correlate with the turbulimetric data
because of the noncorrespondence of these two sets of data in space and time.

Similarity of the respective vertical profiles in Fig. 6 and 7
reflects a layered vertical structure of the hydrophysical fields. Thus,
small-scale oceanic turbulence is determined by local background conditions
in a quasihomogeneous layer. This dependence is illustrated by the
experimental data in Fig. 8 which were obtained at the same levels as
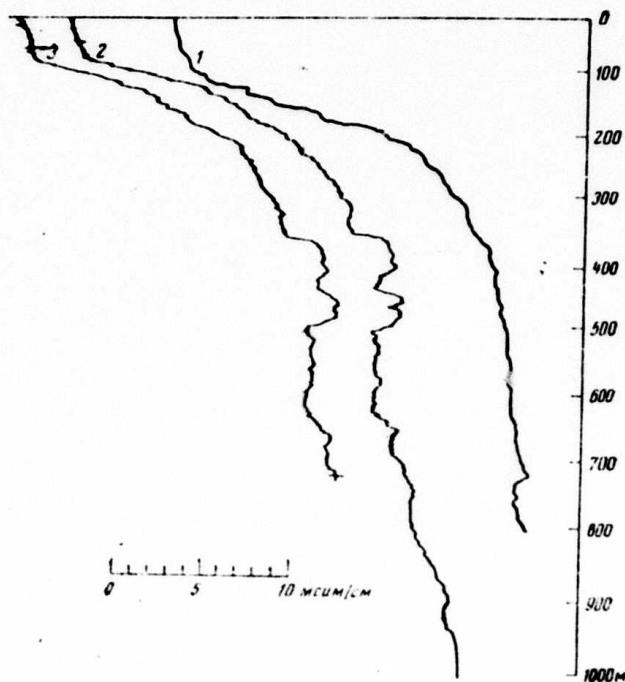
Fig. 6. Vertical profile of electrical conductivity (in relative units) from measurements with the OKB OT probe (curves 2 and 3) and AIST meter (curve 1) at station 497, 18 March 1972, 5:10 PM (2) and 5:40 PM (3) and at st. 495, 16 March 1972, 5:04 PM (1).
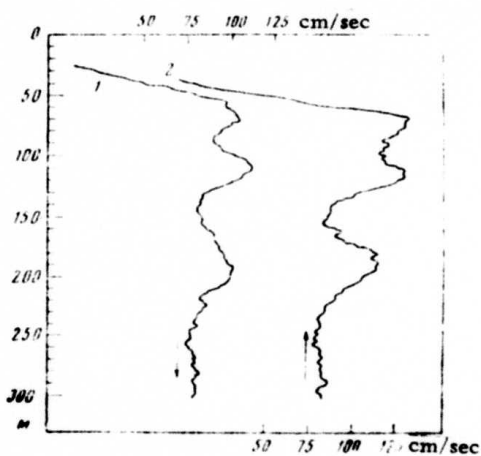
Fig. 7. Current modulus vertical profiles, obtained on board a drift vessel in descent and rise of TO IOAN acoustic meter (arrows indicate meter direction; velocity scales are shifted); st. 506, Mar 23, 1972, 2:14 PM (1) and 2:40 AM (2).

-14-
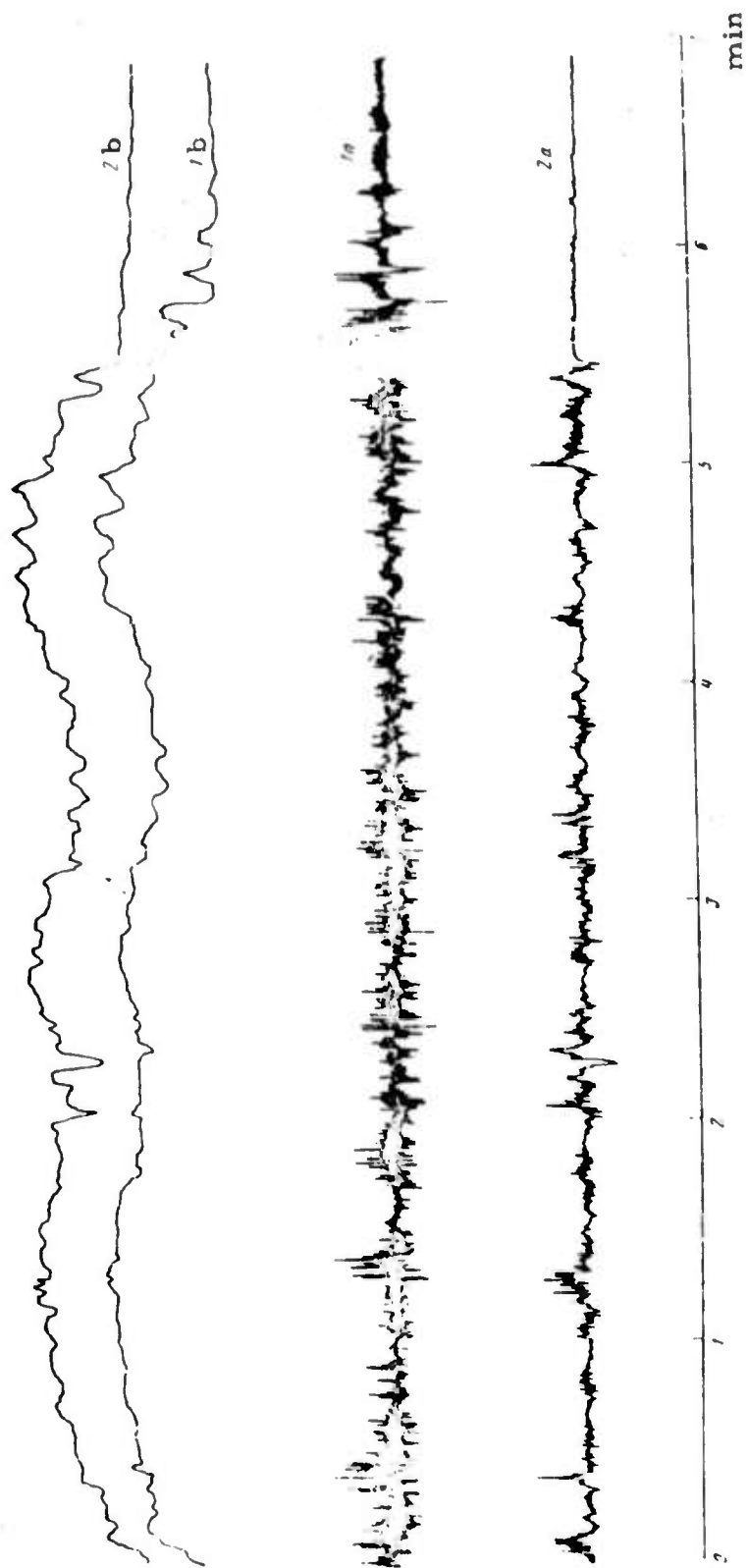
Fig. 8. Oscilloscope traces of average (1b and 2b) and oscillating (1a and 1b) components of electrical conductivity from synchronous measurements at two depth levels with 70 cm vertical spacing.

turbulimetric data. Variability of small-scale fluctuations of
hydrophysical fields in the ocean, even at short horizontal spacings
along a measuring tack is shown in Fig. 9.
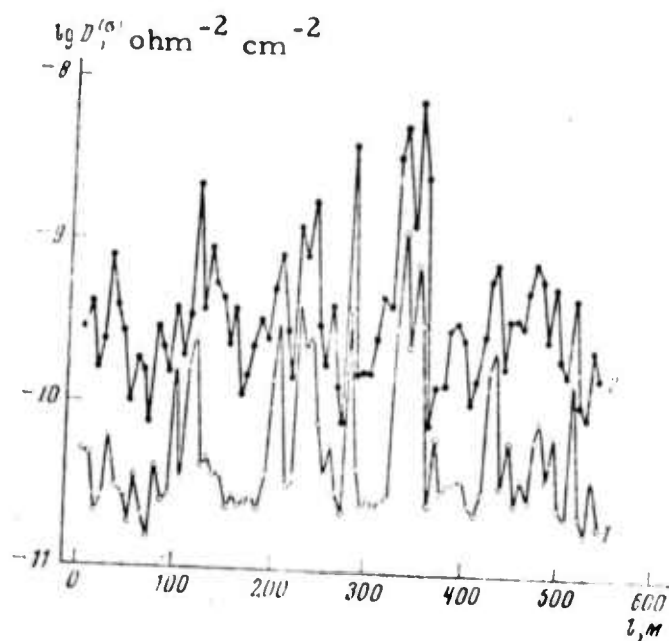
Fig. 9. Slide structural function of electrical
conductivity fluctuations for 2.7 cm (1) and
85 cm (2) spatial shifts along horizontal cross-
section, from data of towed turbulimeters.

The authors show that the measured spectra of current
velocity fluctuations in test area A (Fig. 2) can be described adequately,
at least in their intermediate frequency range, by the universal curve
used by H. L. Grant et al. (J. Fluid Mech, v. 12, no. 2, 1962) to describe
a locally isotropic turbulence. The shape of the spectral curves in Fig. 2
is typical of that of the current velocity spectra at relatively small Reynolds
numbers (10^4 to 4×10^4).

The measured spectra in test area B (Fig. 3) are approximated by the theoretical curve of the Monin model of a stratified fluid. Using this approximation the average dissipation rate of turbulent energy and equalization rate of temperature inhomogeneity were determined to be about 10^{-2} cm^2/sec^3 and 10^{-3} to 10^{-4} deg^2/sec, respectively. The turbulence scale was of the order of step dimensions in the fine density field structure in the ocean.

In summary, small-scale turbulence in a stratified ocean is governed by factors variable in both space and time, which explains the diversity of spectral shapes in fluctuation fields.

Belyayev, V. S., A. S. Monin, and R. V. Ozmidov. A thousand spectra of ocean turbulence. DAN SSSR, v. 217, no. 5, 1974, 1053-1056.

Results of processing the experimental horizontal velocity u, temperature T, and electrical conductivity σ data of the upper 200 m oceanic layer are presented in Fig. 1 in the form of spectral density curves $E_1(k)$ of small-scale fluctuations of the cited variables. The data were recorded at different depths in three and seven test areas during the 9th cruise of the R/V Akademik Kurchatov (Atlantic Ocean, 1971) and the 7th cruise of the R/V Dmitriy Mendeleyev (Indian Ocean, 1972), respectively.

The signal recordings from various sensors towed by the cruising ships were used to calculate the spectra. Each spectrum in Fig. 1 is the average of 5 to 10 spectra, so that about 1000 individual spectra are summarized in this figure. Explanation of the letter indexes in Fig. 1 is given in Table 1. Fig. 1 shows 1) a great variety of turbulence modes in the upper ocean layer, 2) a uniform turbulence at all depth levels in some test

Fig. 1. Families of spectral density curves. Some curves are omitted to avoid overcrowding.

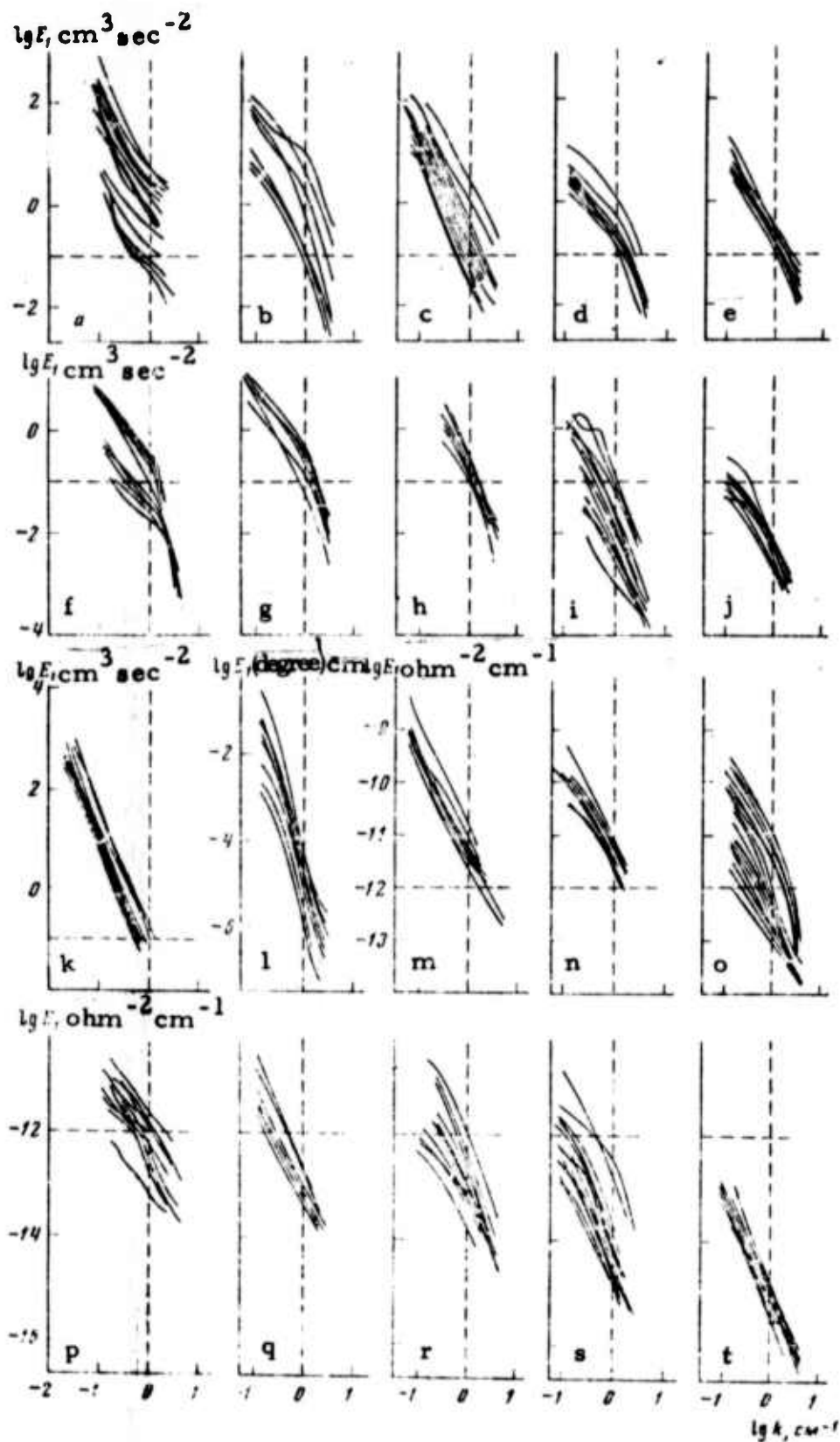| a	b	c	d	e	f	g	h	i	j	k	l	m	n	o	p	q	r	s	t
7.3.u	9.5.u	7.7.u	9.6.u	7.8.u	7.5.u	9.7.u	7.6(2).u	7.4.u	7.2.u	7.6(1).u	9.6.τ	7.8.σ	7.6(1).σ	7.6(2).σ	7.7.σ	7.2.σ	7.4.σ	7.3.σ	7.5.σ
127	70	195	30	55	115	52	107	67	120	90	40	141	54	149	157	77	67	70	187
70	87	157	40	95	115	36	75	120	120	80	50	145	68	149	195	120	65	35	150
70	60	213	60	170	115	140	75	49	138	104	60	170	60	45	94	120	60	35	120
72	80	195	50	161	115	90	106	103	77	128	60	110	14	23	195	120	80	70	105
72	30	213	60	110	115	110	149	60	77	142	50	170	10	217	195	77	70	72	90
35	50	168	77	141	105	73	23	120	181	150	40	175	69	132	213	77	60	52	115
118	40	138	49	102	100		185	60	181	176	77	16	89	23	138	77	75	72	55
35		94		100			125	75	138	163	30		95	75	168		120	70	129
35		103		100			125	65		136			55	75	141		49	91	80
103		138		187			23	80		142				106	174		103	118	100
30		121		120				60						71	138		120	127	
52		77						70						71				103	
91		160												125					
70		168												125					
		141												71					
		77												106					
		20												146					
		55												71					
		33																	

Table 1. Explanation of Fig. 1 letter indexes. The second line index contains cruise number, test area number, and signal type, in that order. Column figures are depths in m. in the same order as the upper left ends of spectra in Fig. 1.

areas, with turbulence nonmonotonically variable with depth in other test areas, i.e., alternating thin layers of weak and strong turbulence; and 3) changing shape of turbulence spectra.

Turbulence modes are correlated with the average hydrological conditions in the test areas and thickness of the upper homogeneous oceanic layer. A trend is revealed towards a weakening of velocity fluctuations with an increase in the average vertical gradient of water density. The slope of nearly all spectral density curves in log-log coordinates is steeper than 5/3, and increases with increase in wave number k from 10^{-1} to 10^{1} cm^{-1}. This conclusion was drawn also from the existence of peaks of dissipation spectra $k^{2}E_{1}(k)$ (not shown). In many cases, the energy spectra $kE_{1}(k)$ indicate small Reynolds numbers of turbulence, the absence of an inertial region, and nonuniversality of small-scale spectral regions.

-19-

Kofanov, Ye. S., N. K. Shelkovnikov, A. A.
Pivovarov, and Yu. I. Gorbatov. Method and
measuring system for study of the structure of
small-scale sea turbulence. VMU, no. 2, 1974,
171-177.

A description is given of a system for measuring temperature
pulsations in the ocean simultaneously at four points in three mutually
perpendicular directions. The article includes a short description of a method
for determining geometry and dynamics of temperature inhomogeneities,
based on the measurements of temperature pulsations at several spaced points,
as well as some sample calculations.

The block diagram of the measuring system is given in Fig. 1.
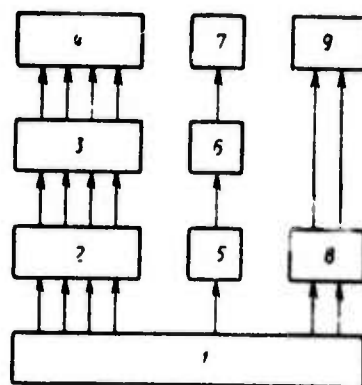
Fig. 1.

1- set of sensors (thermocouples); 2- four-channel
amplifier; 3- control unit; 4- recording unit;
5- measuring bridge; 6- balance unit; 7- automatic
recording potentiometer; 8- two-channel amplifier
for tachometer of current meter; 9- count-rate
recorder.

A complete schematic of a recording channel is also included.

The measuring system includes specially designed high-sensitivity current meters and platinum resistance thermometers. Its characteristics are as follows: drift - ~0.1 sec; sensitivity of recording channel - ~0.002° C /mm; sensitivity of galvanometer - 10^{-5} A (MM) m[sic]; accuracy of temperature gradient measurements - 0.02° C/m in the temperature range of 5-26° C.

The bottom mount for submerged part of the measuring system is illustrated in Fig. 2. The rods with sensors are secured on ball
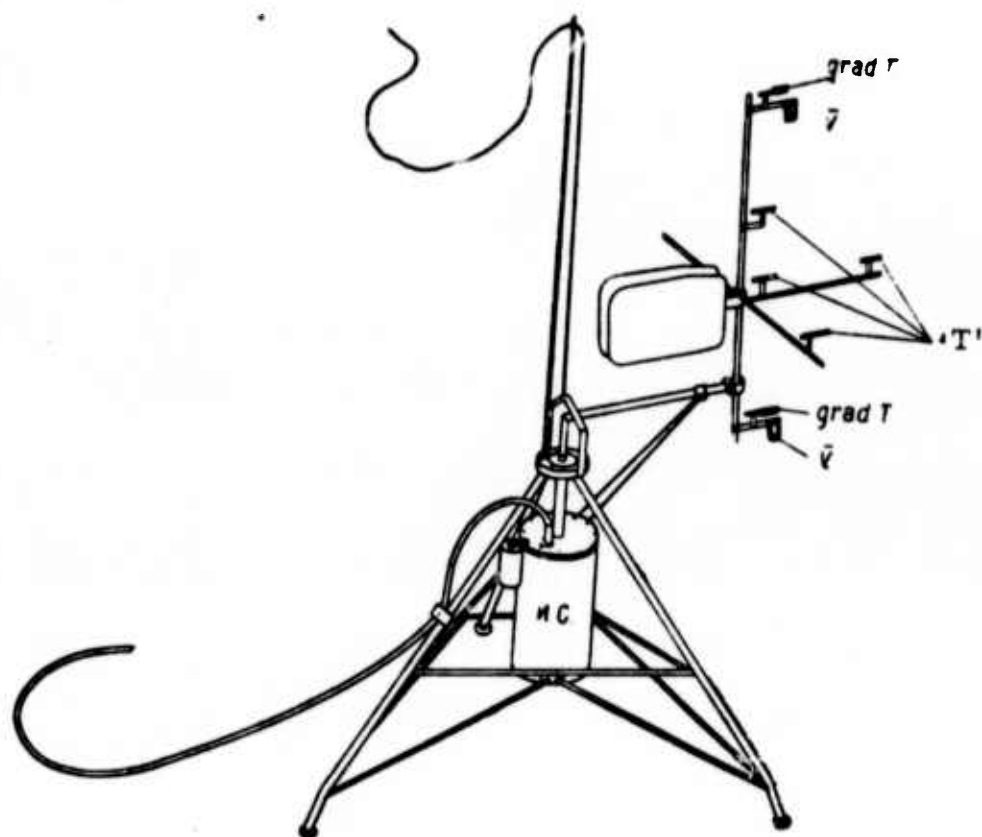
Fig. 2. Sketch of bottom system.

bearings and can be oriented in the flow direction. The mast is positioned vertically for heeling angles not exceeding 30°.

Sabinin, K. D., and A. N. Serikov. <u>Some</u>
<u>results of measurements of space-time character-</u>
<u>istics of short-period internal waves in the tropical</u>
<u>Atlantic.</u> FAiO, no. 10, 1974, 1062-1074.

Temperature fluctuations measured during two days in 1970
from the R/V Sergey Vavilov in the Atlantic are analyzed using Fourier
transforms, and the spectral distribution of internal wave parameters is
discussed. Measurements were made from the drift vessel by means of three
thermistor chains spaced in a layer 90 to 125 m deep, each carrying four
temperature sensors and one depth gauge. Calculations of spectral
distribution were made for each consecutive 40 min. period with a 10 min.
differential between starts of each period.

The internal wave parameters of wave number k, frequency
f, and height h were calculated for more or less well-defined trains of
relatively regular (narrow band) waves within each recording period. The
selected data presented in Table 1 and figures 1, 2, and ? show that the wave

Wave train (period numbers)	Train duration	Wave parameters				
		Period, min.	Length, km.	Height, m.	Orienta-tion, deg.	Mode
8/31/1970						
I (15—19)	00 ч. 02 м. — 01 ч. 26 м.	17÷35.5	0.36÷1.11	8÷15	314÷27	II
II (30—41)	02 40 — 05 18	13÷23	0.57÷0.80	11÷20	331÷335	I
III (46—53)	05 29 — 07 24	15÷25	0.44÷0.85	9÷19	347÷1	I
IV (90—94)	13 10 — 14 33	13÷24	0.50÷1.20	9÷12	32÷71	I—II
V (94—102)	13 52 — 15 38	15÷23	1.30÷2.40	12÷19	356÷24	I
VI (133—137)	20 28 — 21 48	25÷32	1.18÷4.70	13÷15	343÷100	I
VII (141—146)	21 47 — 23 17	21÷31	0.50÷1.60	9÷11	26÷67	II—III
9/1/1970						
VIII (196—205)	6 52 — 9 01	17÷33	1.10÷2.00	8÷13	292÷38	I
IX (197—205)	7 02 — 9 01	15÷25	0.66÷1.20	8÷14	24÷55	I
X (209—212)	9 01 — 10 10	20÷26	0.70÷1.50	11÷15	19÷65	I

Table 1. Principal data on wave trains.
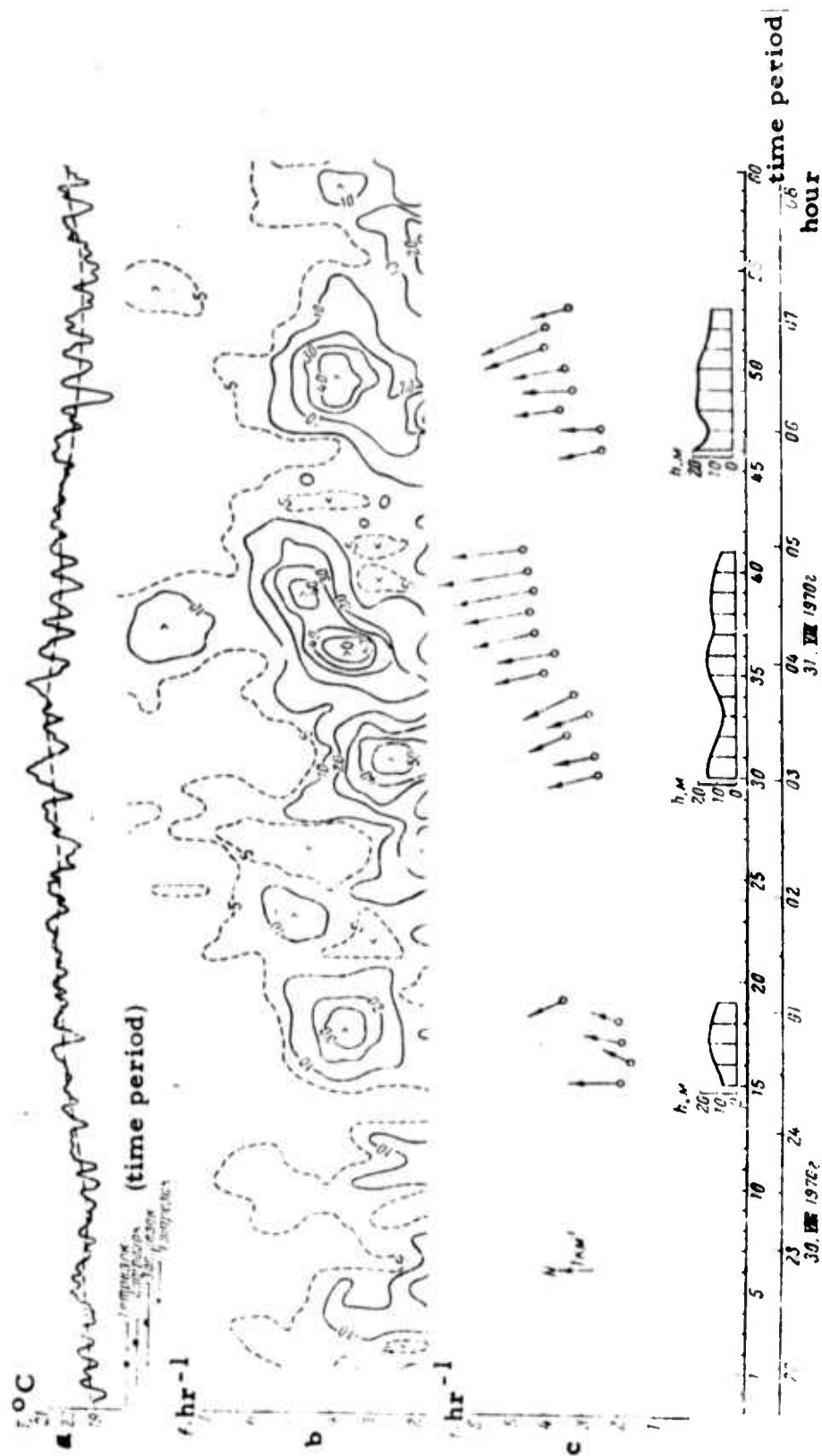
Fig. 1a- temperature fluctuations recording, b- periodogram, c- wave numbers (arrows), frequency (ordinate of arrow origin), and wave height in the trains I, II, and III (lower curves).
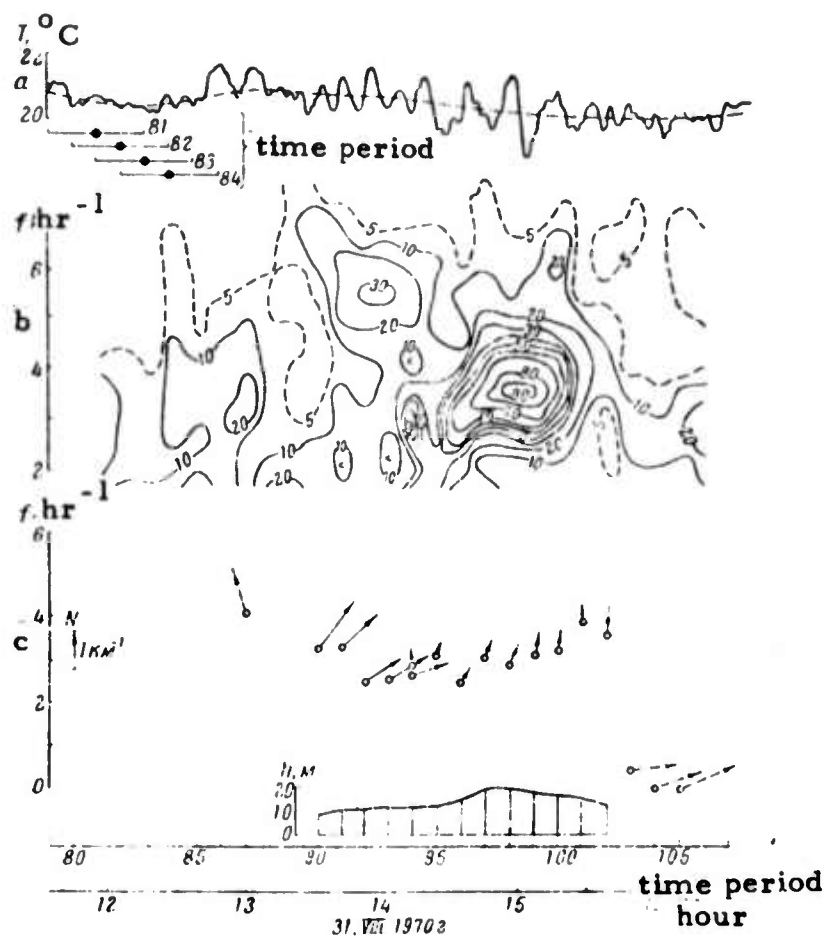
Fig. 2. a- temperature fluctuation recording,
b- periodogram, c- wave parameters of trains
IV and V.

parameters within each wave train are not constant.   An error analysis
was made to determine whether the parameter fluctuations are due to
measurement errors.   Calculations of $< k >$, $< f >$ and the error probability
limits show that   for most wave trains k and f variations in time exceed the
limits of probable deviations from mean $< k >$ and $< f >$ values, attributable
to errors of measurement.   This finding is illustrated for wave train II by
position of the cross, which represents $< k >$, $< f >$, and limits of measure-
ment errors (Fig. 4).   A close examination of the data in Table 1 and Fig. 1
to 4 reveals that most of the energy of the observed internal waves is
concentrated in separate trains of short-period (13 to 35 min.),   360 m to
4. 7 km long waves,which occupy 1/3 of the total recording time.   Each wave
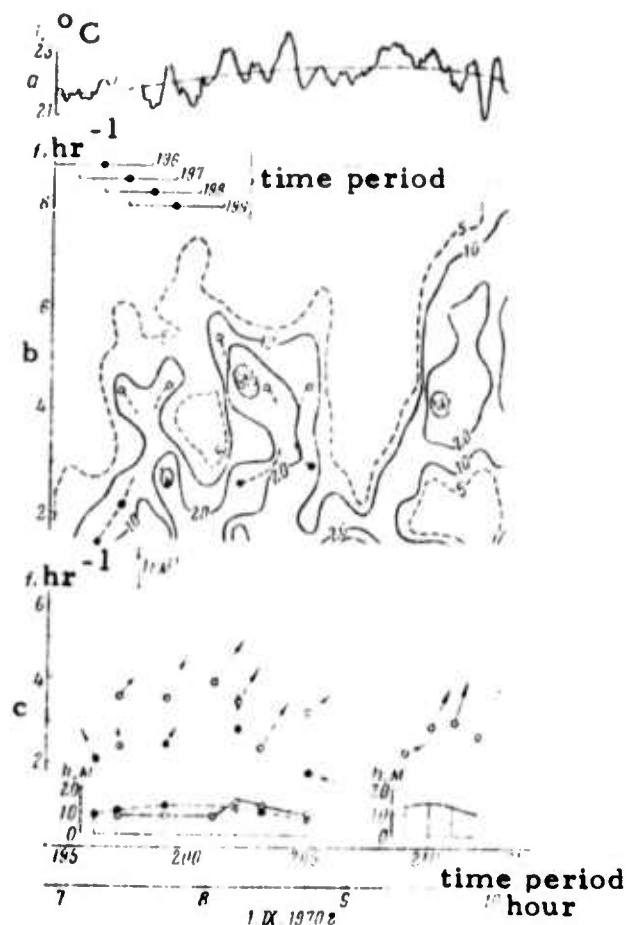
Fig. 3. a- temperature fluctuations recording,
b- periodogram, c- wave parameters of the trains
VIII, IX, and X (same notation as in Fig. 1).

train continues for 1 to 3 hr. Sometimes, as in train II, the waves,
attain h = 20 m. The north, northwest, or northeast directions of wave
propagation are predominant. As Table 1 and Fig. 4 show, most of the
k, f points of the observed wave trains belong to curves such as the dashed
curve in Fig. 4a, which are close to the calculated dispersion curves of
the lowest (I and II) wave modes. A fairly clear pattern of k and f values
increasing in time and space emerges from examination of data for wave
train II. This pattern supports the hypothesis of a locally fluctuating source
of wave train II.
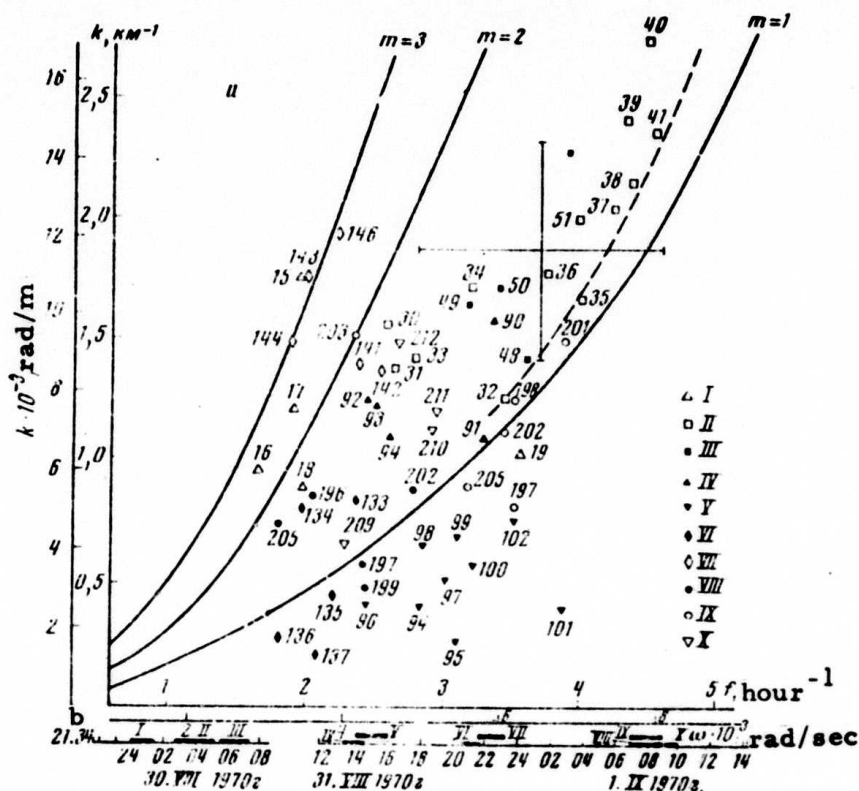
Fig. 4. a- dispersion ratio k_m (f) for modes
m = 1 to 3 of internal waves and k, f points of
different time periods; b- wave train position on
time scale, Roman numerals are train numbers.

The simultaneous existence is also noted of wave trains
VIII and IX, having approximately the same direction and amplitude, but
with k an f values differing by a factor of two. A strong deviation of most k,
f points of train V from the dispersion curve of mode I waves is attributed
to the partly standing nature of the waves which are oriented in a direction
normal to the drift direction of the vessel.

The standing wave ratio calculated by two independent methods
supports the existence of a system of two waves propagating in opposition to
each other. An analysis of directions of all measured waves led to the
conclusion that the short-period internal wave field is anisotropic, although

the existence of western-oriented waves cannot be ruled out. Newly detected characteristics of short period internal waves include frequency fluctuations in time and space, predominance of one direction of wave trains, and the possibility of generation of waves with a standing wave ratio different from zero. The observed phenomena agree with the resonance hypothesis of wave generation.

Leonov, A. I., and Yu. Z. Miropol'skiy. Nonlinear theory of propagation of stationary internal gravity waves. MZhiG, no. 5, 1974, 189-190.

This is the summary of a paper presented on June 6, 1974 at the General Seminar of the Institute of the Problems of Mechanics of the Academy of Sciences. A new nonlinear equation is reported, which describes stationary plane internal waves as a function of a single external parameter-the distributed Vaisalaa-Brunt frequency. The equation is derived on the assumption that fluid stratification is the sole source of vorticity.

In an approximation of weak nonlinearity, solutions to the cited equation are analyzed by the Poincare method for the cases of long internal waves in shallow water and a narrow pycnocline. It is shown that long waves in shallow water are stable against longitudinal disturbance but unstable against transverse disturbance. Nonlinear partial differential equations are set up using the approximation of geometric optics for the amplitude and phase of short internal waves. These equations coincide with adiabatic approximation of the L'yuk-Uizem (?) theory. Particular formulas are derived for linear or weakly nonlinear stratification. The equations of the amplitude and phase characteristics are solved in explicit form for limiting waves (solitons). The parameters of nonlinear internal waves are evaluated for the Vaisalaa-Brunt frequency distributions typical of the ocean.

Leonov, A. I., and Yu. Z. Miropol'skiy.
Stationary internal gravity waves with finite
amplitude. DAN SSSR, v. 218, no. 6, 1974,
1287-1290.

It is shown that nonlinear stationary internal waves in a
steadily stratified fluid can be described by the fundamental hydrodynamic
equation as a function of only one external parameter, namely the Vaisalaa-
Brunt frequency N^{-2}. In contrast with the Long equation, the derived
equation does not contain unknown random functions.

The cited equation with given boundary conditions is solved in
the approximation of weak dispersion and weak nonlinearity. In the case of
long waves, i. e., $\epsilon = H^2/\lambda \leq 1$ (H is the fluid depth, λ is wavelength), there
exists a solution of the form

$$F_1(\zeta, \eta) = W(\eta)U(\zeta), \tag{1}$$

where $\zeta = \theta\lambda^{-1}$ and $\eta = zH^{-1}$ are dimensionless variables, $\theta = x-vt$, x and z
are horizontal and vertical coordinates, and V is the wave propagation rate.
The function $W(\eta)$ is determined by solving the boundary value problem. The
function $U(\zeta)$ is determined from the equation

$$\partial^2 U/\partial\zeta^2 + \gamma U^2 + \beta_1\alpha U = 0, \tag{2}$$

where

$$\gamma = -\beta_0 \int_{-1}^{0} \Omega' W^3 d\eta + \mu\left[\frac{1}{2}\int_{-1}^{0}\Omega(W')^2 W\, d\eta + \int_{-1}^{0}\Omega' W' W^2\, d\eta\right], \quad \alpha = \int_{-1}^{0}\Omega W^2\, d\eta, \tag{3}$$

$\beta = \beta_0 + \epsilon\beta_1 + \epsilon^2\beta_2 + \ldots$ is the eigenvalue of the nonlinear boundary value
problem, $\Omega(\eta - F) = N^2(\eta - F)(N_0^2)^{-1}$ is a dimensionless parameter,
$(0 \leq \Omega \leq 1)$, $F = \psi(Hv)^{-1}$ is a dimensionless variable and ψ is the wave flow
function. Equation (2) coincides with the Korteweg-de Vries equation.
Solution of (2) describes, depending on the ratio of integration constants,
either a solitary wave (soliton)

$$U(\zeta) = -2a \, \mathrm{ch}^{-2}(\overline{\sqrt{a\gamma/6}\zeta}) + b,$$

(4)

or a cnoidal wave

$$U(\zeta) = \frac{2a}{s^2} \, \mathrm{dn}^2\left(\sqrt{\frac{a\gamma}{3}}\frac{\zeta}{s}, s\right) + b,$$

(5)

where a is the wave amplitude, b is an additive constant, and $\mathrm{dn}(x, s)$ is a Jacobian elliptic function with modulus s $(0 < s < 1)$. There can exist, at $\gamma < 0$, solitary internal waves of the trough type as shown in Fig. 1a (curve 1).
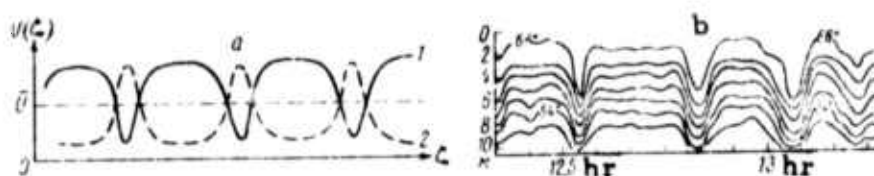
Fig. 1. a- Periodic wave close to solitons sequence: curve 1 - $\gamma < 0$; 2 - $\gamma > 0$; 1b- internal waves in shallow water. Isotherms in $^\circ$F, from the literature.

Solution (5) and that for the frequency ω correspond to each normal mode internal wave. The parameter γ of nonlinear internal waves is calculated for two typical N^2 distributions in the ocean. In the case of $N^2 = N_0^2 = \text{const}$, where N_0^2 is the maximum N^2 value, $\Omega = 1$ and the nonturbulent density distribution ρ_0 (H) is exponential. It is shown that $\gamma_n < 0$ for each odd mode and $\gamma_n = 0$ for even modes. It follows that a general solution would be a set of nonlinear waves close to negative solitons and simusoidal waves. Hence, with N^2 const and the predominant first mode in shallow water, propagation of a group of negative solitons would be observed (Fig. 1b). The second typical case is represented by a stratified model

$$\rho_0 = \begin{cases} \rho_1 = \text{const} & \text{при } 0 > \eta > -l, \\ \rho_2 = \text{const} & \text{при } -l > \eta > -1, \end{cases}$$

(6)

where l is the depth of discontinuity. Then, $\Omega = \delta(\eta + l)$. Calculation of

γ shows that a solution in this case hardly differs from the Boussinesq
approximation. If the upper layer is thinner than the lower, the solitons are
positive ($\gamma > 0$); in the opposite case, the solitons are negative ($\gamma < 0$). At $\ell = 1/2[1 + \mu/8] + O(\mu^2)$, where μ is the characteristic of deviation from
Boussinesq approximation, $\gamma = 0$ and the waves are sinusoidal.

Miropol'skiy, Yu. Z. <u>Propagation of internal</u>
<u>waves in an ocean with horizontal inhomogeneities</u>
<u>in the density field.</u> FAiO, no. 5, 1974, 519-532.

The author notes that most studies of internal wave behavior
in the ocean concentrate on variation of parameters as a function of depth,
while neglecting the horizontal direction. The latter should be accounted for,
however, in view of the typically long horizontal propagation range of internal
waves.

The study accordingly examines free internal waves propagating
in a mean-density ocean as a function of Vaisalaa-Brunt frequency N and
density ρ in both x and z coordinates. The problem is solved by a method
analogous to geometrical optics. The possibility for standing internal waves
in an unbounded ocean is shown. Analysis of internal wave growth shows that
they tend to approach local N frequency; also, wave amplitude increases with
reduction in pycnocline depth. The study demonstrates the possibility of
turbulence being generated by internal waves propagating in an ocean with
horizontal density variability.

Borisenko, Yu. D., and Yu. Z. Miropol'skiy.
Effect of nonlinearity on statistical distributions
of internal waves in the ocean.   Okeanologiya,
no. 5, 1974, 788-796.

Statistical distributions of internal waves in the ocean are
analyzed on the basis of the Longuet-Higgins theory.   Expressions for the
first two moments of distribution are derived from nonlinear equations
based on the theory of internal waves.   Theoretical results are compared
to experimental data obtained from observations on isotherm fluctuations at
two stations in the Atlantic Ocean.

Empirical distributions of probability density for isotherm
fluctuations are given in Fig. 1.
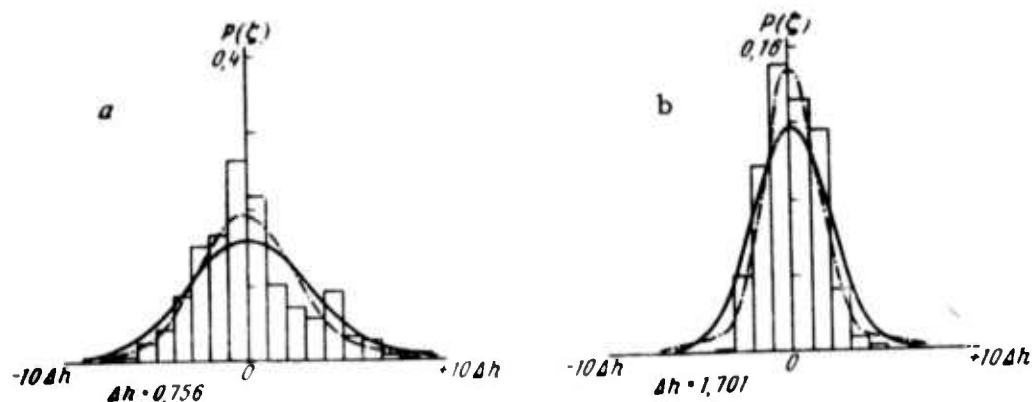
Fig. 1.   Histograms of distribution density
$P(\zeta)$.

a- station 1, isotherm 15° C; b- station 2,
isotherm 17.5° C.   Dashed line - distribution
density calculated by the Longuet-Higgins formula.

Spectral functions of isotherm fluctuations within the
1.96×10^{-2} min^{-1} - 6.27×10^{-1} min^{-1} frequency range, calculated using
data obtained in the Atlantic Ocean (Miropol'skiy, 1973), are shown in
Fig. 2.
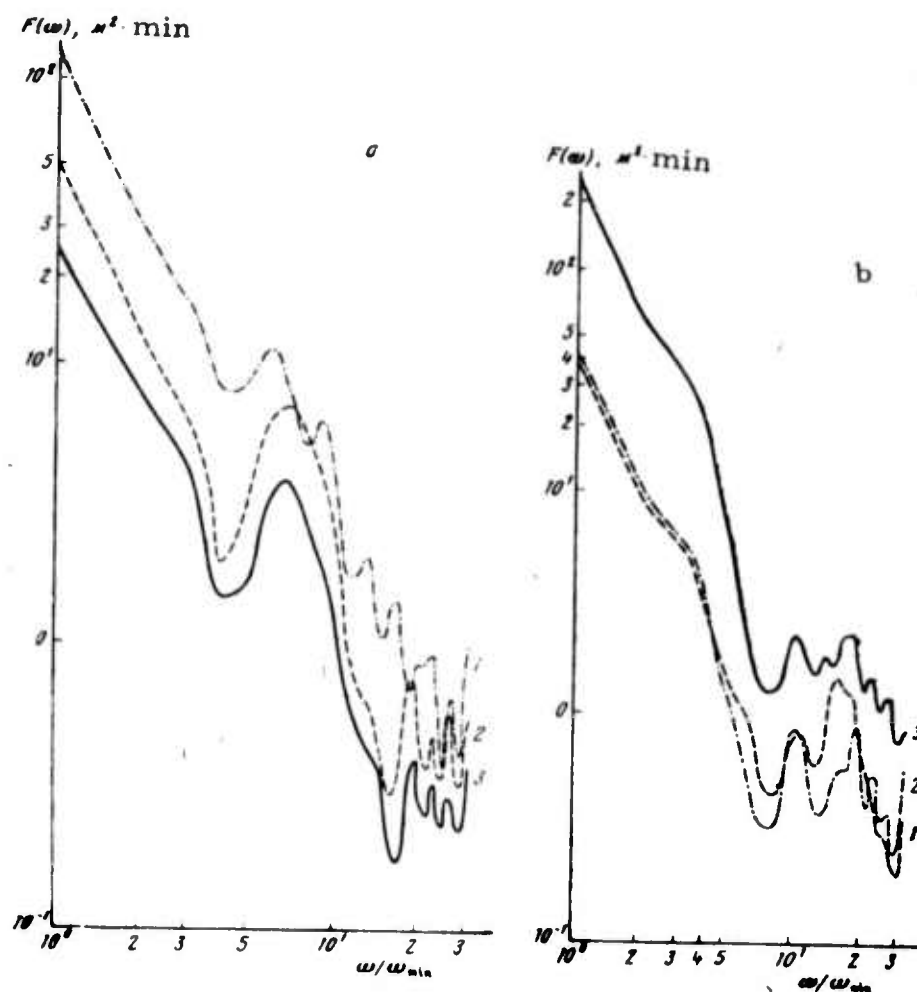
Fig. 2. Spectral functions $F(\omega)$ for various isotherms.

a- Station 1: 1-15°, 2-21°, 3-22.5°;
b- Station 2: 1-16°, 2-17.5°, 3-18°.

Empirical and theoretical values of dispersion μ and coefficient of skewness S for various isotherms are listed in the following table.

The authors conclude that the coefficient of skewness is a positive quantity in the case of a weak nonlinearity and prevalence of the first mode in internal waves.

Isotherm. °C		$\mu_9, \mathcal{M}^8$	$\mu, \mathcal{M}^8$	S_9	S
Station 1	22,5	0,97	1,03	0,369	0,367
	21—	1,56	1,78	0,969	0,527
	19,5	2,68	2,95	1,010	0,687
	18	4,60	4,83	0,682	0,701
	16,5	6,63	6,71	0,400	0,522
	15	6,35	6,81	0,197	0,289
Station 2	18	14,26	14,31	0,104	0,059
	17,5	11,57	11,74	0,044	0,013
	17	11,19	11,33	—0,0048	0,217
	16	12,90	13,03	0,049	0,019
	15	32,07	32,33	0,042	0,077

Table 1

Garnich, N. G., and Yu. Z. Miropol'skiy.
Some characteristics of the fine thermal
structure of the ocean. Okeanologiya, no. 4,
1974, 595-601.

Vertical sounding of the temperature field to a depth of
600 meters was conducted in the central part of the Timor Sea, during the
7th cruise of the R/V Dmitriy Mendeleyev in 1972. Series of measurements
at 2 hour intervals were made using the AIST salinity-temperature probe.

The vertical distribution of the average temperature in the
tested area is shown in Fig. 1, a. Typical vertical distributions of temperature
as detected by the AIST probe are shown in Fig. 1, b.

Spectral functions were calculated for temperature profiles
described by the relation

$$T_i(z) = \overline{T}_i(z) + \theta_i(z), \tag{1}$$

In order to avoid effects of statistical inhomogeneity of the random component $\theta_i(2)$, each θ_i series was divided into n homogeneous depth intervals of length l and new series were calculated by

$$\theta_n = \sum_{i=1}^{I} \theta_{l,i}$$

(2)

The length of new series was $L = Il$ where $I = 7$ is number of subintervals.

Spectral functions calculated for n = 7 depth intervals are shown in Fig. 1.

Fig. 1.   Spectral functions $S_n(\kappa)$ for depth intervals

n = 1 - 50-120 m; 2- 100-170; 3- 150-200; 4- 200-270;
5- 300-370; 6- 400-470; 7- 500-570.

Spectral functions $S_n(k)$ shown in Fig. 1 are seen to be similar to each other, and decrease monotonically as k^{-3}.

Depth dependences for the vertical gradient of the average temperature $(d\bar{T}/dz)_n$, standard deviation $\sigma_n (d\bar{T}/dz_n)^{-1}$ are shown in Fig. 2.
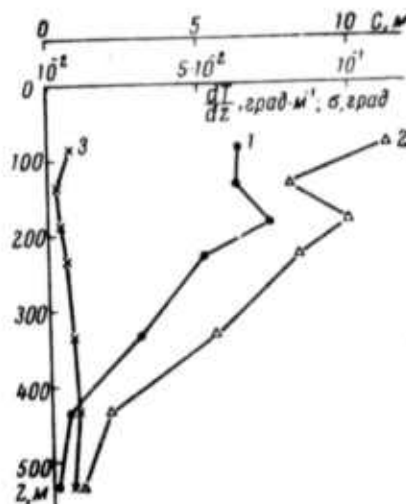
Fig. 2. Depth dependences for $(d\bar{T}/dz)_n$ (1), σ_n (2), and C_n (3).

The fact that the standard deviations are proportional to the vertical gradients of the average temperature, i.e., C = const (see Fig. 2) suggests that the depth dependence for $S_n(k)$ may be determined by the depth dependence for $(d\bar{T}/dz)_n$. In that case the following relation may be assumed:

$$S_n(k) \sim k^{-a}. \tag{3}$$

The spectral functions normalized by $(dT/dz)n^2$ are shown in Fig. 3.

As can be seen in Fig. 3, equation (3) is satisfied only for small wave numbers, i. e., large scale inhomogeneities, $\lambda > 10$ m. The average value of β is 7×10^{-4}. The results shown in Fig. 4 confirm that conclusion.

Hence the relation C = const is satisfied only for small wave numbers, i. e., large-scale vertical inhomogeneities in the temperature field. An explanation offered for this result is that vertical

microstructure in the ocean is generated by different mechanisms: by breaking of high-amplitude internal waves at small λ, by layer convection, and by "salt fingers" at small λ. More refined experiments are needed to resolve this question.
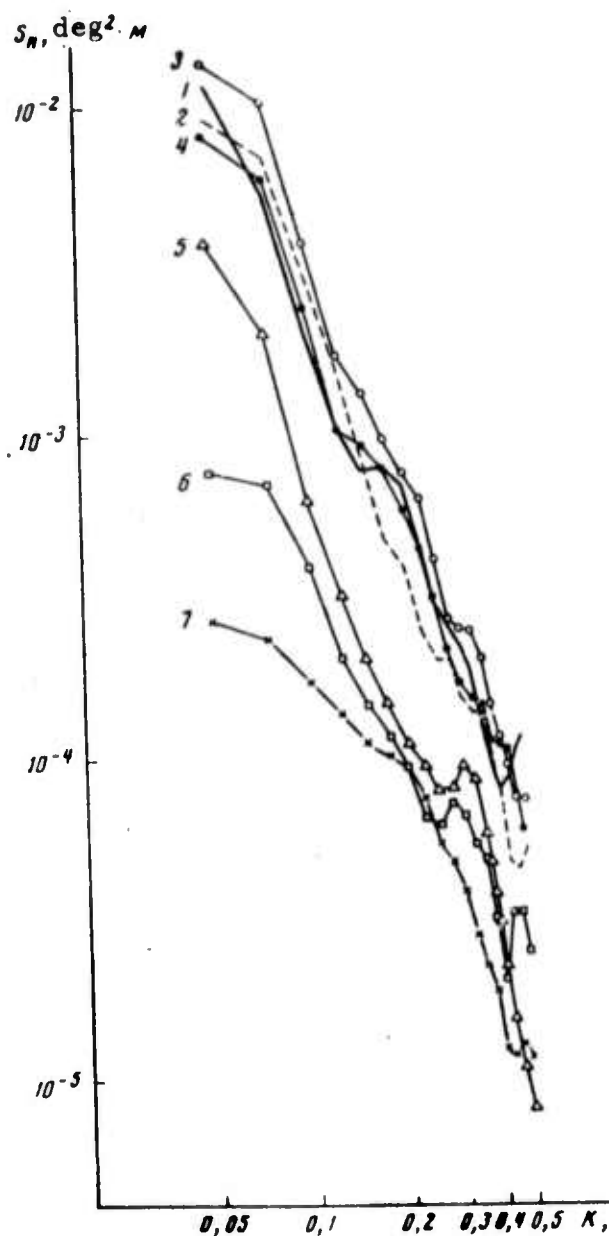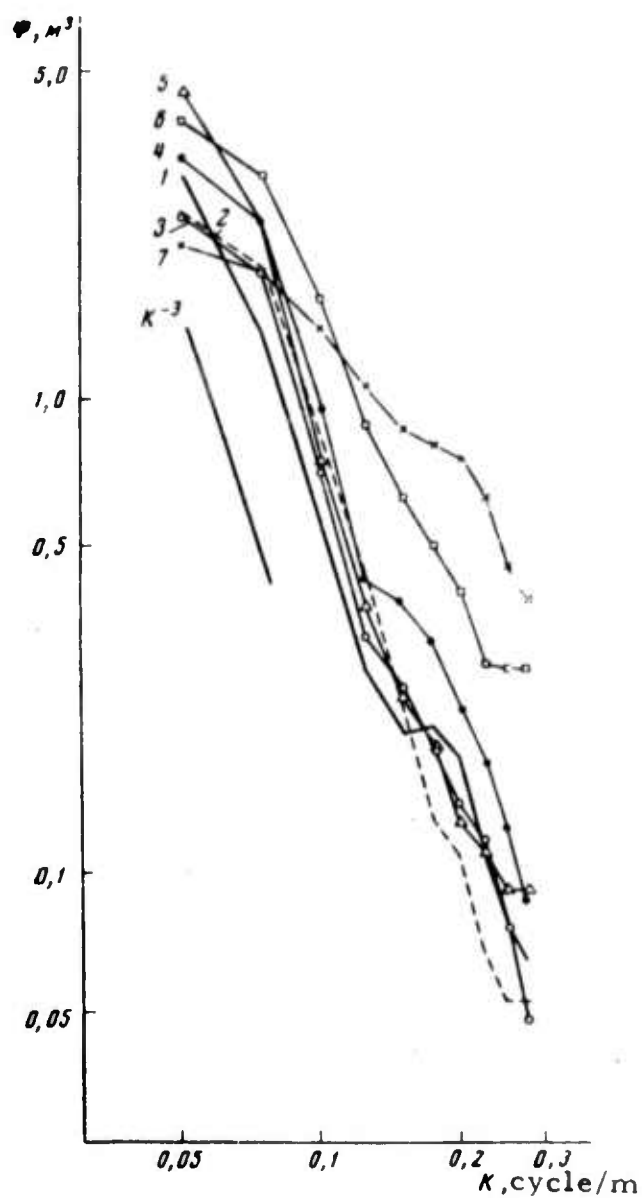

Fig. 3. Normalized spectral functions $\psi_n(k)$ for n depth intervals.

n = 1- 50-120 m; 2- 100-170; 3- 150-200; 4- 200-270; 5- 300-370; 6- 500-570.
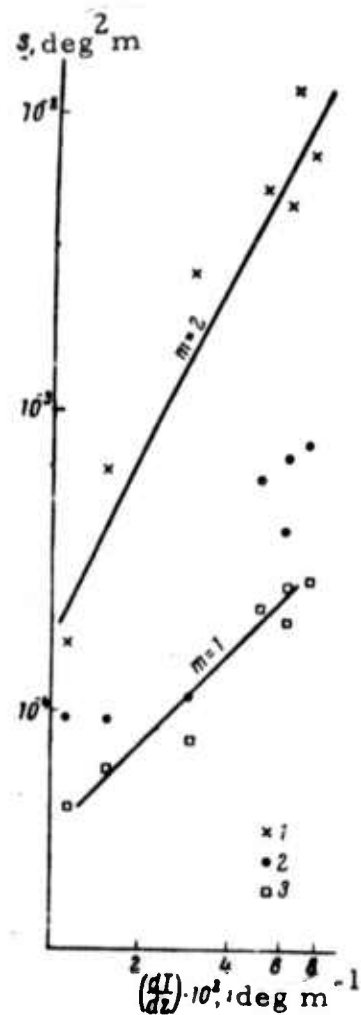
Fig. 4. Dependence of S_n on $(d\bar{T}/dz)_n$ at different k.

1- k = 0.025; 2- k = 0.2; 3- k = 0.275.

Desnyanskiy, V. N., and Ye. A. Novikov.
Modeling of cascade processes in turbulent
currents. PMM, v. 38, 1974, 507-513.

Modeling of cascade processes of energy transmission,
vorticity, and nonuniformity of admixture concentration using the spectrum
of turbulent motion is of special interest in the study of turbulent flows.
Cascade processes control the internal structure of flows and mechanisms.
of turbulent dissipation.   It has been possible in recent years to obtain
computer modelling of a two-dimensional spatial-periodical flow at modest
viscosity, and to obtain the portion in the energy spectrum $E(k) \sim k^{-3}$
(Batchelor, 1969; Lilly, 1969, 1971; Gavrilin et al., 1972) which corresponds
to the cascade process of vorticity transmission (Batchelor, 1969; Kraichman,
1967).   The authors are aware of only one work on numerical modeling of
three-dimensional periodical flows (Orszag and Patterson, 1972), in which
the Reynolds numbers are however still too small to trace the cascade process
of energy transmission and to obtain the portion of spectrum with the -5/3
power law.   In addition to improving numerical experiments with a large number
of degrees of freedom, it is also of interest to develop methods for reducing
the number of degrees of freedom in a way that would not prevent realization
of cascade processes.   Such a method is suggested in the present work.

Model equations for collective degrees of freedom - Fourier
amplitudes of velocity field, summed over an octave of wave numbers (wave
number modulus changes by a factor of two within an octave), are derived
from the hydrodynamics equation.   The stationary solutions of these
equations which give similarity laws in corresponding inertial intervals
($k^{-5/3}$ in three-dimensional, or k^{-3} in two-dimensional turbulence) are analyzed.
Nonstationary problems of formation of cascade processes have been
numerically analyzed by Desnyanskiy and Novikov (1974).

Bogdanov, Yu. A., V. A. Burkov, V. M. Pavlov,
and Ye. A. Plakhin. Some inhomogeneities of
water stratification in the Gulf Stream area.
Okeanologiya, no. 5, 1973, 755-759.

Results of integrated observations of fine structure in the
Gulf Stream waters are reported and discussed. The observations were
made in February 1972 during a cruise of the R/V Dmitri Mendeleyev. They
included measurements of the absolute attenuation coefficient ϵ and transparency
$0 = 10^{-\epsilon}$ of water samples; vertical distribution of ϵ and temperature T; and
composition and content of suspended particles in the same water samples.
The SGN-M spectral turbidity meter, the FPR vertical profiling transparency
meter coupled with a bathythermograph, and the AIST-STD recording meter
were used to measure absolute ϵ, $\epsilon(z)$ and T(z), respectively.

The cited optical and hydrologic parameters were measured
at three ship stations: no. 351 at latitude $28^{\circ}46'$ N and longitude $78^{\circ}48'$ W;
352 at $28^{\circ}44'$ N and $79^{\circ}26'$ W, and 354 at $28^{\circ}44'$ N and $79^{\circ}50'$ W. The
vertical profiles of the measured parameters are shown for all three
stations. Homogeneity of the upper 100 m oceanic layer is deduced from the
profiles at the station 351. The profile of suspended particle concentration shows
a sharp increase in concentration at 10 m, and a decrease to a minimum at
100 m. The profiles at stations 352 (Fig. 1) and 354 (Fig. 2) are especially
revealing, insofar as these stations were located near mid-Gulf Stream.
They indicate optical stratification of waters, which is supported fully by the
quantitative distribution of suspended particles. In the 200 to 300 m layer at
station 352, the particles are rich in coarse carbonate material. At the same
station, the T(z) profile plotted from AIST recordings exhibits three steps within
the 0 to 200 m layer having small T gradients. The centers of these steps
coincide with observed optical anomalies.
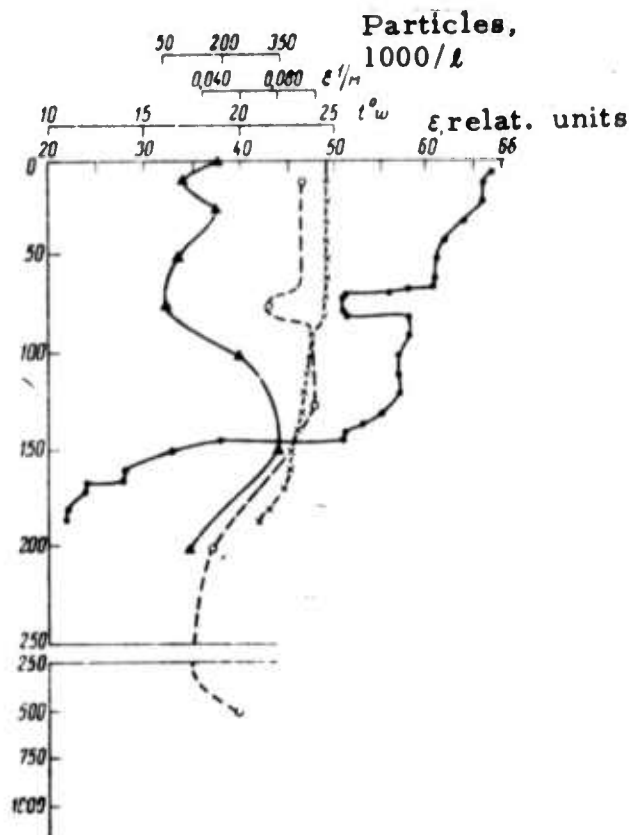
Fig. 1
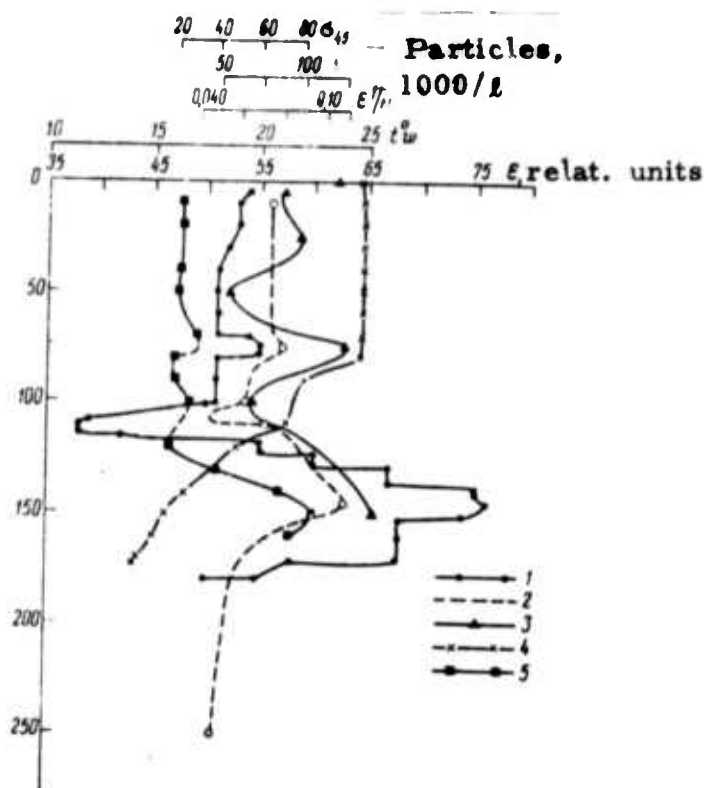
Fig. 2

Fig. 1 and 2. Vertical profiles of optical and hydrologic parameters at stations 352 and 354: 1- ϵ given by FPR meter; 2- ϵ given by SGN-M meter; 3- suspended particle concentration; 4- water T from bathythermograph data; 5- light scattering coefficient σ_{45} at 45°, in relative units.

At station 354, the optical structure of the upper 200 m layer (Fig. 2) appears to be very complex. The turbid (to 78% transparency) layer, 60 m thick, centered around 145 m depth, is correlated with T discontinuity. Transparency at the 250 m level increases to 89%.

A summary of the cited data led to the conclusion that the 50 to 75 m upper layer is occupied by Gulf Stream waters, and may be in turn subdivided into several layers of decreased transparency and increased suspended particle content. Such a clear stratification of waters may be attributed to the hydrologic structure of the area. The depth of a sharp peak of suspended particle concentration within the 0 to 50 m layer coincides with that of minimum salinity and the steps of the T(z) profile. The low salinity indicates a possible influx of coastal waters.

Stiro, D. B. Study of vertical turbulent
diffusion in the Baltic Sea. IN: Sb. Fiz.
atmosfery, Vil'nyus, no. 1, 1973, 163-166.
(RZhGeofiz, 4/74, no. 4V42). (Translation)

The coefficient of vertical eddy diffusion was calculated
from an equation which describes tracer distribution (Ozmidov, Popov,
1965) using published data on Sr^{90} concentration. The coefficient K varies
from 0.6 to 0.9 cm^2/sec. The calculated data are compared with results
of other authors. The Sr^{90} concentrations on the surface and at 200 m depth
in the Baltic Sea in 1960 and 1961 were calculated.

Bogdanova, A. K. The structure of the
turbulent velocity field in the Bosporus area
of the Black Sea. IN: Sb. Materialy Vses.
simpoz. po izuchennosti Chern i Sredizemn.
morey, ispol'z. i okhrane ikh resursov,
Sevastopol', 1973, Ch. I, Kiyev, Izd-vo
Nauk dumka, 1973, 59-63. (RZhGeofiz, 4/74,
no. 4V49). (Translation)

Current velocity measurements by means of a BPV-2 meter have
been carried out for 2.5 days in calm weather at 10, 25, 50, and 85 m. levels
at one point, at 91 and 91.5 m levels at another point in the Bosporus area
of the Black Sea. Using the current velocity observation series (at 10 min.
discrete time), mean square root deviations, turbulence intensity, and
coefficient of horizontal turbulent transport are calculated with different
averaging periods. The coefficients of vertical turbulent transport are
calculated from the equations of turbulent kinetic energy. Also, correlation
functions, spectral density, and energy spectra are calculated. Analysis of
the cited parameters indicated that, in the upper layer of Black Sea waters,

small-scale eddies play the major role in eddy thermal diffusion.
Importance of intermediate-scale eddies increases in the Black Sea-to-
Mediterannean transition layer.   The 12 h. eddy is predominant in the
bottom current of Mediterannean waters.   Concurrently with the decrease
in vertical diffusion momentum in the layer (85 m) of a sharp density
jump, an increase in horizontal transport is noted.   In that case, energy
increases on account of the large-scale spectral region of turbulent eddies.

Gagoshidze, Sh. N.   The transformation of
stationary internal and surface waves in the
presence of a stationary current and depth
variability.   IN: Trudy. Zakavkaz. n. -i.
gidrometeorol. in-t, no. 31(37), 1973, 26-38.
(RZhGeofiz, 4/74, no. 4V219). (Translation)

The problem of wave parameter transformation under
conditions of variability in depth and in stationary current velocity is
analyzed, on the basis of a linear theory of plane waves propagating on the
surface of contact discontinuity and the free surface of two ideal flows with
different densities.

Fundamental correlations of the amplitude and wavelength
transformation coefficients for both interface and free surfaces are derived
from the energy balance equation and the condition of periods equality in
deep and shallow waters.   Simplified design correlations of the cited
coefficients are derived for certain specific ranges of depths and stationary
current velocities.

Abramov, A. A., B. A. Tareyev, and V. I.
Ul'yanova. Long waves and baroclinic instability
on the inclined surface of an interface. IN:
Vnutrenniye volny v okeane. SO AN SSSR,
Novosibirsk, 1972, 244-256.

Results are given of a numerical analysis of frontal waves instability at a discontinuity surface in a stratified flow. The analysis covers the range of long waves and baroclinic instability, i.e., the $3 \leq \alpha \leq 12$ range of Richardson numbers and $0 \leq \beta \leq 1$ range of Rossby numbers $\beta = kU/f$, where U is the characteristic velocity and f is the Coriolis force. Thus the analysis previously made by Orlanski (Jour. Atmosph. Sci., v. 25, no. 2, 1968) is extended to cover the range of higher Ri numbers, and then to determine applicability ranges of the Kotsohin and the quasigeostrophic Phillips models of instability on the inclined surface of an interface.

Solution of a set of differential equations for the amplitude of small pressure disturbances on the inclined interface (Fig. 1) reduces
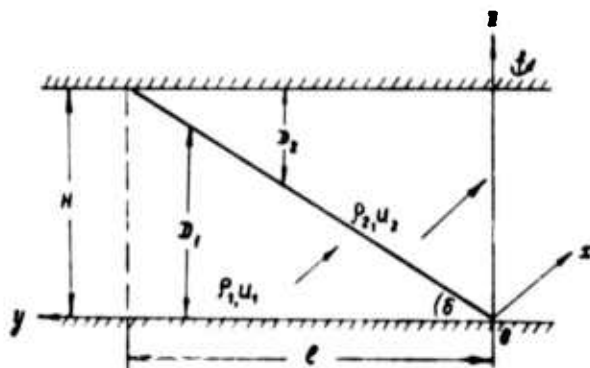
Fig. 1. Geometry of stratified flow.

to the problem of determining the eigen value of the instability increment τ as a function of α and β. In the most general case, $\tau = \tau_r + \tau_i$ is a complex number. The complex τ values are calculated for baroclinic instability of

the vortex gradient and internal gravity waves. In the case of the vortex gradient waves, τ_i and τ_r are calculated by integration of the set of differential equations using the method of successive calculations described by the authors in FAiO, no. 2, 1972, 139. The τ_i and τ_r values are plotted versus α at $\beta = 0$ to 0.4. The contour map of τ_i eigenvalues (Fig. 2) shows that, within the Kotschin instability region (above the
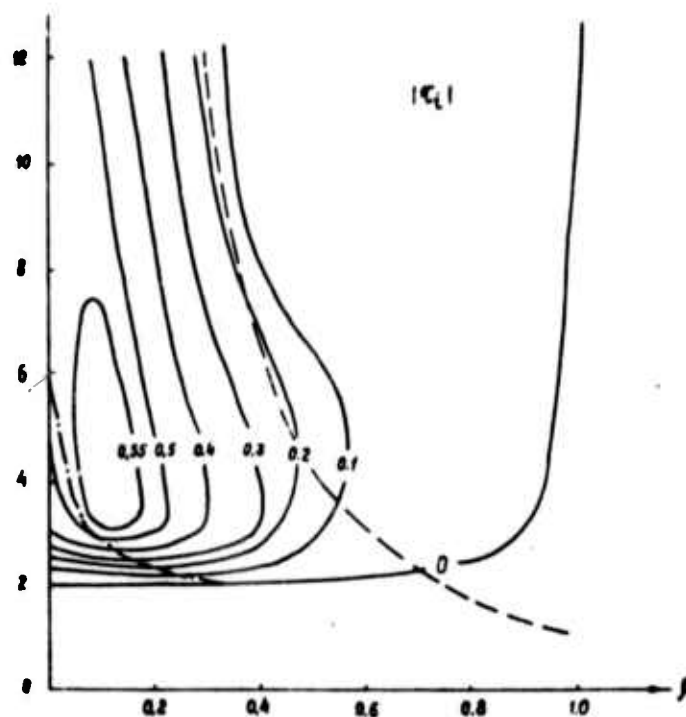
Fig. 2. Contour map of τ_i within the Kotschin instability region: the region of solely imaginary τ is to the left of the dot-dash line; the dashed line is the neutral line of the Phillips geostrophic model in the absence of beta-effect.

$\tau_r = \tau_i = 0$ curve) at $\alpha > 6$ τ becomes complex and a second τ eigenvalue appears, which is always smaller than the fundamental eigenvalue. At high α and small β, $\tau_r = 0$ in the Phillips model. Approximation of τ_r in the Phillips model becomes satisfactory only at very high α values, e.g., $\alpha = 100$ and $\beta = 0.02$.

In the case of internal gravity waves, numerical analysis shows that τ eigenvalues are real ($\tau_i = 0$) and are outside the boundaries of the unit circle in the τ - plane. The approximation $\tau = (\alpha - 1) + \beta^{-2}$ shows that, within the analyzed α and β ranges, the Kelvin-Helmholz instability of gravity waves is absent. This is illustrated by the table of selected τ eigenvalues and the corresponding $\tau_r = \tau_r (\beta)$ plots (Fig. 3).
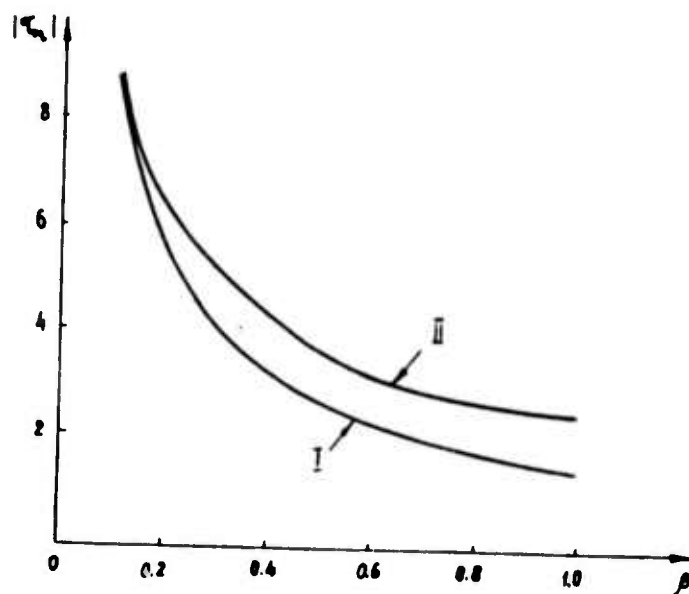
Fig. 3. Dimensionless phase velocity τ_r versus Rossby number β (proportional to wave number) for internal gravity waves. Curve I - $\alpha = 4$, curve II - $\alpha = 9$.

The cited data thus confirm the insignificance of the beta-effect on behavior of internal gravity waves.

Yefimov, V. V., and V. M. Kushnir.
Analysis of the high-frequency portion of an
ocean wave spectrum. Okeanologiya, no. 1,
1974, 30-36.

Results are described of the statistical processing of natural
recordings of ocean waves. The functional mode of the HF portion of wave
spectra obeys the expression ω^{-p}, where $4 < p < 6$. For determining the
probable value of exponent p in the case of wind waves, recordings of the
surface waves were used, which were obtained in the storm test area of the
Marine Hydrophysical Institute in the Black Sea.

Surface waves were measured by capacitive string wavemeters,
attached to a fixed pole at 300 m from the coast at a depth of 15 m. Signals
from the sensors were transmitted to the coast by cables, where they were
converted to digital code and recorded on magnetic tapes. Values of
discreteness in measurements were varied as a function of the statistical
structure of the measured process, such that the ordinal number is maintained
at a fixed level, at which the spectral density decreases from maximum at
$\omega = \omega_o$ to a quantization value, determined by noise. Observation series
treated were as long as 10^4 numbers. Intervals of discreteness in different
cases were varied from 0.06 to 0.5 sec.

In the present work, frequency spectra of surface waves are
calculated and their behaviors analyzed. Table 1 shows the calculated results
of the most likely exponent of the function, which is close to the behavior of
the HF portion of the spectrum. It is seen that the exponent p' for different
series of measurements lies in the range of 4 to 5; the average value of p'
is 4.36. It is noted that the difference between the obtained average value
of p' = 4.36 and the usually accepted value p' = 5 is not great. However, this
may indicate the fact that during shaping of the HF portion of the sea wave
spectrum, it is necessary to consider some other physical mechanism,
which is different from that used in the expression based on the hypothesis

Table 1

Wave frequency, f_o Hz	Ave. wind velocity, $\bar{u}$ m/sec.	Exponent p'	Criterion ϵ/D	F-distribution quantiles at $\alpha = 0.05$	Frequency range for analysis, $1.3\,f_o - f_{max}$, Hz
0,183	7—8	4,2	1,08	1,3	0,238—1
0,183	9—11	4,4	1,25	1,3	0,238—1
0,266	7—11	5,3	1,2	1,4	0,346—0,835
0,234	7—9	4,5	1,42	1,32	0,302—0,92
0,29	5—7	4,2	1,5	1,45	0,37 —0,8
0,316	3—4	4,4	1,56	1,37	0,41 —1,23
0,286	5—7	4,4	1,4	1,45	0,37 —0,84
0,167	9—11	5,3	1,15	1,25	0,216—0,84
0,15	8—12	4,0	1,17	1,35	0,195—0,85
0,266	9—10	4,2	1,0	1,40	0,238—1
0,268	4	4,5	1,45	1,40	0,346—0,82
0,218	5—7	4,2	1,72	1,45	0,28 —0,65
0,183	6,5	4,4	1,2	1,3	0,238—1
0,322	4—6	4,1	1,35	1,5	0,416—3,2
0,322	4—6	4,8	1,08	1,5	0,416—3,2
0,322	4—6	5,0	1,43	1,5	0,416—3,2
0,322	4—6	4,0	1.05	1,5	0,416—3,2
0,322	4—6	4,2	1,23	1,5	0,416—3,2
0,322	4—6	4,4	1,30	1,5	0,416—3,2
0,21	7—9	4,2	1,06	1,3	0,27 —1,75
0,18	7—9	4,2	1,20	1,3	0,238—1
0,30	9,5	4,0	1,15	1,45	0,39 —0,8
0,266	9,5	3,9	1,58	1,50	0,346—0,7
0,266	9,5	3,8	1,82	1,6	0,346—0,68

of Phillips, namely

$$S(\omega) = \beta g^2 \omega^{-5},$$ (1)

where $S(\omega)$ - spectral density; β - dimensionless constant; q- acceleration of gravity; ω - angular frequency.

Ivanov, Yu. A., and Ye. G. Morozov.
Deformation of internal waves by a flow with
horizontal velocity shift. Okeanologiya, no. 3,
1974, 457-461.

A mathematical model is discussed for deformation of internal gravity waves by a flow with horizontal velocity shift. A numerical

analysis was carried out for negative values of $k_x x - \omega t = \pi/2$ in a flow with horizontal velocity shift is given in Fig. 1.
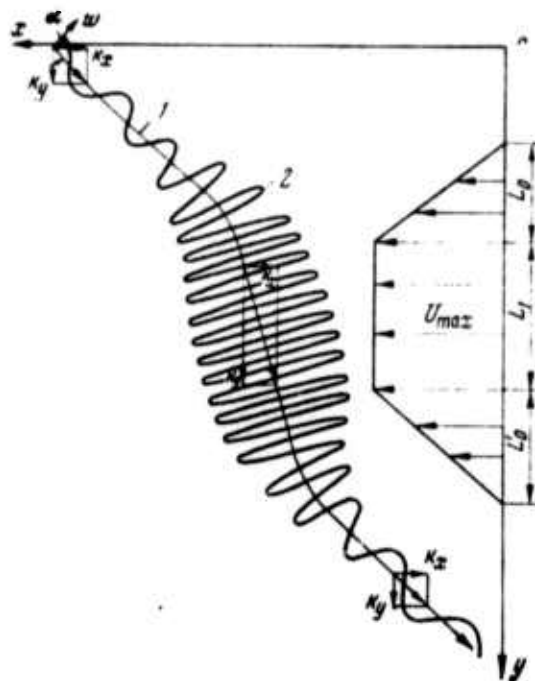
Fig. 1. Qualitative picture of the distribution of the average flow velocity U and deformation of internal waves.

1 - wave propagation direction; 2 - variation of w along the ray.

Variation of the amplitude of internal waves in a flow with horizontal velocity shift is illustrated in Fig. 2 and 3.

Numerical analysis shows that a large horizontal velocity shift induces significant deformation of internal waves over a wide frequency range. As the horizontal velocity shift decreases the frequency range narrows toward the high frequencies. However, deformation of internal waves does not depend on L_0 (see Fig. 1). Furthermore, calculated values
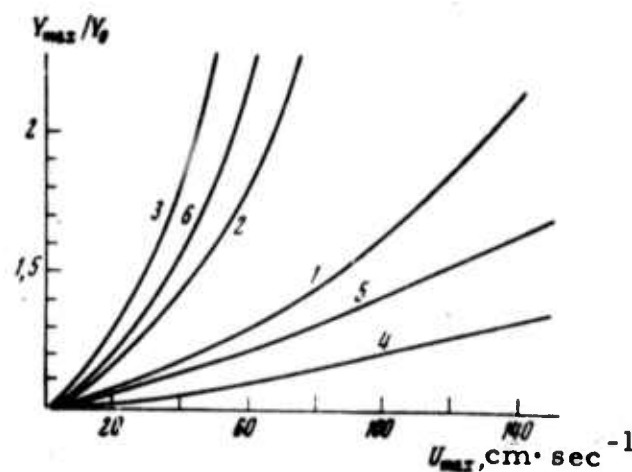
Fig. 2. Dependences of the ratio between the maximum and initial amplitude of internal waves on the maximum velocity shift for different modes and frequencies:

1 - $\omega = 0.20 \times 10^{-2}$ sec^{-1}, n = 1; 2 - 0.20 x 10^{-2} sec^{-1}, n = 2; 3 - 0.20 x 10^{-2} sec^{-1}, n = 3; 4 - 0.6 x 10^{-3} sec^{-1}, n = 1; 5 - 0.17 x 10^{-2} sec^{-1}, n = 1; 6 - 0.25 x 10^{-2} sec^{-1}, n = 1.
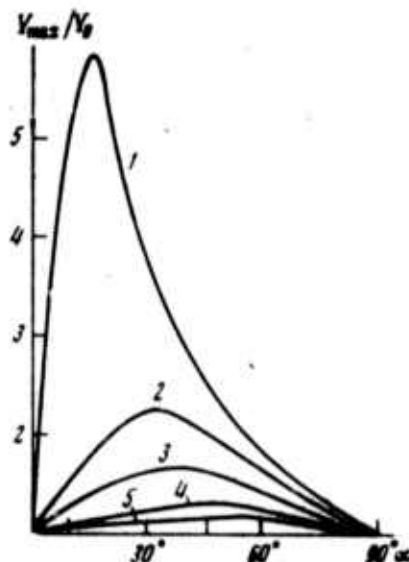
Fig. 3. Dependences of the ratio between the maximum and initial amplitude of the first mode on the initial incident angle α at U_{max} = 100 cm x sec^{-1} and different frequencies:

1 - 0.24 x 10^{-2}; 2 - 0.22 x 10^{-2}; 3 - 0.20 x 10^{-2}; 4 - 0.14 x 10^{-2}; 5 - 0.6 x 10^{-3}.

of wave numbers at the beginning and end of the L_0 interval agree very well with values obtained using the Jones formula (1974) approximated for the present problem.

Chistyakov, A. I. <u>The use of depth-stable bodies</u>
<u>with towed oceanographic measurement systems.</u>
IN: Sb. Issled. okeanich. turbulentnosti, Moskva,
Izd-vo Nauka, 1973, 139-142.

A mathematical model of a filtration process is developed for
the effects of wave-induced ship motion on oceanographic measurements
made with towed systems. Filtration is accomplished most simply and
efficiently by using a passive intermediate depth-stable fish attached to the
faired towing line, as described by Ozmidov (Report no. 2 of this series,
Oct. 1974, p. 4). The filtering effect of the depth-stable fish is evaluated
in terms of three main factors: the length of towing line from the stern
to the depth-stable fish (X_1), the position of diving planes of the depth-
stable fish (X_2), and the position of the fish suspension point coordinate
on the horizontal axis in relation to the fish's center of gravity (X_3). A
factorial experiment is described to establish the effect of the cited factors
on the filtration process. The experiment was set up with the towed system
assembled from devices widely used for oceanographic studies. A hydro-
dynamic body of airplane-like design was used as the depth-stable fish. The
upper and lower limits of factor variations were: 45 and 30 m, -12 and +19
deg, and 1.2 and 1.1 m for X_1, X_2 and X_3, respectively. The angle of
deflection of the tow line varied from 18 to 30 deg. The experiment made it
possible to obtain the regression function $y = f(X_1, X_2, X_3)$, where y is the
process output. The regression coefficients b_i taken as the measure of X_n
effects on the process were calculated. The significance of b_i for a 95%
confidence coefficient was given as $b_i > 0.123$. Standard dispersion σ^2
of angular displacements of the instrument packages was evaluated by
statistical treatment of experimental data. Results of the experiment are
summarized in Table 1. The following conclusions are drawn from the
analysis of the factorial experiment.

It is concluded that a significant improvement in the motion
dynamics of oceanographic instrument packages is made possible by

Experiment No.	Factors			Output $y = 1/\sigma^2$ $1/grad^2$	Matrix row	b_i
	x_1	x_2	x_3			
1	−	−	−	0,132	$\cdot 1 \cdot$	2,06
2	+	−	−	0,188	X_1	0,216
3	−	+	−	0,350	X_2	0,375
4	+	+	−	0,286	$X_1 X_2$	0,00875
5	−	−	+	2,8	X_3	1,82
6	+	−	+	3,63	$X_1 X_3$	0,371
7	−	+	+	4,05	$X_2 X_3$	0,298
8	+	+	+	5,07	$X_1 X_2 X_3$	0,0387

Table 1. Results of factorial experiment.

the use of an intermediate depth-stable body.   The most significant factor
of filtration is X_3.   To increase the effect of filtration of interference
from tow ship motion, the suspension point of the depth-stable body must
be in the forward-most possible position.   The X_1 and X_2 factors are
mutually independent.   The X_3 factor interacts positively with either
X_1 or X_2, thus,   the higher is X_3, i. e., the more forward the suspension
point, the greater is the filtration effect from the increase in X_1 or X_2
(upward deviation of the diving planes).

Fel'zenbaum, A. I.   A method for calculation
of flow velocity, temperature and salinity fields in
the ocean.   DAN SSSR, v. 217, no. 1, 1974, 79-82.

A method is proposed for calculation of flow velocity,
temperature and salinity fields in the ocean as functions of near-surface
atmospheric processes.   The method is based on a generalization of multi-
parametric models of temperature and salinity, and integral equations of
turbulent temperature conductivity and salt diffusion for a multilayered ocean.

The multilayer ocean model consists of a stratosphere for which temperature and salinity are specified, and a troposphere in which these parameters are to be determined. The troposphere consists of a quasi-isothermic layer and seasonal and main thermoclines. The thickness of the quasi-isothermic layer is a function of horizontal coordinates and time, while the thickness of other layers are unvariable and specified. After some simplification, all calculations are done in the framework of a plane problem.

The equations derived are applicable to the ocean in general, including equatorial zones. If nonlinear accelerations were to be taken into account, however, the cited planar model would not suffice.

Mogilko, V. A., and Yu. A. Shcherbina. A new characteristic of the structure of turbulent pulsations. Tr. 18-y Nauch. konf. Mosk. fiz. -tekhn. in-t, 1972. Ser. Aeromekhanika. Protsessy upr. Dolgoprudnyy, 1973, 31-36. (RZhMekh, 4/74, #4B1039). (Translations).

A new characteristic was proposed for describing the scale of irregularities in a turbulent flow, named the S-function. This function is introduced as the distribution of probabilities of intervals between two successive zeros of the equation $c(t) = c_i$ (c_i is an arbitrary number; $c(t)$ = concentration of passive tracer, and is assumed to be a stationary random function). Apparatus is described for measuring the S-function, and results are given of measurements in a submerged axially symmetric jet. It was established that the S-function is described by a log normal distribution of probabilities within a wide range of c values.

Karabasheva, E. Z., N. G. Kozhelupova,
Yu. Z. Miropol'skiy, V. T. Paka, and B. N.
Filyushkin.   Some data on the spatial structure
of internal wave fields in the ocean.   Okeanologiya,
no. 3, 1974, 462-467.

Measurements of spatial variations in ocean temperature,
performed during the 2nd cruise of the R/V Dmitriy Mendeleyev in 1969
are described.   The experiments were conducted in a test area in the
North Atlantic along four pairs of tacks (see Fig. 1, a), using towed
thermistor chains.   Control experiments were conducted by using a
hydrological buoy with a BPV current meter and photothermograph, and a
radio buoy with an 8-thermistor chain set at depths of 40-180 m.

The area of measurements was found to be characterized by
a distinctive seasonal thermocline at depths of 30-90 m, as illustrated in
Fig. 1, b.
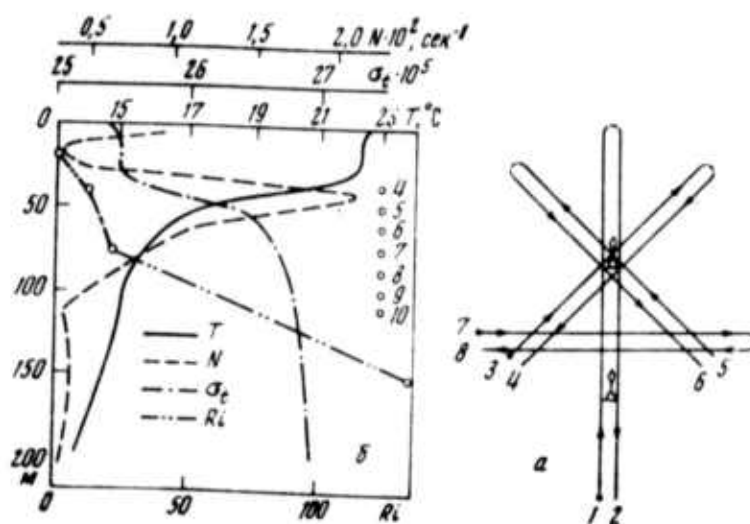
Fig. 1.   Layout of tacks (a) and vertical
distributions of temperature $T(^\circ C)$, conditional
density σ_t, Vaisalaa frequency N, and Richardson
number R_i in the test area.

One-dimensional spectra of spatial temperature pulsations
along individual tacks are shown in Fig. 2.   They follow fairly well the
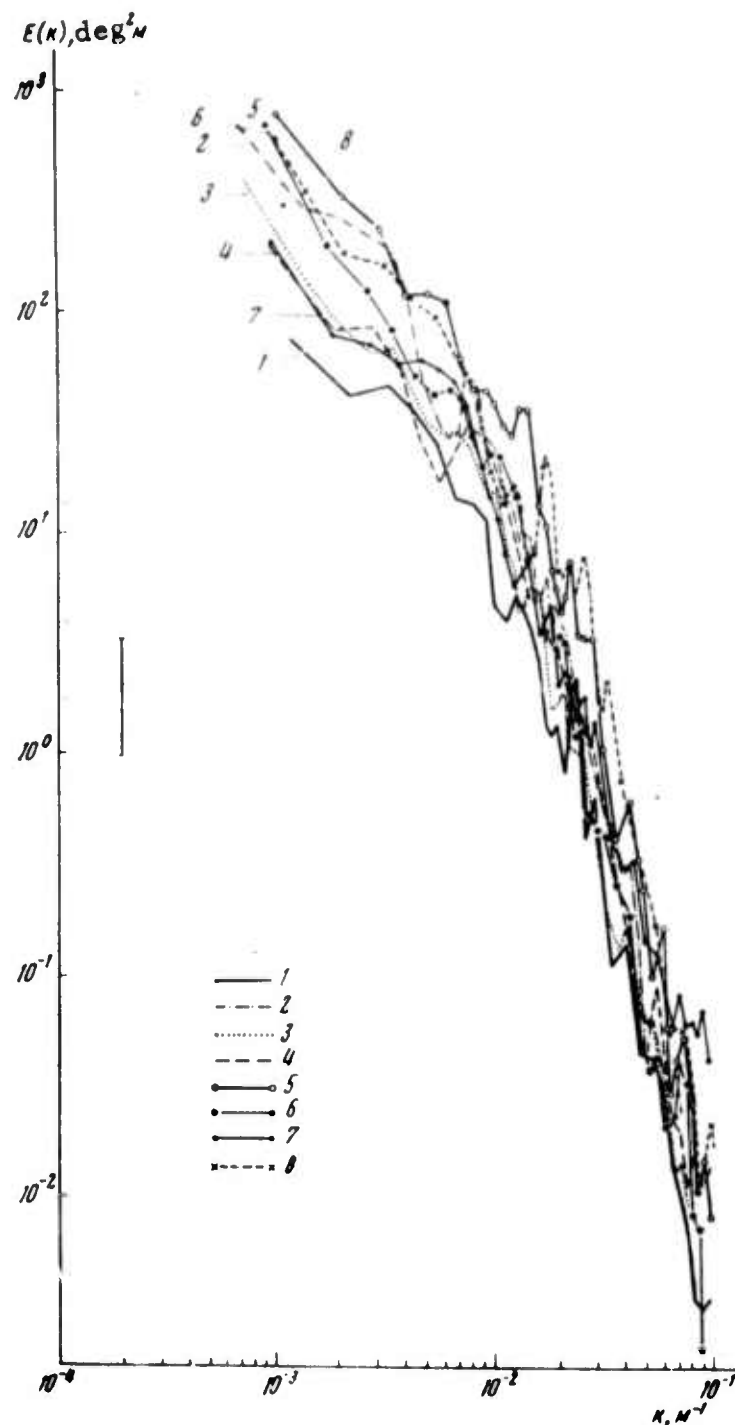
Fig. 2. Spectra of temperature pulsations
along tacks 1-8 (sensor 5).

inverse power law $S \sim k^{-n}$ where $3 \leq n \leq 4$. The results shown in Fig. 2
suggest an isotropic temperature field at $k \geq 2 \times 10^{-2}$ m^{-1}, and an anisotropic
one at $k \leq 2 \times 10^{-2}$ m^{-1}.

Two dimensional correlation functions for temperature pulsations are shown in Fig. 3. These were calculated by a method developed by Laykhtman et al., (1973) for four outgoing and return tacks with angles of $\pi/4$ between them.
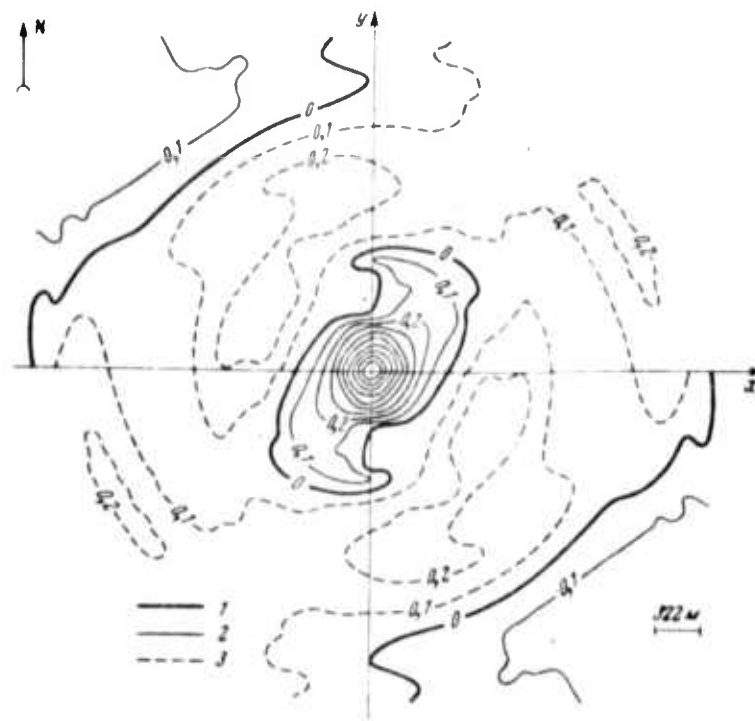
Fig. 3. Two-dimensional spatial correlation function for temperature pulsations at a depth of 60 m.

1 - zero values of correlation function; 2 - positive; 3 - negative.

As Fig. 3 shows, the internal wave field is isotropic over small intervals (~300 m) but anisotropic over large intervals. It is also somewhat directional in a NE-SW line.

Babiy, M. V., and L. V. Cherkesov. The
effect of an underwater obstacle on long wave
deformation. IN: Sb. Mor. gidrofiz. issled.,
no. 2(61), 1973, Sevastopol', 5-14. (RZhGeofiz,
1/74, no. 1V83). (Translation)

The title problem is examined in the framework of the linear
theory of long waves in a homogeneous rotating liquid of variable depth.
The Coriolis coefficient is assumed to be constant. A two dimensional
periodical flow is postulated. The free surface is described by the expression
$\zeta(x, t) = \zeta(x) \exp(-i\sigma t)$. The effect of localized variations of depth on wave
profile is analyzed for the cases of wave crest and trough at a constant
ocean depth, and for several constant-depth regions interconnected with
regions of linearly variable depth. A solution is derived for each region.
The level and speed of current at the boundaries are assumed to be
continuous. Variations in reflected and refracted wave profiles are
calculated for different depths and obstacle dimensions.

Geshev, P. I. Characteristics of the coefficient
of turbulent exchange in a viscous sublayer.
ZhPMTF, no. 2, 1974, 61-66.

Nonstationary equations are examined for longitudinal
(flow direction) pulsations in velocity and concentration within the bounds
of a viscous sublayer. Evaluations based on experimental data permit one
to neglect certain terms in these equations in the case of turbulent exchange.
In the resulting approximation expressions are obtained for coefficients of
turbulent viscosity and diffusion. The variation in behavior of these
coefficients is discussed for the case of large Schmidt (Prandtl) numbers.
The behavior of turbulent Schmidt number in the viscous sublayer is
analyzed.

Sekerzh-Zen'kovich, Ya. I. Steady state,
finite amplitude capillary gravity waves
generated by periodic pressure on the surface
of a fluid flowing over a wavy bottom. DAN SSSR,
v. 215, no. 1, 1974, 68-71.

A rigorous solution is obtained to the problem of an ideal
incompressible fluid subjected to periodic surface pressure, expressed
by an infinite trigonometric series, and acting over a periodic wavy bottom,
also expressed as a trigonometric series. The particular case is examined
in which the arc length of the bottom surface wave coincides with the length
of a developed free linear wave, corresponding to a viscous flow for the
case of a plane horizontal bottom and a constant pressure over the surface.
Some approximate solutions are discussed. This work is an extension of
an earlier paper by the author on an analogous problem, except that the
surface pressure was constant rather than periodic.

Samodurov, A. S. Internal waves in a
medium with a Vaisalaa-Brunt frequency
dependent on the horizontal coordinate.
FAiO, no. 3, 1974, 306-310.

Behavior of internal waves in an ocean region, where wave
frequency ω approaches the Vaisalaa-Brunt frequency $N(x, z)$, is analyzed
for the particular case of $N = N(x)$, where x is the horizontal coordinate in
Cartesian coordinates. The problem of determining small deviations u and w
of the waves' velocity components from the average stationary state is
reduced to solving the expression for the flow function

$$\Psi = q(x, z)e^{i\omega t}.$$

(1)

Then the deviations u and w can be determined from

$$u = \partial\varphi/\partial z, \qquad w = -\partial\varphi/\partial x$$

(2)

The function φ in (1) is determined for an infinite ocean with a linear
vertical density profile $\rho(z)$ using a Boussinesq approximation, i.e.,
assuming ρ_0 constant. Typically, the linear ρ distribution in the ocean
is maintained by a geostrophic current perpendicular to the x-z plane.

Under the cited conditions, the governing set of equations
of motion for an incompressible stratified liquid reduces to a single equation
for the function φ in the orthogonal system of coordinates r and q. These are
defined in terms of ω, N, x, z, H, and L, wher H and L are the vertical and
horizontal distances, respectively, corresponding to the maximum $(\sim 10^{-3})$
relative ρ variation in the ocean.

The main conclusion from the analysis is that the amplitude
and length of internal waves increase and decrease, respectively, toward
decreasing N(x) and, ultimately, break down in the vicinity of $N(x) = \omega$
with the resulting generation of turbulence in a stratified layer. During
measurements, local increase in amplitude of internal waves in the vicinity
of a breaking point is visualized as a wave train.

Karyakin, Yu. Ye., and V. G. Sharov. <u>A</u>
<u>finite difference method for calculating the</u>
<u>turbulent boundary layer of an incompressible</u>
<u>liquid.</u> I-FZh, no. 2, 1974, 298-304.

Numerical computation of a turbulent boundary layer is made
using an implicit finite difference method to solve the equations of the layer
motion, both in the presence and absence of injection on a streamline surface.
The equations of motion are presented in the form of a single differential
equation in Leese variables ξ and η. Two numerical grids are used for
the approximation. Both approximation methods produced finite-difference

equations of the type

$$a_i F_{i-1, j+1} + b_i F_{i, j+1} + c_i F_{i+1, j+1} = g_i, \quad i = 1, 2, \ldots, N-1. \tag{1}$$

where $F = \partial f / \partial \eta$ is the unknown grid function; a_i, b_i, c_i, and g_i are variable factors; and N is the number of nodal points across the boundary layer. Equation (1) is solved by iteration with successive calculations of f in each layer at ξ = const. A certain point $x = x_t$ was used as the starting point in computation; this point is assumed to be the transition from laminar to a developed turbulent boundary layer.

Calculations for the main region of flow are in good agreement with experimental data. The theoretical data calculated on the basis of the local similarity hypothesis are acceptable only for flows with a negative pressure gradient. In the presence of injection into boundary layer, the finite-difference method adequately describes the deformation in velocity profile, even at fairly high injection parameter values.

Pavel'yev, A. A. Development of grid turbu-
lence in a flow with a fixed velocity gradient.
MZhiG, no. 1, 1974, 38-47.

A mathematical model is developed to calculate a boundary layer flow, a pipe flow, a mixed flow, or any other turbulent shear flow. To simplify the analysis a homogeneous grid turbulence in a flow with constant velocity gradient $\partial u_1 / \partial X_2$ is assumed. Two mathematical models of such a flow are developed from the Napier-Stokes equations. One model of five partial differential equations can be used to calculate a flow at any arbitrary Reynolds number, Re; the other model of three such equations describes the flow at a large Re. The five equations of the first model give the mean fluctuating velocity components $< u_2^2 >$ and $< u_3^2 >$ along two axes, the mean Reynolds stress $< u_1 u_2 >$, the turbulent energy E, and the turbulence

length scale L. The equations for $<u_1 u_2>$, E, and L represent the second model.

Solutions for the derived equations were obtained by computer. Calculated results have compared favorably with available experimental data.

Gledzer, Ye. B. Solution of functional
equations in a theory of turbulence. MZhiG,
no. 1, 1974, 21-28.

The author analyzes equations defining turbulent flow of a viscous incompressible fluid. Small scale turbulence is described by a Guassian field of external forces with Gaussian mean value equal to zero. Using this model, a set of functional equations is solved for the characteristic functional $\Phi[z]$ of the spatial-temporal Fourier transform of turbulent velocity field, u (x, t).

Next a closed set of functional equations is derived to determine the functional $\psi_{ij}[z]$ of the true tensor ψ_{ij} of velocity field reaction to an infinitesimal external force. Both functionals $\Phi[z]$ and $\psi_{ij}[z]$ are expressed through the true spectral tensor B_{ij} of velocity field and the true tensor ψ_{ij} of the cited reaction. An approximate solution of the functional equation for $\Phi[z]$ is obtained in the form of a Gram-Charlier series in which Gaussian characteristic functional with B_{ij} is the zero approximation. A method of graphical repesentation of functions and operators is used to determine $\psi_{ij}[z]$ and $\Phi[z]$.

The approximate solution obtained indicates an upper frequency bound in large-scale fluctuations of a velocity field.

Dotsenko, S. V. Teoreticheskiye osnovy
izmereniya fizicheskikh poley okeana
(Theoretical fundamentals of measuring
physical fields of the ocean). Leningrad,
Izd-vo Gidrometeoizdat, 1974, 152 p.

The author, who publishes frequently on oceanographic
instrumentation, deals in this monograph with the theory of measurement
of various physical fields of the ocean and with the corresponding measuring
instruments. The monograph summarizes both Soviet and non-Soviet publi-
cations on theoretical aspects of some specific instruments or methods used
in hydrophysical studies. Dotsenko's original studies make up a significant
part of the published sources cited.

Chapter 1 discusses problems of hydrophysical measurements,
including classification and mathematical descriptions of the operation of
linear measuring instruments, capable of averaging in space and time.
A mathematical description is also given of the instrument range function
and multidimensional determinate and random fields.

In Chapter 2 the equation relating output signal of a moving
instrument to the magnitude of its measured field is derived and anlyzed.
Hydrophysical field measurement by vertical probing is the subject of the
third chapter. Distortions of measured characteristics, caused by the
instrument moving at a constant speed or rolling with the vessel are studied
here.

The fourth chapter concerns measurement of statistical
characteristics of isotropic or locally isotropic hydrophysical fields by
an instrument towed or drifting at a constant speed. Typical spectra of an
output signal are shown, and the concept of equivalent spectral characteristic
is introduced. Field measurement with sensors of different configurations
and different orientation with respect to direction of instrument motion is
analyzed.

In Chapter 5, distortions of the spectra caused by the vessel rolling during measurement of random field components are studied, and tolerance limits of the instrument to roll or pitch are evaluated.

The sixth chapter treats measurement of random field components, using instruments with a multielement sensor array. Spectral characteristics of such instruments are examined in relation to different methods of connecting the elements, and the effect of spectral characteristics of the elements is evaluated. A method for designing such an instrument with preselected spectral characteristics is given.

In the final chapter methods of calculating spread functions of various sensors designed for measuring physical fields are described, and directions are indicated for experimental determination of spread functions. Most study results have been reduced to directly applicable formulas. Graphs and tables applicable to all practical cases are offered because of difficult application of certain formulas.

There are 11 appendices (calculations and tables) and 93 references, about 80% of them Soviet.

Davidan, I. N., T. A. Pasechnik, and V. A. Rozhkov. Determining the components of a wave energy balance equation in a spectral form, and some results of model calculations of probability characteristics of wave conditions. Trudy GOIN, no. 122, 1974, 59-78. (RZhMekh, 10/24, no. 10B602). (Translation)

A wave energy balance equation is presented, and a discussion given on the right-hand components of this equation. Based on generalized experimental data individual component values are calculated. Some cases of a partial analytic solution to the balance equation are given, together with the algorithm for its numerical solution. Results are discussed of modelling actual wave situations.

Kononkova, G. Ye., L. V. Boborchaya, T. I. Kavasheva, T. P. Petrovskaya, K. V. Pokazeyev, and V. A. Razumov. Effect of turbulent flow on wind waves. Vod . resursy, no. 1, 1974, 179-182. (RZhGeofiz, 8/74, no. 8V70)

An experiment was performed in an aerohydrodynamic channel to evaluate the effect of turbulent flow on wave formation, specifically on its energy and spectrum. Wind range was 8.3 - 14.5 m/sec. Turbulence was generated by injecting a horizontal jet at a depth of 10 to 20 cm, with $Re = 3 \times 10^4$. The range of mean wave periods was 0.32 - 0.45 sec, mean wave height was 2.4 to 4.5 cm. Wind and turbulent jet directions were the same. Waves were registered with a wire wave gage, while turbulent flow velocity was recorded by motion pictures of floating neutral particles in the stream. Calculations are made for dispersion, autocorrelation function and wave spectrum on the water surface. The drop in wave energy caused by turbulent flow is analyzed; the degree of suppression is evaluated as a function of dispersion, both with and without turbulent flow. Energy loss occurs mainly at the high-frequency spectral ranges, and is apparently caused by energy transfer from the surface to the turbulent layer.

Shekhvatov, B. V., and E. V. Suvilov. A temperature recording current meter with a magnetic recorder. Okeanologiya, no. 5, 1973, 883-886.

The type TsITT improved self-contained recording meter for simultaneous measuring of speed and direction of currents and water temperature is described in detail. The improvements include a digital data recording system which provides direct data input to a computer with a large-capacity magnetic storage. The meter was designed at the Academy's

Shirshov Oceanographic Institute, for measurements from aboard ship, buoy stations, piers, etc.

The measured parameters are converted into variable resistances, measured by the method of ordered weighing on a bridge. The data are recorded on magnetic tape using a progressive binary code. A general view and a block-diagram (Fig. 1) of the meter show its main components. The components are enclosed in a cylindrical casing designed
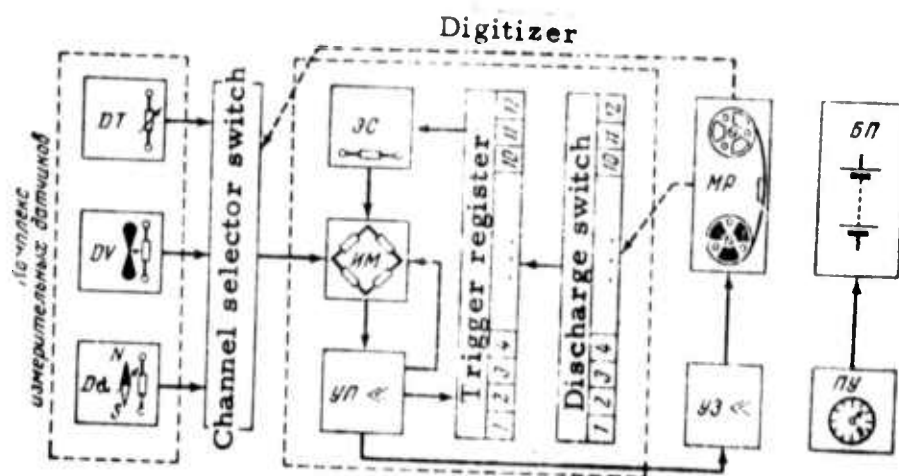
Fig. 1. Temperature and current recording meter. DT-temperature sensor; DV-current velocity sensor; Dα -current (direction) indicator; $\mathcal{K}$ -standard resistance, БП-power supply; MP-magnetic recorder; УЗ-write amplifier; ПУ -timer.

to withstand 200 atm hydrostatic pressure. All electromechanical systems are combined into a single unit which is fastened to the upper lid of the instrument. The temperature sensor, a solid-state thermistor, is mounted on the outer face of the lid. The current velocity sensor assembly and its magnetic coupling with the potentiometer are mounted on the bottom lid; this sensor rotates on a vertical axis. The current-direction indicator is a self-correcting potentiometric compass. Start-stop operation of the magnetic recorder is optimized by its synchronization with the discharge switch and tape drive mechanism of the magnetic recorder. In this way, a constant on-off time of pulse signals is assured, regardless of speed variations of the tape-drive mechanism and in the absence of stabilization

of rotational velocity. The write amplifier combines a coded pulse shaper and amplifier of the magnetic recorder output.

Specifications of the TsITT are as follows:

Current speed measurement range - 2.5 to 150 cm. sec^{-1}	
Speed measurement accuracy to 10 cm. sec^{-1}	$\pm 10\%$
Speed measurement accuracy from 10 to 150 cm. sec^{-1}	$\pm 3\%$
Direction measurement accuracy	$\pm 5^{\circ}$
Temperature measurement range	1 to 30° C
Temperature measurement accuracy	$\pm 0.02^{\circ}$ C
Duration of a three parameter measurement cycle	18 sec
Intervals between measurement cycles	5, 15, and 30 min.
Capacity of magnetic recorder	10,000 cycles
Supply voltage	12 v
Battery capacity	3 a-hr
Maximum immersion depth	1.5 km
Duration of self-contained operation	6 months
Dimensions of instrument less stabilizers -length, diam.,	840 mm 220 mm
Instrument weight in air	60 kg

Akhmedov, T. Kh., and A. I. Kvasov. Possibilities for applying laser optical methods for image analysis in the study of turbulent flows. IN: Sb. Probl. gidroenerg. i vod. kh-va. Vyp. 11, Alma-Ata, Nauka, 1974, 150-157. (RZhMekh, 8/74, #8B958) (Translation)

A discussion is given of a directional optical filtering system for two-dimensional images. The design makes it possible to separate out lines with a preselected direction from a negative which is characterized by a variable amplitude transmission coefficient. The possibility was discussed for applying this design in analysis of the velocity field of visualized turbulent flow during the diffusion of an aerated water jet in a rigid diffusion funnel.

Chistyakov, A. I. <u>Automatic control of towed</u>
<u>systems for oceanographic measurements.</u> IN:
Sb. Issled. okeanich turbulentnosti, Moskva,
Izd-vo Nauka, 1973, 143-148.

The dynamics of a towed system with an automatically
depth-stabilized towed body are analyzed by a method of experimental
programming. The purpose of the analysis was to develop a mathematical
model for automatic stabilization of the depth-stable body's longitudinal
motion. Such a model would be helpful in synthesizing a control system
for a towed system with an active depth-stable body.

The output of the automatic stabilization process is formulated
in terms of four main factors,

$$y(X_1, X_2, X_3, X_4) = \frac{1}{\sigma^2}, \tag{1}$$

where σ^2 is the standard deviation of angular displacements of the instrument
package; X_1, X_2, X_3, and X_4 are factors which represent the effects of the
signals from the sensors for trim θ and angular velocity $\dot{\theta}$ of the depth-stable
body, and the sensors for depth variations H_k and trim θ_k or angular velocity
$\dot{\theta}_k$ of the instrument package, respectively. The factorial experiment was
set up to reveal the effects of each sensor signal and the interaction between
the signals on automatic stabilization of the instrument package. The
automatic control system consisted of elements of the AP-5 and AP-61
automatic pilots.

The experimental program and the calculated regression
coefficients b_i in the regression function (1) are tabulated. Statistical analysis
shows that $|\theta b_i|$ values > 0.0156 are significant with 95% confidence level.
Using the tabulated b_i values, the regression function y is given in final
form, which describes filtration of interferences from towing vessel motion
with an active depth-stable body.

Table 1. Results of complete factorial experiment.

Experimental No.	Factors				$y = 1/\sigma^2$ $1/\text{grad}^2$	Matrix row	b_i
	$X_1(\theta)$	$X_2(\dot\theta)$	$X_3(H_к)$	$X_4(\theta_к)$			
1	−	−	−	−	0,222	«1»	0,266
2	+	−	−	−	0,229	X_1	0,0250
3	−	+	−	−	0,181	X_2	−0,00840
4	+	+	−	−	0,298	X_1X_2	−0,0436
5	−	−	+	−	0,115	X_3	0,0108
6	+	−	+	−	0,203	X_1X_3	0,0357
7	−	+	+	−	0,215	X_2X_3	0,00525
8	+	+	+	−	0,279	$X_1X_2X_3$	−0,0112
9	−	−	−	+	0,272	X_4	0,0486
10	+	−	−	+	0,351	X_1X_4	−0,00365
11	−	+	−	+	0,371	X_2X_4	−0,0340
12	+	+	−	+	0,121	$X_1X_2X_4$	−0,0545
13	−	−	+	+	0,216	X_3X_4	0,0255
14	+	−	+	+	0,590	$X_1X_3X_4$	0,0323
15	−	+	+	+	0,320	$X_2X_3X_4$	−0,0132
16	+	+	+	+	0,279	$X_1X_2X_3X_4$	0,00550

Analysis of the factorial experiment data led to the following conclusions: the factors X_1 and X_4 are positive and significant, while factors X_2 and X_3 are insignificant. But X_2 interferes negatively and X_3 interferes positively with X_1 and X_4 significant factors. Thus, allowance for signals from the sensors of θ is not appropriate, but allowance for signals of H_k of a twin instrument pod is advisable in formulation of the control law for an active depth-stable body.

In summary, the control function of automatic stabilization must include signals from sensors of θ of the depth-stable body and sensors of θ_k and H_k of one instrument package along the towing line. This conclusion can serve as the basis for designing the control system for any given towed system with an active intermediate depth-stable body.

Lyamshev, L. M., S. A. Salosina, and A. G. Shustikov. <u>Pressure pulsations in a turbulent boundary layer during discrete fluid suction.</u> Akusticheskiy zhurnal, no. 3, 1974, 435-442.

An analysis was given of correlation and spectral characteristics of wall-pressure fluctuations in a turbulent boundary layer during discrete fluid suction. The fluid suction was carried out in three ways: through a system of slots, with a porous belt, and with a perforated belt. The experiments included measurements of the average flow velocity in an uncontrolled boundary layer. Results are shown graphically.

It was established that fluid suction results in a decreased longitudinal and lateral correlation as well as power spectrum of wall-pressure fluctuations in the low frequency range. The decrease is smaller in the case of fluid suction through a system of slots, and larger in the case of suction through porous or perforated belts. However, in the high frequency range the power spectrum of wall pressure fluctuations increases during fluid suction.

Trapeznikov, Yu. A. <u>Study of two-dimensional spectral density of sea waves from records of disturbed surface at several points.</u> Trudy GOIN, no. 122, 1974, 47-58. (RZhMekh, 10/74, #10B604). (Translation)

Problems are considered in calculating the Fourier coefficients of a two-dimensional spectrum of sea waves by the Longuet-Higgins-Sveshnikov method, using records of a disturbed sea surface at several points. It is shown that the cited method can be applied for the study of time variability in the spectral structure of sea waves. The effect of sensor spatial resolution on the calculation of spatial derivatives of a disturbed sea surface is evaluated.

Leonov, A. I., and Yu. Z. Miropol'skiy.
Nonlinear internal gravity waves in a steady-
state mode. Okeanologiya, no. 3, 1974, 575-
576. (Translation)

This paper undertakes a study of finite-amplitude internal
gravity waves in a steady-state mode, i.e., those waves for which the flux
function and all other characteristics have the form $\psi(t, x, z) = \psi(\theta, z)$
where $\theta = x-vt$, θ = phase and v = phase velocity. As is generally known,
complete hydrodynamic equations for two-dimensional steady-state waves
in a stratified fluid account for the first two integrals, and as a result an
equation containing two undetermined arbitrary functions is obtained for the
flux function. The presence of two undetermined arbitrary functions
complicates the problem considerably. Since the vertical profile of undisturbed
Vaisalaa-Brunt frequencies $N(z)$ can be measured, it is reasonable to use it
in calculations of internal waves, both in the atmosphere and the ocean.
Therefore it is of interest to express the unknown arbitrary functions through
$N(z)$. Determination of N from the solution with an arbitrary function leads
to a complex or unsolvable inverse problem.

The authors of this paper show that, with certain assumptions,
the undetermined arbitrary functions can be expressed through $N(x)$. Thus
they obtained the following equation describing propagation of nonlinear
steady-state internal waves in a fluid at rest:

$$\Delta\Psi + \left\{ \frac{\Psi}{v^2} + \frac{1}{2\omega g}\left[\left(\frac{\partial\Psi}{\partial\theta}\right)^2 + \left(\frac{\partial\Psi}{\partial z} - v\right)^2 - v^2 \right]\right\} N^2\left(z - \frac{\Psi}{v}\right) = 0. \tag{1}$$

here $\Delta = \left\{ \frac{\partial^2}{\partial\theta^2} : \frac{\partial^2}{\partial z^2}\right\}$ and g is acceleration of gravity. This equation does
not contain the unknown arbitrary functions since $N^2(z)$ and $N^2(z-\psi/v)$ are
predetermined.

Asymptotic solutions of equation (1) are considered for the
following cases: propagation of internal waves in a shallow-water basin in
the presence of weak nonlinearity and dispersion; propagation of internal
waves in a narrow pycnocline; and propagation of short internal waves
(wave length L much smaller than fluid depth H).

At $\epsilon = H/L$, solution of equation (1) is obtained in the form
of an asymptotic expansion in terms of ϵ by a method analogous to the
Poincare method in the theory of nonlinear oscillations. It is shown that
equation (1) allows solutions for both periodical and solitary waves. Frequency,
wave number and amplitude of periodical waves are connected by a nonlinear
dispersion relation. A calculation of wave parameters for $N(z)$ in the ocean
shows that both positive and negative solitary waves can exist. In addition,
the possibility of using the Boussinesque approximation was analyzed. It
was established that in certain cases the use of this approximation results
in some errors.

At $\epsilon = \delta/L \ll p$, where δ is pycnocline depth, the solution of
equation (1) was obtained in the form of an expansion in terms of ϵ, which
is valid within the pycnocline. It was combined with the solution for a
nonstratified fluid, which is valid outside the pycnocline. The problem was
reduced to solving a nonlinear boundary-value problem for the Laplace
equations. This problem also allows for solutions both for nonlinear
periodical and solitary waves. However, in contrast to the case of a shallow-
water basin, the dispersion relation does not exist in an ordinary sense,
and wave velocity is arbitrary. A sample calculation (for N^2 = const) shows
that both positive and negative solitary waves can exist in a narrow pycnocline.

At $\epsilon = L/H \ll 1$, solution of equation (1) was found by an
asymptotic method and the problem was reduced to a system of equations in
terms of the first-order partial derivatives of wave amplitude and vector
slowly changing in space. This system was analyzed by the method of

characteristics. A number of conservation laws relating to the characteristics were obtained, and an amplitude increase at the resultant caustics was noticed.

In conclusion the authors discuss numerous unsolved problems, and point out the importance of studying the stability of the obtained solutions in order to understand turbulence generation in a steady-state stratified fluid.

Shelkovnikov, N. K. Techniques for studying the structure of turbulent flows. VMU, no. 2, 1974, 205-209.

A simplified method is proposed for studying the structure of turbulent flows using data on velocity or temperature pulsations measured simultaneously at several spaced points. An example is given for calculation of propagation rate and scale of turbulent inhomogeneities from measurements of velocity pulsations in the main flow direction at two points.

Assuming that velocity or temperature pulsations are stationary in time, the author analyzes the turbulence structure using the space-time correlation function

$$R_{ij}^{(k)}(x_1, x_2, x_3, \tau) = \frac{\overline{(u_i')_A (u_j')_B}}{\sqrt{\overline{u_i'^2}} \sqrt{\overline{u_j'^2}}}. \tag{1}$$

where x_1, x_2, x_3 are spacings between points in the longitudinal, lateral, and vertical directions respectively. Longitudinal integral scales of turbulence in this case are

$$L_{ij}^{(1)} = v \int_{-\infty}^{+\infty} R_{ij}(x_1, 0, 0, \tau) d\tau, \tag{2}$$

where v is the variation rate of the space-time correlation function.

For the correlation function assumed, the longitudinal integral scales of turbulence are given by

$$L_{ij}^{(1)} = v \int_0^\tau R_{ii}(x_1, 0, 0, \tau)\, d\tau,$$
(3)

or using the mean-value theorem, by

$$L_{ij}^{(1)} = v\tau_o h,$$
(4)

where h is some mean value of R_{ij}. The variation rate of space-time correlation function is then $v = x_1/\tau$.

The scale of turbulent inhomogeneities at the zero correlation level hence is $\ell_o = v\tau_o$, and at the 0.5 correlation level, $\ell = v\tau_{0.5}$. Form anisotropy of turbulent inhomogeneities is given by $\ell_1 = \ell_1/\ell_2$, $\ell_2 = \ell_1/\ell_3$, $\ell_3 = \ell_2/\ell_3$, where ℓ_1, ℓ_2 and ℓ_3 are turbulence scales in three mutually perpendicular directions.

The cited calculations show that the turbulence propagation rate is equal to the average flow velocity, and that the turbulence scale decreases with time.

Nozdrin, Yu. V. Effect of buoyancy force on spectra of turbulent processes in the ocean. Okeanologiya, no. 5, 1974, 797-801.

The author analyzes the behavior of the three-dimensional energy spectrum of kinetic energy of a turbulent upper ocean layer. Theory predicts that in spectra of temperature and salinity fluctuations there will be an inertial-convective interval where energy E relates to wave number k by $E(k) \sim k^{-5/3}$ and a viscous-convective interval where $E(k) \sim k^{-1}$. However, experimental results have shown some disagreement with these relationships, and it is suggested that this is attributable to buoyancy forces

on volumes of water having a local density difference.

Nozdrin accordingly analyzes small-scale turbulence with effects of buoyancy and thermal diffusion taken into account, and establishes the conditions for which one would indeed expect a deviation from the "5/3" curve.

Navrotskiy, V. V. Amplitude structure of velocity and temperature fluctuations in the upper oceanic layer. FAiO, no. 7, 1974, 771-781.

An analysis is given of probability distribution functions for medium-scale fluctuations of current velocity and temperature in the upper oceanic layer. The results were compared to theoretical probability distributions. The following model turbulence processes were considered:

$$y(t) = a \sin (\omega t + \alpha) \tag{1};$$

$$y(t) = a \sin (\omega t + \alpha) + x_N(t). \tag{2}$$

where $x_N(t)$ has a distribution close to normal; and

$$y(t) = f(t) x(t). \tag{3}$$

where $f(t)$ is a deterministic periodical function, $x(t)$ is a random stationary function.
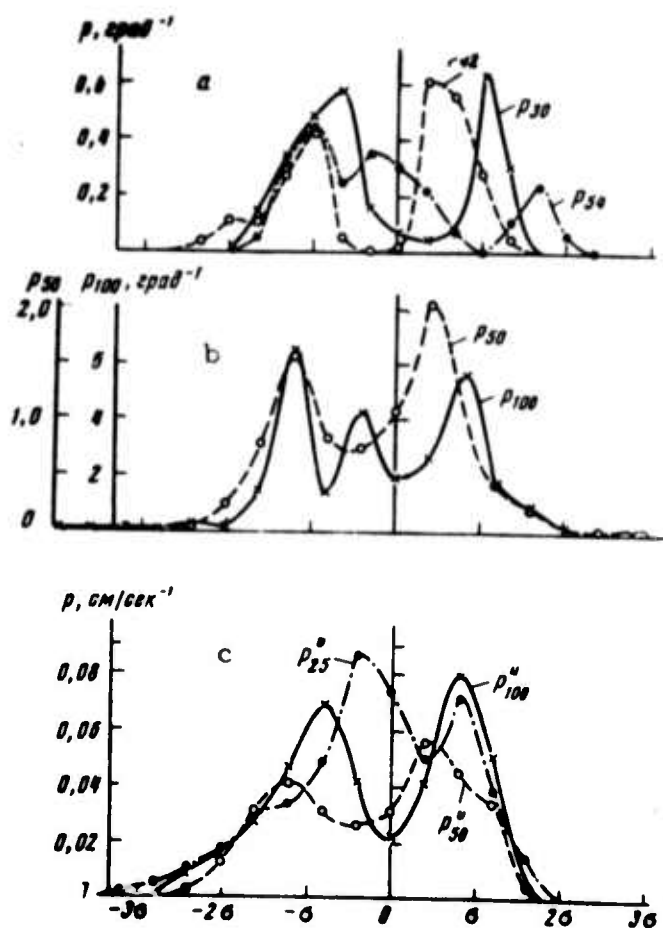
The results are shown in Figs. 1-6.

Fig. 1. Density of probability distribution for
spatial (a) and time (b) temperature fluctuations,
and spatial current velocity fluctuations (c) (3rd
cruise of the R/V Academician Kurchatov). Mean
values at different depths are:

a - T_{30} = 25.5, σ_{30} = 0.32; T_{42} = 22.8, σ_{42} = 0.63;
T_{54} = 19.8, σ_{54} = 0.52.

b - T_{50} = 18.2, σ_{50} = 0.27; T_{100} = 15.9, σ_{100} = 0.10.

c - $\bar{v}_{25}$ = -9, σ_{25} = 5.2; $\bar{v}_{50}$ = -15.4, σ_{50} = 7.9;
$\bar{u}_{100}$ = -17.8, σ_{100} = 6.1.
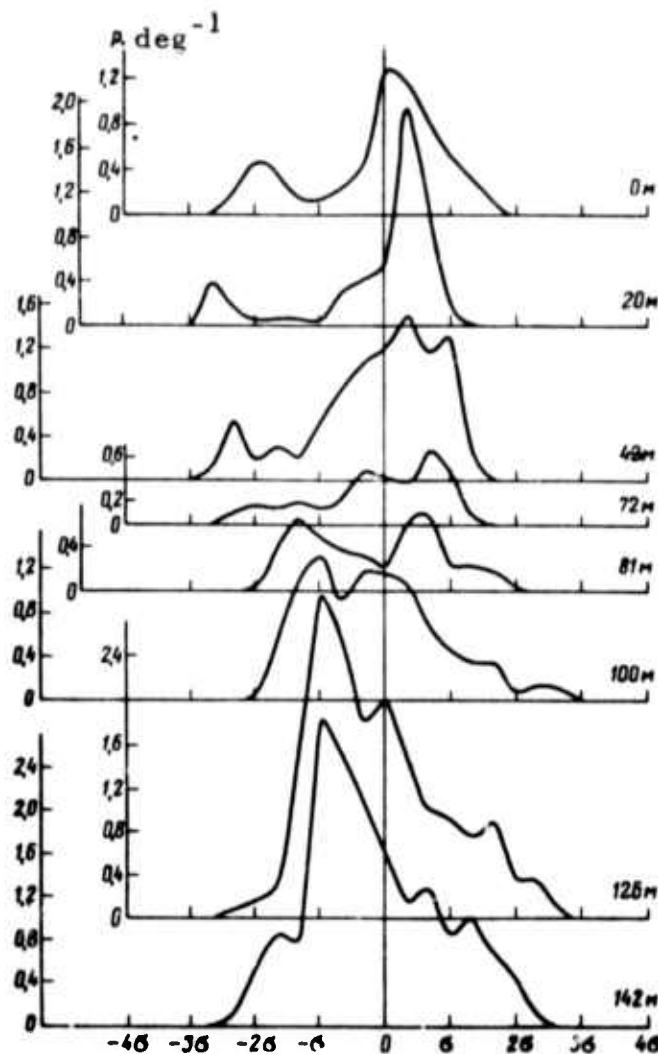
Fig. 2.   Density of probability distribution
for temperature fluctuations at different
depths (16 May 1968, 3 rd cruise). Vertical
distributions of the mean and rms values are
shown in Fig. 3.
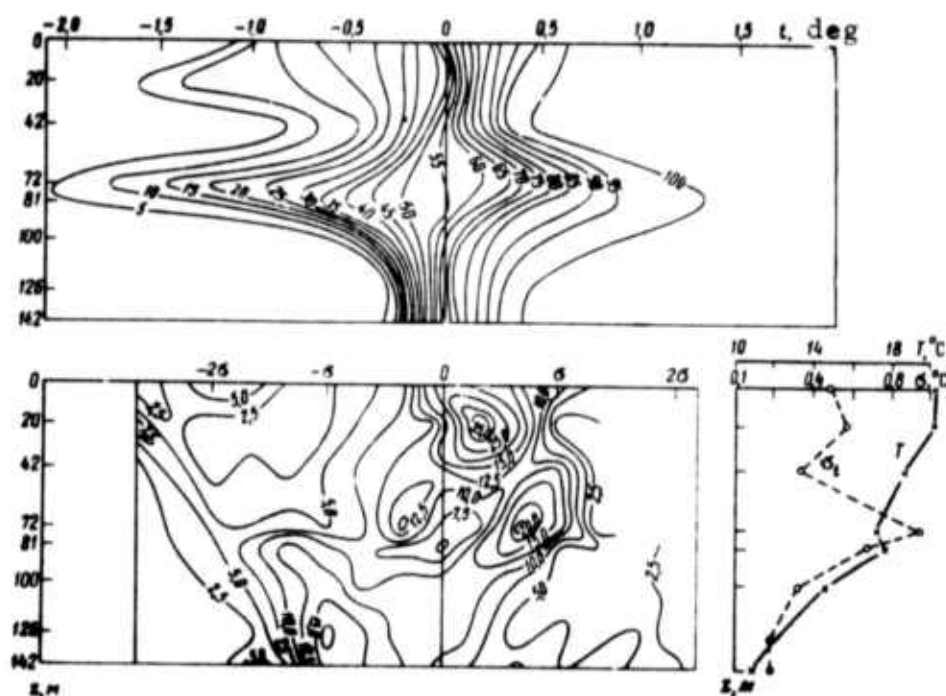
Fig. 3. Cross-section of probability distribution (above) and hit probability (below) for spatial temperature fluctuations (16 May, 1968, 3rd cruise).
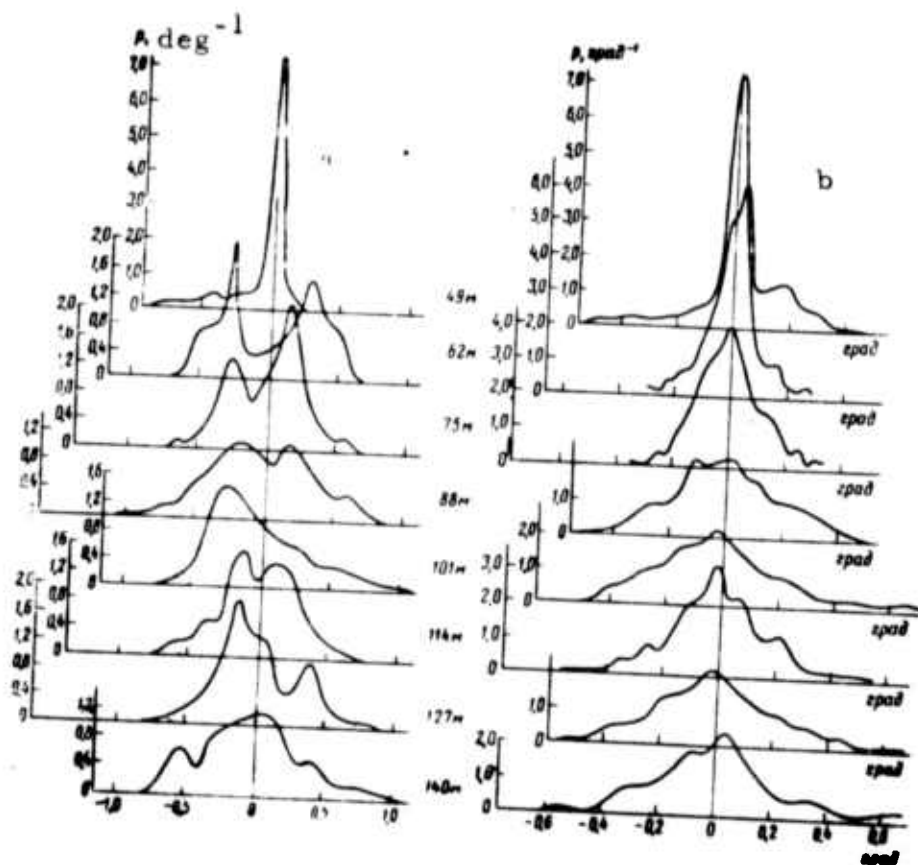
Fig. 4. Density of probability distribution for spatial temperature fluctuations before (a) and after (b) filtering (cruise 8, line 1).

Fig. 5. Vertical distribution of probability for spatial temperature fluctuations before (a) and after (b) filtering (cruise 8, lines 1 and 9). Vertical distributions of the mean temperature $T(z)$, the temperature difference between adjacent horizons $\Delta T(z)$, and rms fluctuations before and after filtering $\sigma_t(2)$ and $\sigma_t'(2)$ are shown on the right-hand side of the figure.
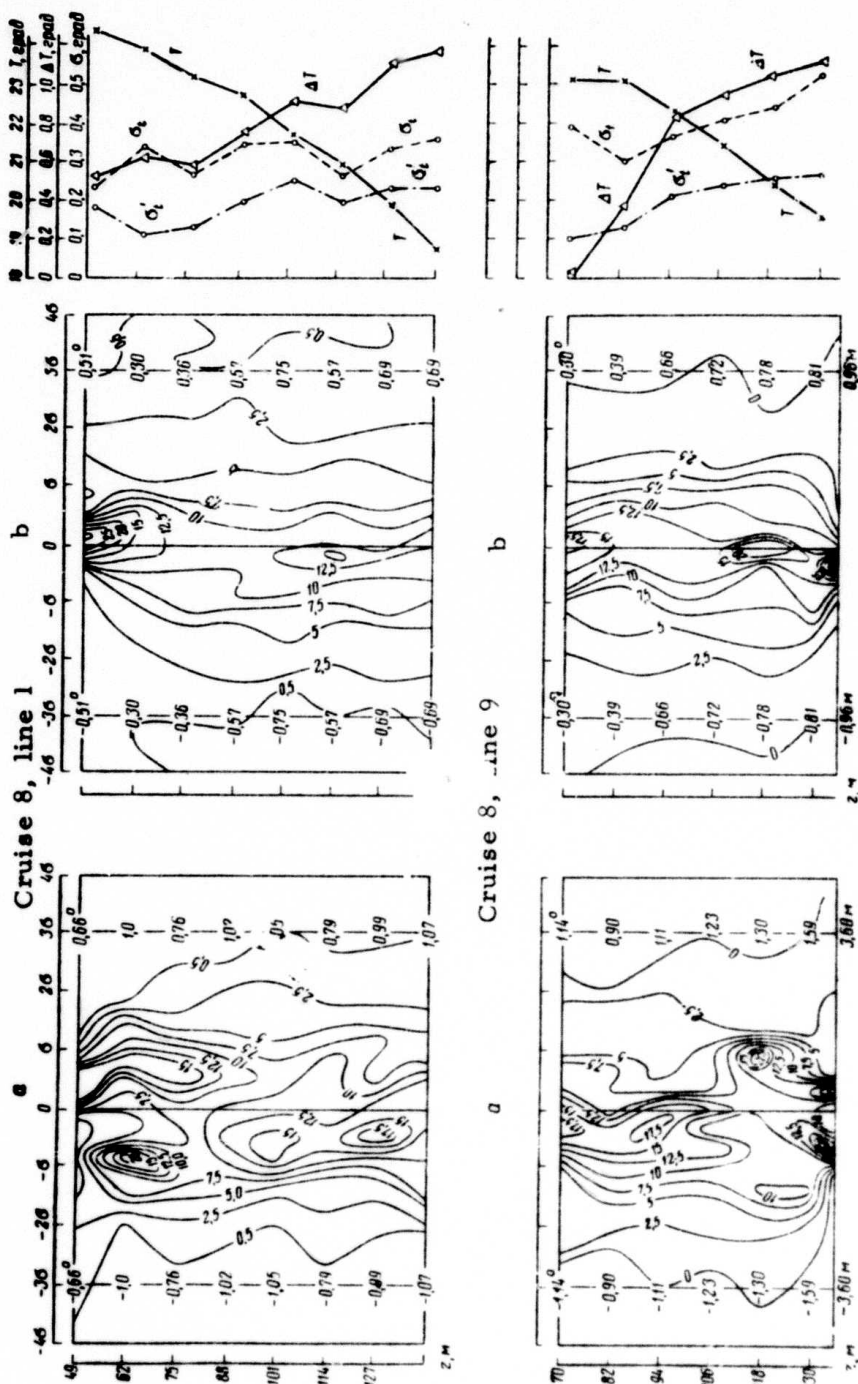
Fig. 6. Vertical distribution of probability for time velocity fluctuations before (a) and after (b) filtering (Buoy station C in upper graphs; buoy station D in lower graphs).

The probability distributions shown in Fig. 1 indicate the presence of wave oscillations in the temperature fluctuations. If side maxima are associated with internal waves, then the amplitudes of the internal waves are evaluated to be: 2 and 5m at depths of 50 and 100 m respectively in the case of time temperature fluctuations; and 3.5, 5, and 10 m at depths of 30, 42, and 54 re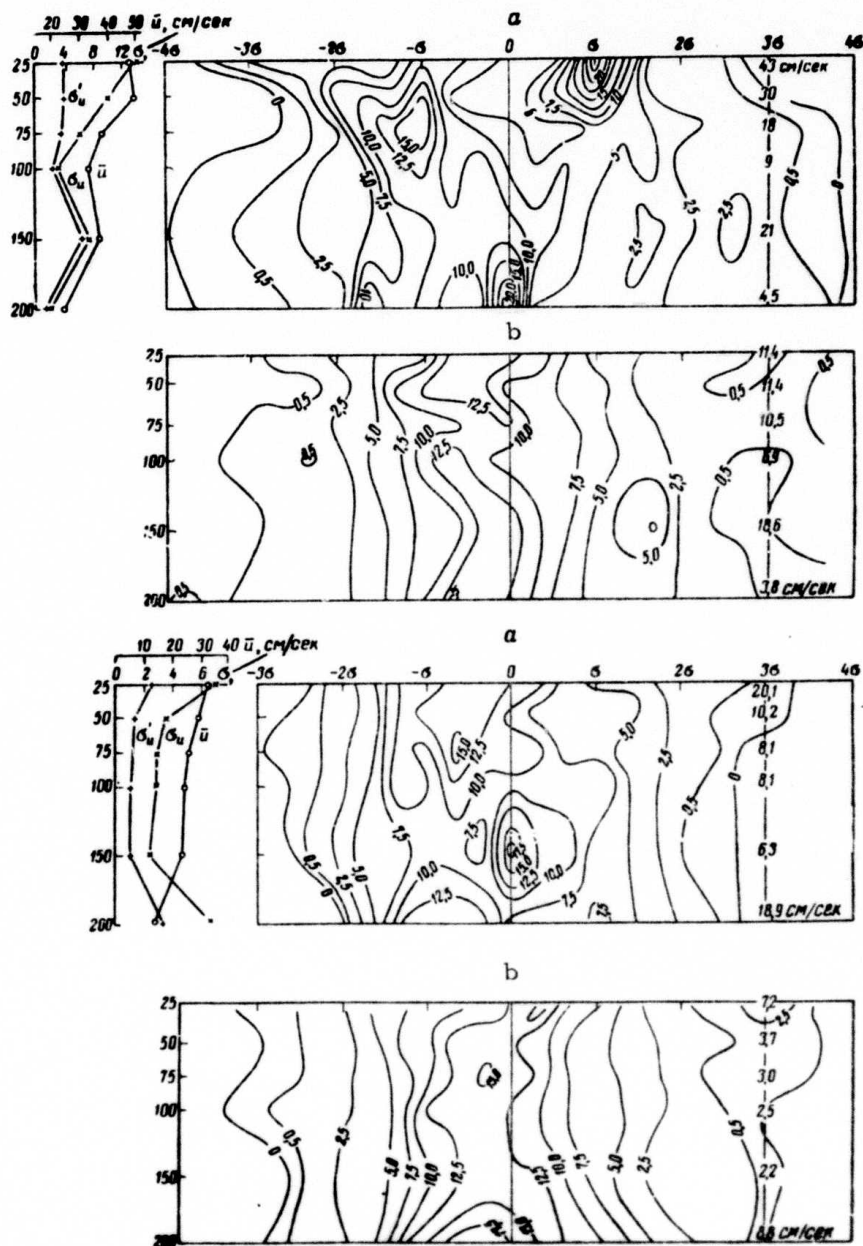spectively in the case of spatial temperature fluctuation. It was pointed out that instability in the phase and amplitude of the sinusoidal process can result in a quasinormal distribution. A possible distortion of probability distribution caused by deviation of wave motion from sinusoidal oscillations is illustrated in Fig. 2. The observed asymmetry of probability distribution and change of its sign with depth is explained on the basis of the theory which takes into account nonlinear effects for high-amplitude waves.

In many cases, experimental data can be approximated by model (3). As can be seen in Fig. 4, probability density peaks sharply at zero values of σ. An analysis shows that this is caused both by small-scale turbulence and by decrease of the mean temperature gradient. A comparison of experimental and theoretical data shows the following: 1. Probability distribution for velocity fluctuations, including large-scale ones, approaches a Gaussian or Rayleigh distribution only in the uppermost layer (25 m). After filtering out fluctuations exceeding 11 hours, the probability distribution approaches Gaussian or Rayleigh at greater depths. 2. The measured probability distribution of spatial and time temperature fluctuations on a medium scale do not compare favorably with theoretical values.

Rudenko, O. V., L. I. Soluyan, and R. V. Khokhlov. Problems in the theory of nonlinear acoustics. Akusticheskiy zhurnal, no. 3, 1974, 449-457.

This is a short comprehensive review of theoretical studies on nonlinear acoustics. The published data of Soviet and Western authors

are treated in an attempt to derive a unified approach to the problem, as well as to identify insufficiently covered areas and to stimulate further studies in these areas.

The unified system of phenomena classification is based on a set of three dimensionless numbers Γ, D, and N which are used to compare relative effects of dissipation, dispersion, and diffraction, respectively, on distortion of an acoustic wave profile in a nonlinear medium. This distortion is described completely by the numbers $\Gamma^{-1} = 2\epsilon$ Re, $D = m/2\epsilon M$, and $N = (\lambda/a)^2/2\pi^2\epsilon M$, where Re and M are the Reynolds and Mach numbers; $m = c_\infty^2 - c_o^2$, C_∞ and C_o are high and low-frequency sound velocities, λ is the wavelength in the medium, $\epsilon = (\gamma + 1)/2$, γ is the adiabatic exponent, and $\underline{a}$ is the acoustic beam radius.

Using the cited numbers the authors describe propagation of plane, spherical, and cylindrical acoustic waves separately in dissipative ($D = N = 0$, $\Gamma \neq 0$); relaxing ($\Gamma = N = 0$, $D \neq 0$); and diffractive ($\Gamma = D = 0$, $N \neq 0$) media. The theory of nonlinear deformation of wave spectra is reviewed in the presence of wave interaction of different types. Mathematical expressions for finite-amplitude wave propagation are presented in second and third order. f approximation. A description of acoustic wind is given in terms of nonlinear acoustics and hydrodynamics.

It is emphasized that the method of approximation of a slowly-changing acoustic wave profile, which is used in most of the studies reviewed, is a powerful tool for analyzing various problems of nonlinear acoustics. All Soviet studies discussed (80% of the total number) were made at Moscow State University.

Maderich, V. S. Vertical structure of the
main oceanic thermocline. Meteorologiya i
gidrologiya, no. 10, 1974, 67-74.

The effect of vertical intermixing in a baroclinic ocean
on formation of the main oceanic thermocline is analyzed, on the assumption
that vertical diffusion is small in relation to vertical and horizontal advection.
A stationary ocean model is considered, having remote horizontal boundaries,
and outside the Ekman layer.

In the first approximation, vertical motion, continuity, and
density transport are described by a single equation for the baroclinic
correction function $M(x, y, z)$, where x, y, and z are the coordinates oriented
eastward, northward, and downward respectively. This approach treats the
main thermocline as a baroclinic boundary layer at the ocean surface, with
an underlying nearly barotropic abyssal region. Three particular solutions
to the equation for M are obtained using the method of asymptotic expansion
and assuming the parameter $\epsilon = \chi/W_0 H_*$ to be small; $\chi = 1 \text{ cm}^2/\text{sec}$ is the
coefficient of vertical diffusion, and W_0 and H_* are characteristic scales of the
vertical velocity W and the depth z of the main thermocline, respectively.
The solutions take into account the particular solution of Welander (Tellus,
v. 11, no. 3, 1959, 309) for $M_0(x, y, z)$ in the diffusion boundary layer within
the main thermocline.

Solutions for M_0 are thus derived and the density anomaly
$\delta = \rho - \rho_0$, where ρ_0 is the density of a homogeneous liquid, is formulated
for three cases: $\epsilon^{1/2} < \omega \leq 1$ (I), $\omega \leq \epsilon^{1/2}$ (II), and $\omega \leq \epsilon$ (III), where
$\omega = W_{oe}/W_0$ is the amplitude of vertical Ekman velocity. The formulas
for δ show a significant dependence of the vertical density gradient on
magnitude and direction of w_e and density flux q at the lower boundary of the
Ekman layer.

The anomaly δ has two components: advective and diffusional. Particular solutions are discussed with respect to variations of q, magnitude and direction of w_e. The cases are examined when condition I exists in the center of oceanic cyclonic ($w_e < 0$) or anticyclonic circulations while conditions II or III are realized at the periphery of the oceanic circulations.

A graphical comparison between theoretical δ data and the vertical density profiles observed in the Pacific Ocean (Fig. 1) demonstrates a qualitative agreement between two sets of data, e.g., between the curves (25) and (13) or (36) and (88) of Fig. 1.
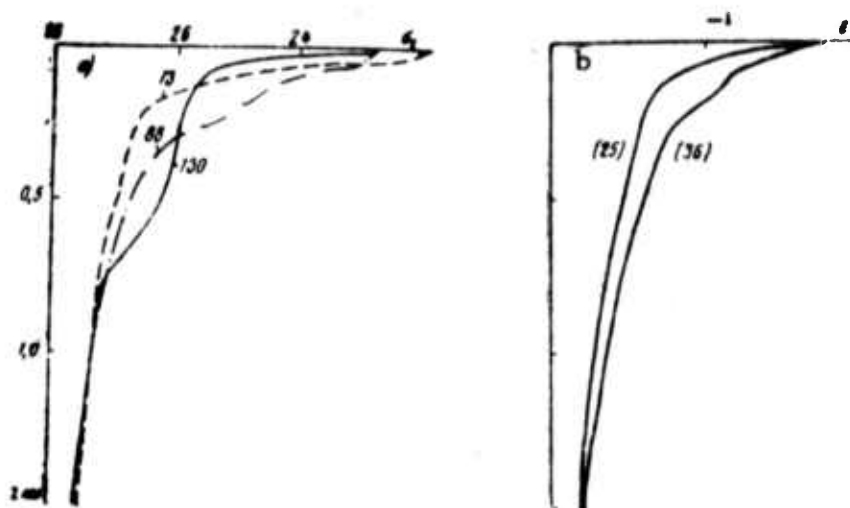
Fig. 1a. Vertical profiles of relative density in square areas 13 (in October, in the center of tropical cyclone), 88 (in September, at the periphery of anticyclone), and 130 (in July, in the center of anticyclone); b- density anomaly calculated for cases I (25) and III (36).

In summary the cited theoretical model indicates that an advective thermocline with a surface diffusion layer can exist, at least in a limited range of w_e and q.

Burtsev, G. A. <u>On a theory for the magnetic field of ocean waves</u>. GiA, no. 2, 1974, 345-349.

Burtsev, G. A. <u>Theory of the magnetic field of sea waves in a finite-depth sea</u>. GiA, no. 3, 1974, 516-521.

Wave motion of seawater in the geomagnetic field generates internal currents, with associated secondary magnetic fields. A rigorous theory for the field induced by small waves in an unbounded ocean was developed by Weaver (J. Geophys. Res, 70, 1965, 1921). The present work applies this solution over a wide range of frequencies, introduces similarity criteria for wave-generated magnetic fields, and gives a comparison of rigorous and approximate solutions of the formulas.

Results show that even for a simplified model, the wave magnetic field has a very complex nature. For the more realistic case of statistically nonuniform wind waves over a rough bottom at some finite depth, the problem is further complicated. It is concluded that more rigorous solutions are needed for cases of realistic ocean parameters.

In Burtsev's second cited paper, the foregoing analysis is extended to the more practical case of a finite-depth sea. Following Weaver's theory, a set of four linear differential equations is derived from Maxwell's equations to completely define the vertical component h_z of magnetic field strength in the sea, air, and sea bottom. The cited set of equations is solved for h_z by known methods, taking into account the conditions at the air-sea and sea-bottom interfaces. The bottom effect as a function of magnetic field frequency is evaluated.

The solution was used to evaluate the applicability of some earlier approximate solutions to the problem. The author concludes that his method can also be used to calculate the magnetic field from sea surface turbulence with very long periods, such as swells or tides.

Savin, M. T. <u>Oscillations at the Vaisalaa</u>
<u>frequency in the field of a geostrophical current.</u>
Meteorologiya i gidrologiya, no. 5, 1974, 94-97.

Oscillations of a water particle in a continuously stratified
ocean in the presence of a geostrophical current are analyzed theoretically,
on the assumption of horizontal gradients of density and pressure and
oscillations normal to an isobaric surface. Such an assumption is reasonable
for a real ocean; presumably the isobaric surfaces P = const are randomly oriented.

An elemental volume dxdydz in a static equilibrium is
subjected to the force of gravity $g \rho$ dxdydz and the resulting pressure
$g \rho$ dxdydz $1/n$, where ρ is density and $n = \cos \theta$, where θ is the angle between
the normal to an isobaric surface and the Z axis. The resultant of these
two forces must be in equilibrium with the Coriolis force. Thus a particle
in a state of static equilibrium moves horizontally at a constant geostrophic
speed which is defined by its projections u_0 and v_0 on the x and y axes,
respectively. In an intermediate position (x, y, z), the elemental volume
is subjected to the same force of gravity and the resulting pressure
$$g \left(\rho + \frac{\partial \rho}{\partial x} x + \frac{\partial \rho}{\partial y} y + \frac{\partial \rho}{\partial z} z \right)$$

Motion of the elemental volume subjected to the cited forces
is described by a set of three second-order partial differential equations,
taking into account static equilibrium conditions. This set of equations is
reduced to a known equation which describes the motion of a particle in a
calm stratified ocean in which ρ and pressure horizontal gradients are
absent. In the particular case of isobars inclined in the x-z plane only, at
an angle θ with the horizontal plane, the set of three equations of motion
is reduced to

$$\frac{d^2 x}{dt^2} + M^2 l x = - N^2 l z,$$

$$\frac{d^2 z}{dt^2} + N^2 n z = - M^2 n x,$$

(1)

where $N^2 = \frac{g}{\rho}\frac{\partial \rho}{\partial z}$, N is the Vaisalaa frequency, $M^2 = \frac{g}{\rho}\frac{\partial \rho}{\partial x}$, $n = \cos\theta$, $l = \sin\theta$. Equations (1) are solved for the coordinates x and z of an oscillating particle, allowing for the fact that $tg\theta = \lambda/gV_0$, where λ is the Coriolis parameter. The author concludes that in a real ocean, where isobaric surfaces are not horizontal and geostrophic currents are present, particle oscillations have a horizontal component whose amplitude is 10^{-5} to 10^{-6} that of the vertical component. The oscillation frequency with allowance for isobars inclination is given by the approximate formula

$$ \Pi = \sqrt{N^2 + \frac{\lambda}{\rho} v_0 \frac{\partial \rho}{\partial x}}, \tag{2}$$

different from the known formula of N insofar as Π is a function of geostrophic current speed and the horizontal ρ gradient in addition to the vertical ρ gradient. In most cases, the addend with v_0 is small ($\sim 10^{-12}$)

In the case of the fine structure of internal waves e. g., their stability, it may hence be necessary to take into account the frequency variations due to horizontal components of particle oscillations in the fields of a geostrophic current.

Trofimov, I. L. Effect of spatial inhomogeneities of the magnetotelluric field on its vertical distribution in the sea. GiA, no. 3, 1974, 560-563.

A theoretical solution to the title problem is obtained, using a horizontal layer model of geoelectric cross-section and an arbitrary electromagnetic field source. Horizontal (e_2, e_1, h_2, h_1) and vertical h_{z2}, h_{z1}) components of the complex electric $\underline{e}$ and magnetic $\underline{h}$ vectors at the levels z_2 and $z_1 < z_2$ within the nth layer are intercorrelated, assuming that e and h in each layer obey the Helmholz equation for electromagnetic waves. Then approximate correlations between the components E_2, E_1, H_2, H_1 and H_{z2}, H_{z1} of the integral complex vectors E(x, y, z) and H (x, y, z) are derived for variations of magnetotelluric fields with periods of up to 30 min. or more.

It follows from analysis of the approximate correlations and evaluation of the spectral impedance $Z^* = e_x/h_y = e_y/h_x$ of the sea geoelectric cross-section, that vertical distribution of the horizontal components of the magnetotelluric field in a seawater layer is nearly independent of the field spatial inhomogeneity, and practically coincides with their distribution in the case of a plane wave. Also it follows that variations of the vertical component of magnetic field are identical with the variations of electric field in a vertical direction. Consequently, at e-m wavelengths $\lambda > 10\ d$, where d is the depth of the first layer, the vertical component of magnetic field practically does not vary. Measurement of the $(E_2 - E_1)$ and $(H_2 - H_1)$ differences between the horizontal components of E and H may be used as an indirect method of measuring E and H, respectively. In practice, a magnetometer which measures the modulus of the integral magnetic field vector T can be used for a gradient magnetic sounding. The T variations are given by

$$\delta T(t) = \cos I \delta T_H(t) + \sin I \delta T_z(t), \tag{1}$$

where $\delta T_H(t)$ and $\delta T_z(t)$ are the variations of horizontal and vertical components of T and I is the magnetic inclination. Limitations of the proposed sounding method result from its theoretical base, i. e., the horizontally homogeneous geoelectric cross-section model. This model, however, is applicable to significant surface areas of the global ocean. Advantages of sounding with a component magnetometer are listed as follows: 1) the same apparatus measures E and H, 2) the absence of spatially oriented parts, and 3) potential for a very precise determination of impedance since present magnetometers have resolutions down to a fraction of a γ.

Anuchin, V. N., A. M. Gusev, and Yu. G.
Pyrkin. The turbulent structure of bottom
density currents. Meteorolog. i gidr., no. 2,
1974, 85-88.

A theoretical interpretation is given of the flow characteristics
of stable bottom currents in the ocean. This interpretation is based on the
fact, confirmed by numerous experimental studies, that there is an
inflection in the vertical profiles of current velocity and fluid density ρ at the
fluid interface in the mixing zone. It follows that $d\rho/dz$, hence stability E
of a water mass, attain their maximum values in that zone, while the
turbulence transfer coefficient

$$k = \frac{k_0}{1 + cE}.$$
(1)

where c is the impurity concentration, is at its minimum.

The vertical diffusion profile is evaluated from the equation

$$\lambda \frac{\overline{\partial c}}{\partial z} - \overline{w'c'} = A,$$
(2)

where λ is the coefficient of molecular diffusion, w' is the current velocity
component, and A is an integration constant. Equation (2) is derived for a
stationary two-dimensional current, on the assumption that $\partial c/\partial x$ is
negligible. The effects of molecular viscosity and λ can be neglected in the
central zone with a developed turbulent flow, but not in the mixing zone, where
the coefficient of eddy diffusion is minimum.

The current velocity gradient and turbulent stress exhibit
maxima in the region of the profile inflection, as confirmed by several
experimental studies. The presence of the maximum turbulent stress in the
mixing zone allows us to draw an analogy between the processes at the
interface of two fluids of different density and fluids at a wall.

Published experimental data on turbulent stresses at the fluid interface and near the bottom lead to the conclusion that viscosity exerts a strong influence at the interface of two fluids of different density. The experimental data of Barr plus those of the authors are cited to support the conclusion that the bottom density currents can be considered as nearly plane-parallel, with different turbulent stresses at the boundaries. The strong effect of viscosity must be taken into account at the bottom boundary and at the fluid interface. Propagation of bottom currents over great distances from their origin is explained by the minimum turbulent diffusion across the interface.

All the cited data point to the dual nature of the bottom density currents; i. e. laminar or turbulent, depending on whether analysis is made on a large or a small scale.

Kuznetsov, O. A., and G. N. Panin. Effect of a surface oil film on turbulence in the near-water atmospheric layer. Meteorologiya i gidrologiya, no. 5, 1974, 97-99.

An experimental study of sea-atmosphere interaction was carried out in 1971 in the Caspian Sea from an offshore platform over a sea surface area partly covered with an oil film. The urgency of the study is emphasized in view of increasing oil exploration in sea shelf regions, the colossal volume of oil transported in big tankers and the inevitable risk of oil pollution.

During the cited study fluctuations of vertical wind velocity component and atmospheric moisture content were measured, and integral moisture flow was determined. The measuring instruments were an acoustic anemometer and a spectrally selective hygrometer operating in the u-v range.

The data are compared with the measurements under similar wind and sea conditions in the absence of oil film.

The comparative wind velocity data (Fig. 1) show the wave
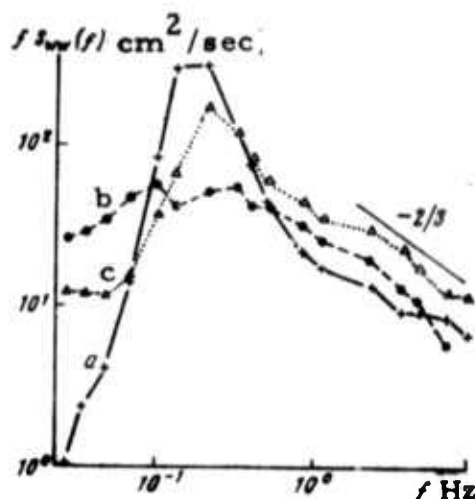

Fig. 1. Wind velocity vertical component spectra $fS_{WW}(f)$ measured above the surface covered by oil film at 2.45 m (a) and 11.0 m (b) altitudes, and above oil free surface at 2.45 m (c) altitude during decaying sea roughness (swell).

peak of $fS_{WW}(f)$ to be more pronounced over the oil film (Fig. 1a) than above an oil-free surface (Fig. 1c). This fact is due to the structural similarity of an oil-covered surface with ocean swell. The $fS_{WW}(f)$ spectrum measured at 11 m. altitude does not reflect any wave turbulence. The spectral energy decay at $f > 1$ cps closely conforms to the -2/3 law. In the spectral range, the calculated average wind dynamic velocities $U_* = 9$ and 15 cm/sec in the cases of Fig. 1a and 1b, respectively, do not differ from U_* data usually observed over a sea surface at average wind velocities $\bar{U}_{10} = 2.5$ and 3.5 m/sec. at 10 m. altitude. This finding confirms the conclusion of the 1968 U. S. experiment (Barger et al, J. Appl. Meteorol, v. 9, no. 3, 1970) that an oil film does not significantly affect momentum flow between atmosphere and ocean. However, measurements of moisture flow indicated a tremendous effect of oil film on evaporation. The integral moisture flow E over the oil-covered surface was found to be 4×10^{-3} g/m^2 sec versus

$E = 1.1 \times 10^{-2}$ g/m^2 sec in the absence of film. The moisture gradient was hardly detectable, because of a very small evaporation. Under the given conditions, even a very substantial increase in wind velocity cannot cause a corresponding increase in evaporation in the presence of an uninterrupted surface film. This fact points to the need for a thorough study both of film behavior and atmospheric turbulence over a film under a variety of conditions.

Shifrin, K. S. <u>Effect of wind on effective sea radiation</u>. FAiO, no. 7, 1974, 803-805.

A theoretical evaluation is made of the effects of wind-generated sea surface roughness, increase in sea surface area, spray, and foam on thermal radiation of the sea.

The effect of sea surface slope $t_g \, \theta_n$, where θ_n is the zenith angle of the normal to the surface, on the water emission coefficient ϵ is evaluated approximately by averaging, over different wind directions, the probability P of steep surface slopes, as determined from the formula of Cox and Munk (Bull. Scripps Inst. Oceanogr, v. 6, 1956, 401). At a typical 10 m/sec wind velocity, dispersion σ in the cited formula is $= 0.164$, i.e., 95% of the slopes are confined within 2σ limits, or in the region of $\theta_n \leq$ 18 degrees. The calculated ϵ values (Table 1) are constant within a fraction of a percent, hence a more accurate evaluation of ϵ is unnecessary.

Table 1. Water emission coefficient at different θ_n.

λ, μ	θ_n, degree		
	0	10	20
8,0	0,9834	0.9833	0,9832
9,0	0,9856	0,9856	0,9854
10,0	0,9901	0,9901	0,9900
11,0	0,9927	0,9927	0,9927
12,0	0,9853	0,9853	0,9851

The effect of an increased radiating surface area is evaluted by means of the Cox-Munk formula. The increase is given by

$$S/S_o = 1 + \frac{1}{2}\sigma^2 - \ldots = 1 + \frac{1}{2}10^{-4}(15+25.4v) - \ldots \tag{1}$$

where v is wind velocity and $\sigma^2 = 0.03$. The increase in S/S_o is correlated with the change in effective radiation temperature by

$$T_{eo} = T\left(1 + \frac{1}{4}\frac{\Delta S}{S_o}\right) \quad \text{or} \quad \Delta T = T_{eo} - T = \frac{1}{4}\frac{\Delta S}{S_o}T. \tag{2}$$

The $\Delta S/S_o$ and ΔT values calculated from (1) and (2) for $T = 300^{\circ}$ K (Table 2)

Table 2

v, m/sec	σ	$\Delta S/S_o$, %	ΔT, °C
5	0,119	0,7	0,5
10	0,164	1,4	1
15	0,200	2,0	1,5
20	0,230	2,6	2

show that in moderate winds, a sea roughness-caused increase in thermal radiation is equivalent to 1 degree rise in T. This is considered to be a significant effect, which must be taken into account in calculations. The $\Delta S/S_o = 2\%$ value in Table 2 coincides with the four $\Delta S/S_o$ values calculated by Monin (FAiO, no. 6, 1967) for four different models of sea roughness and the mean square wave slope $k = 0.2$ ($k \sim \sigma$).

The negative sea radiation balance R during the night is decreased by fog from water spray. In the absence of large water drops in the fog, the decrease ΔR can be evaluated from

$$\Delta R/R = -6w\%. \tag{3}$$

where w is the amount of water in the fog layer over the sea. Assuming the

fog water content to be 0.2 g/m^3 and fog layer thickness to be 1 m, Eq. (3) gives $\Delta R/R = -1\%$. This value of the effective sea radiation change is balanced by the equal radiation loss from the fog cover into the atmosphere, so that R of the sea-fog system remains unaffected by fog.

A detailed calculation of the IR emission coefficient of sea foam indicates that the presence of foam for any $v \geq 10$ m/sec. should not change ϵ of the sea in the spectral region of the atmospheric window.

Volkov, Yu. A., L. G. Yelagina, and B. M. Koprov. Spectral characteristics of turbulent exchange between the ocean and atmosphere in the tropical Atlantic. FAiO, no. 6, 1974, 619-627.

Spectral treatment is described of a tape recorded set of experimental data on wind velocity components, atmospheric temperature T and humidity e at 10 m. altitude above the sea surface. Systematic simultaneous measurements of the vertical turbulent fluxes of heat, moisture, and momentum were carried out during the TROPEKS-72 Atlantic expedition in the summer of 1972 from the R/V Akademik Kurchatov. (The methods used and the results obtained in this field experiment are described in Sb. Tr. "TROPEKS-72". Gidrometeoizdat, 1974).

Fig. 1 shows a general view of the instrument boom extended from the ship's bow. During measurements, the ship was either moving to windward or drifting. The angle of roll ψ was of the order of 1 deg; the vertical displacement amplitude, about 1 m, and the vertical velocity amplitude, 1 m/sec.
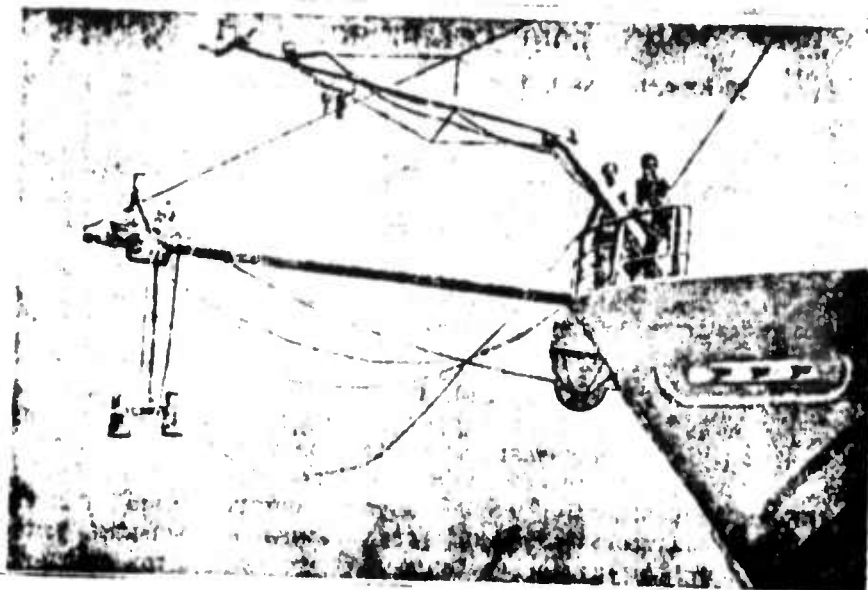
Fig. 1. Instrument boom.

The formulas of the real component (cospectrum) $\Phi_{\alpha\beta}$ (f) and imaginary component (quadratic law spectrum) $\psi_{\alpha\beta}$(f) of the reciprocal spectrum $F_{\alpha\beta}$(f) of measured quantities α, β are derived from the expressions

$$w_x{}' = w' + \bar{u}\varphi + \dot{z},$$

(1)

and

$$\gamma_x^{\varkappa(i)} = \gamma^{(i)} + z\partial\gamma^{(i)}/\partial z, \quad i=1,2,3,$$

(2),

where w_x' and $\gamma_x^{(i)}$ are the measured fluctuations of the vertical velocity component w; $\gamma^{(1)} = T$, $\gamma^{(2)} = e$; $\gamma^{(3)} = u$, the horizontal velocity component; z is deviation from mean value of the vertical coordinate of sensor suspension point, and $\dot{z}$ is the time differential of z. The vessel's reaction to fluctuations w' and u' in the suspension point, and φ, z, and $\dot{z}$ correlation with the wave induced fluctuations of u, w, T, and e, are neglected.

A method of compensation for the ship's pitching effect on the measured fluxes, or the corresponding cospectra, was used. The method consisted of measuring u and φ, hence $u\varphi$ and correcting the measured w_x' signal by the value of $u\varphi$. Such compensation may not be sufficiently

-92-

accurate, as illustrated by the spike on the $fF_{ww}(f)$ plot at f near the
predominant pitch frequencies. The true of $\Phi_{ww}(f)$ and $f\Phi_{w_\chi w_\chi}(f)$
values, however, can be reconstructed with sufficient accuracy in a
narrow frequency range, using an interpolation method. Numerical results
from 12 data series are tabulated and the functions

$$S_{\alpha\beta}(\Omega) = \Omega\bar{\Phi}_{\alpha\beta}(\Omega) \Big/ \int_{\Omega_1}^{\infty} \bar{\Phi}_{\alpha\beta}(\Omega)\,d\Omega,$$

(3)

where $\Phi_{\alpha\beta}(\Omega) = f\Phi_{\alpha\beta}(f)/\Omega$, are plotted (Fig. 2 and 3) against the wave
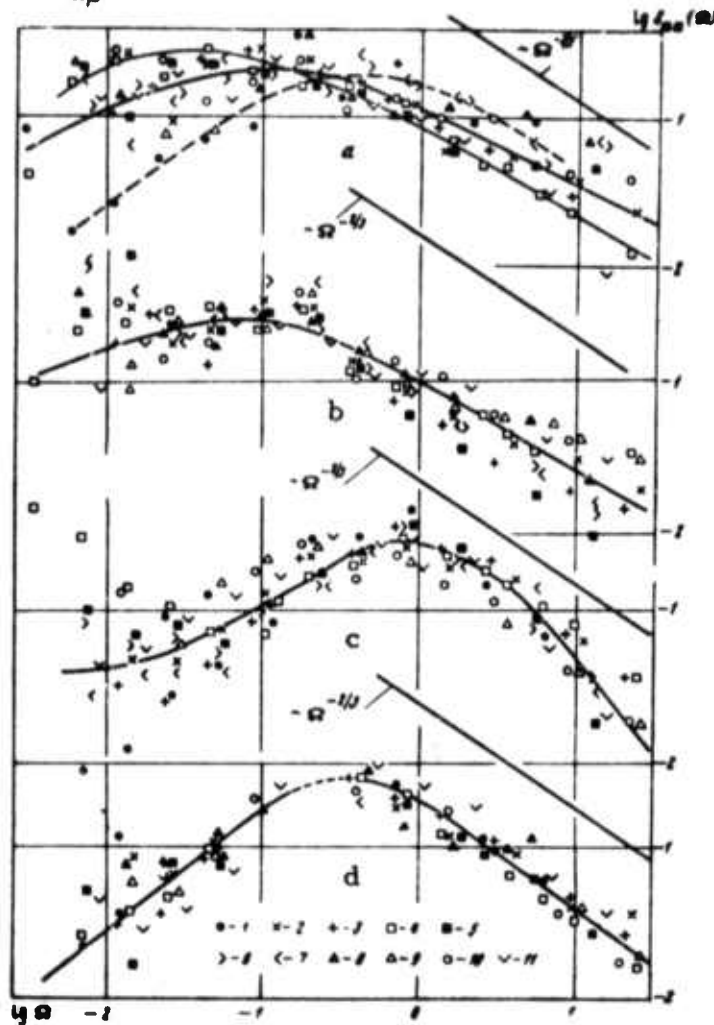

Fig. 2. $S_{\alpha\alpha}\,\Omega$ functions of fluctuation spectra
in log coordinates. Heavy continuous lines
correspond to averaged values of the functions
$S_{ee}(\Omega)$ (a), $S_{uu}(\Omega)$ (b), $S_{TT}(\Omega)$ (c), and $S_{ww}(\Omega)$
(d). Dashed and fine continuous lines of $S_{ee}(\Omega)$
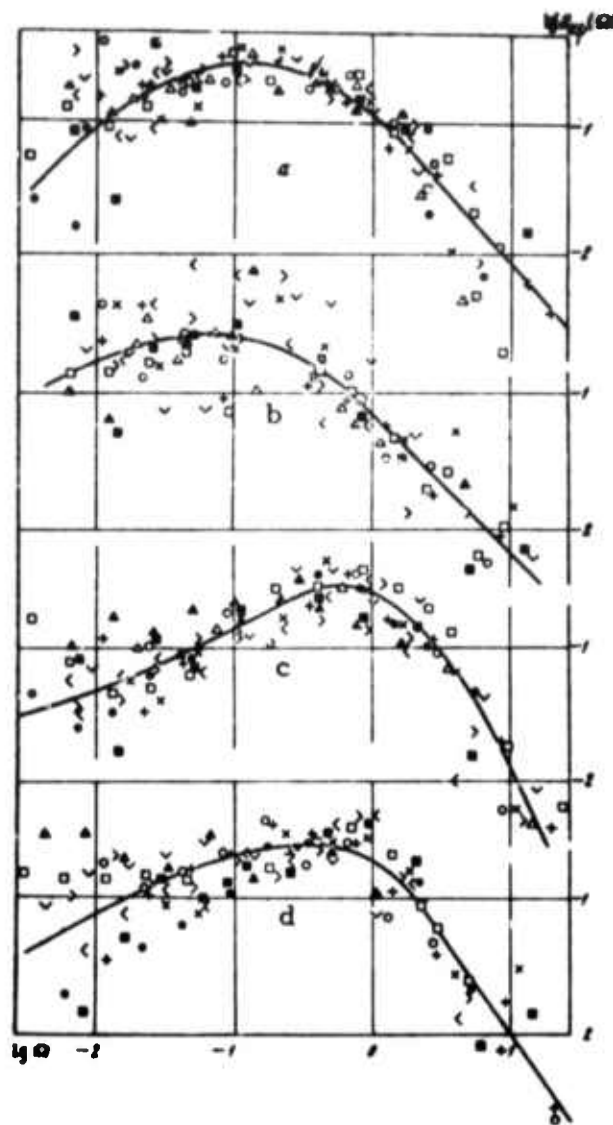plot represent two different data series, 1 and 4.

Fig. 3. $S_{\alpha\beta}(\Omega)$ functions of turbulent flux spectra in log coordinates: $S_{we}(\Omega)$- a, $S_{wu}(\Omega)$ (with inverse sign) -b, $S_{wT}(\Omega)$- c, and $S_{eT}(\Omega)$- d curve. Same notations as in Fig. 1.

numbers $\Omega = fz/u$ in the 10^{-2} to 20 range, where u is the total (vessel plus wind) velocity of the incoming flow.

A detailed analysis of the $S_{TT}(\Omega)$ and $S_{ee}(\Omega)$ plots (Fig. 2c and 2a) revealed a significant difference between these functions in the $\Omega < 1$ range. This difference is interpreted as the result of different $T(z)$ and $e(z)$ vertical profiles. The low-frequency fluctuations more significantly contribute to e fluctuations than to T fluctuations, because significant T inhomogeneity arises

only near the surface, while e inhomogeneity occurs at any altitude owing to unstable stratification by density.

At the surface T and e profiles must be similar. This conclusion is confirmed by the fact that the $S_{TT}(\Omega)$ function shows a maximum at the same Ω as the $S_{eT}(\Omega)$ function (Fig. 3d) and the spectral correlation coefficient $r_{eT}(\Omega) = \Phi_{eT}(\Omega)/\Phi_{ee}(\Omega)\Phi_{TT}(\Omega)$ (Fig. 4).
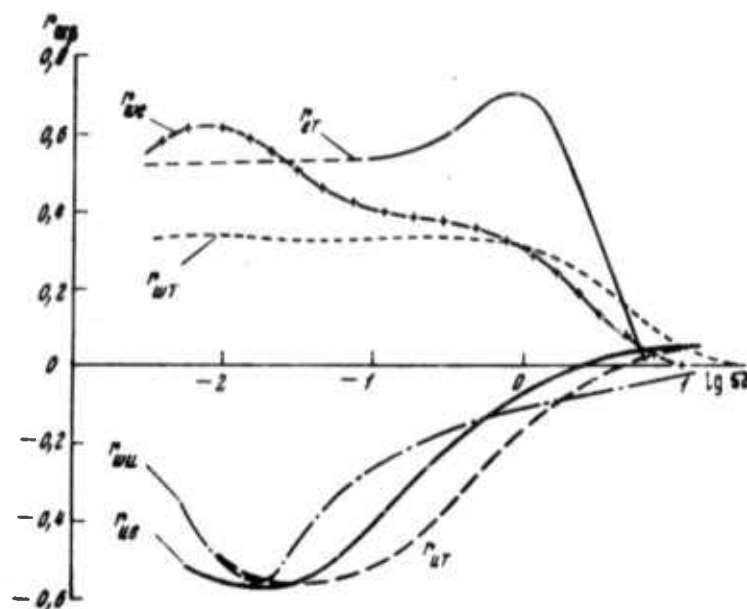

Fig. 4. Spectral correlation coefficients $r_{\alpha\beta}(\Omega)$.

A decrease of $S_{eT}(\Omega)$ at $\Omega < 1$ is correlated with the appearance of large inhomogeneity at high altitudes, simultaneously with lesser T inhomogeneity. Similar considerations may explain the difference between the $S_{wT}(\Omega)$ and $S_{we}(\Omega)$ functions (Fig. 3c and a).

The underlying cause of peculiar T spectra is a small difference between water and air temperature, which was also observed during the BOMEX expedition. The turbulence parameter $\lambda = \rho w'T;/0.61\ Tw'e'$, analogous to the Bowen number, is introduced and found to be about two, as in the BOMEX expedition.

The $r_{wT}(\Omega)$ data (Fig. 3) and other turbulence spectral characteristics are in good agreement with data of the BOMEX expedition. This agreement is considered to be an additional confirmation of the possibility of studying turbulence characteristics on shipboard using the cited method.

Kuchumova, L. S., V. V. Khlopov, and O. I. Sheremetevskaya. Heat balance and its role in the change of temperature of the surface oceanic layer. IN: Trudy AANII, no. 315, Leningrad, 1974, 41-52.

Components of the oceanic surface heat balance are calculated, using meteorological data obtained during the fourteenth and fifteenth cruises of the R/V Professor Vize in the test areas off the Azores and in an equatorial region of the Atlantic, respectively.

A formula for calculating total solar radiation flux

$$Q_\odot = Q_{max}(0.80 - 0.60 N^2_*)(1 - A).\qquad(1)$$

where Q_{max} is the maximum solar radiation in the absence of atmosphere, N_* is the half-sum of the total, and lower cloudiness, and A is the sea albedo, was derived by unifying the actinometric observation data in the seas and oceans. The radiation balance was calculated from

$$B = Q_\odot - Q_{rad}\qquad(2)$$

where Q_{rad} is the effective heat loss due to backscatter. Comparison of the Q_o and B data calculated from Eqs. (1) and (2) with direct measurement data shows that this method can be used to calculate Q_o and B within 8 to 12% in both test areas.

Other heat balance components were calculated using known formulas from the literature. The vertical gradients of wind velocity, air temperature and moisture were the logarithmically approximated observation data. The calculated heat balance data plotted in Figs. 1 and 2 show significant fluctuations in the solar heat flux and sharp differences in heat
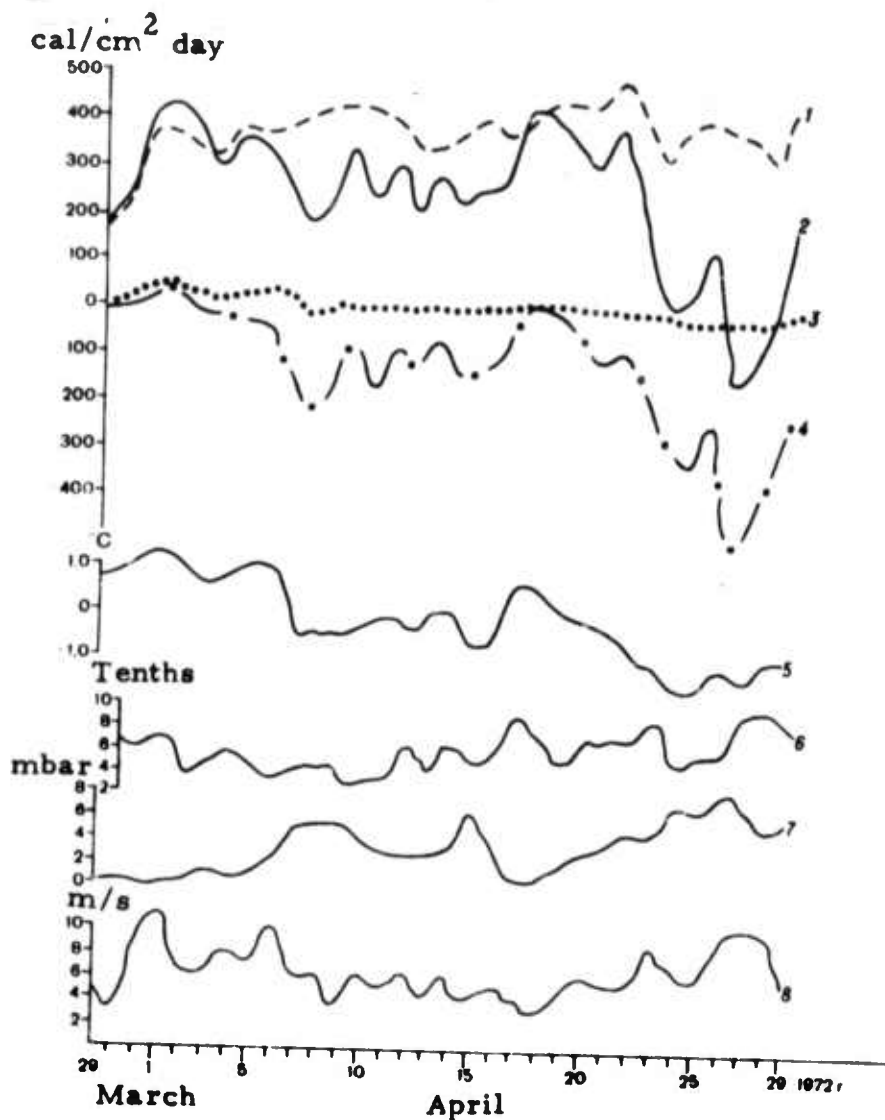

Fig. 1. Heat balance components (1, 2, 3 and 4) and their calculation base data (5, 6, 7 and 8) from observations made during the 14th cruise of the R/V "Professor Vize": 1- radiation balance, 2- total heat balance, 3- turbulent heat transfer, 4- heat loss by evaporation, 5- temperature difference between air and water, 6- half sum of total and lower cloudiness, 7- moisture deficit, 8- wind velocity.
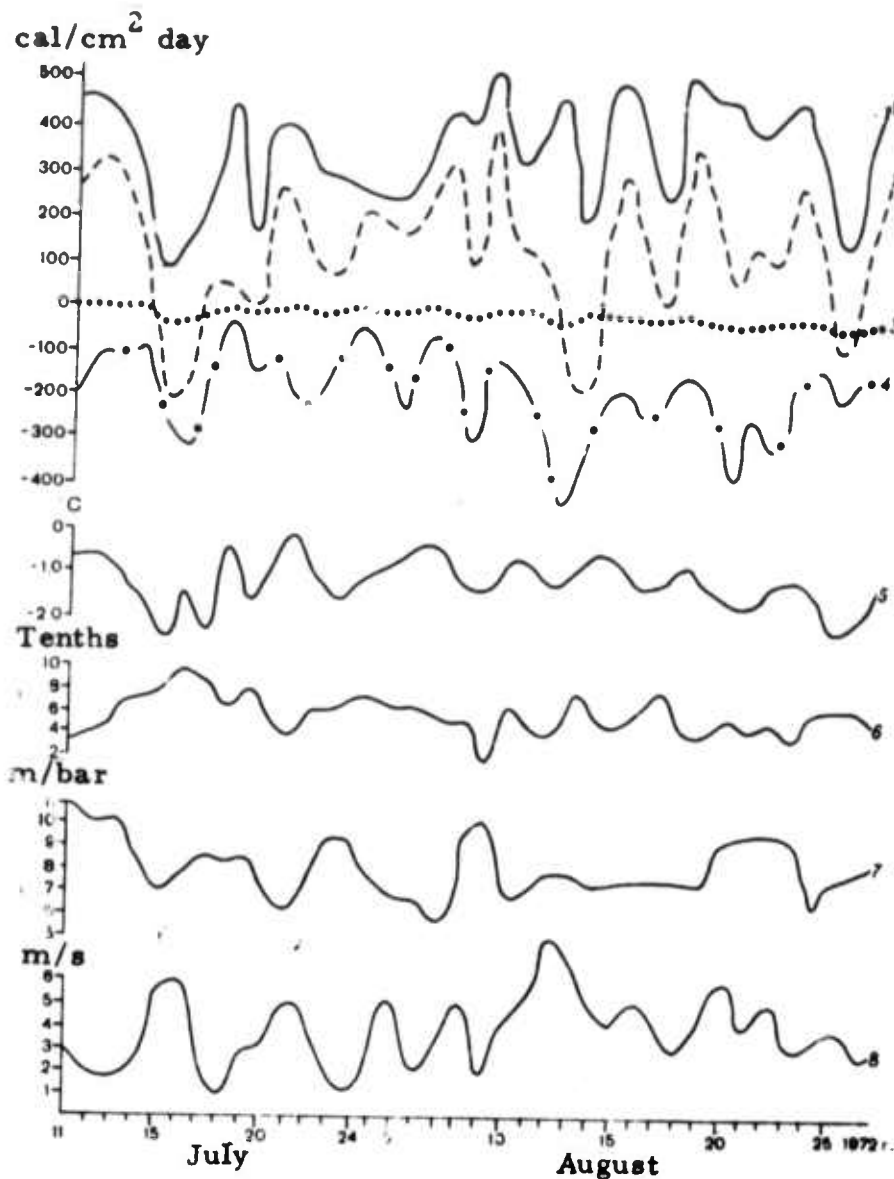
Fig. 2. Heat balance components (1, 2, 3, and 4) and their calculation-base data (5, 6, 7 and 8) from observations made during the 15th cruise of the R/V "Professor Vize". Conventional indicators are the same as in Fig. 1.

loss by evaporation. Evidently, B and Q_{ev} are the principal factors in total heat balance.

Analysis of the calculated heat balance indicates the fluctuations of the basic heat balance components are dependent on hydrometeorological factors. Fluctuations in the subtropical region near the Azores are explained

by activity of the Azorian anticyclone; those in the equatorial region are interpreted as the result of an increased activity of the intertropical convergence zone during the July-August test period. Statistical treatment of the data confirm that evaporation and total solar radiation are subjected to greater fluctuations in the subtropical region.

The authors conclude that heat transfer fluctuations were significant during the observation period in the test area and did correlate with changes in weather conditions. Heat losses due to evaporation and turbulent heat exchange were relatively stable. Advective and local variations in temperature of the oceanic upper layer were calculated using the observed temperature and current velocity data and the calculated heat balance data, respectively. Local temperature variations in the upper oceanic layer during the observation periods were calculated to be 1.9^{o} and 1.6^{o}, respectively, in the Azores region and in the Atlantic equatorial region. Heat balance fluctuations are estimated to cause about 85% of temperature variations, with the remainder attributable to advective heat transfer.

Zykov, I. D., and K. S. Pomeranets. Results of calculating statistical characteristics of currents. IN: Trudy Arktich. i antarktich. n. -i. inst., Leningrad, vol. 312, 1974, 192-196.

The statistical treatment is described of current velocity data, collected in the northeastern Atlantic at 400 m depth over a thirty day period at half-hour intervals. Variable mathematical expectation M_i and spectral density function S_k of the meridional vector component of the current are calculated by the method described by Ozmidov (Horizontal turbulence and turbulent exchange in the ocean, Moskva, 1968). Also a procedure of separating out long-period fluctuations of sea waves was used. M_i was thus calculated using preassigned values of the smoothing interval δ of long period fluctuations (Fig. 1). This reveals irregular background fluctuations with a
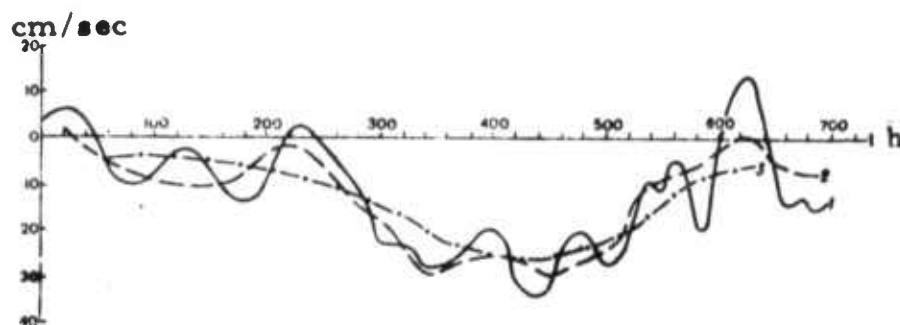
Fig. 1. Variable mathematical expectation at different smoothing intervals: δ_1 = 12.5 h, δ_2 = 25 h., and δ_3 = 87.5 h.

period twice the observational interval.

The effects of duration of the observation series, the discrete interval Δ of time series, and the degree of freedom $\gamma = 2N/m$, where N is the number of observations and $\underline{m}$ is the shift of correlation function, are then evaluated from comparison of the S_k maxima for different periods. A comparison between S_k values in Table 1 shows that

Table 1. Spectral characteristics for different durations of observation series.

Ordinate	Quantity of ordinates	Spectral density cm^2/s^{-2}, h		
		$T_1 = 75\,h$	$T_2 = 24\,h$	$T_3 = 12.5\,h$
1—1440	1440	470	1620	290
1—720	720	50	1400	100
721—1440	720	550	1170	150
1—480	480	—	830	75
481—960	480	—	910	110
961—1440	480	500	350	145
1—960	960	65	1560	195
481—1440	960	390	1075	200

S_k calculated for a part of the observation series equal to 1/2, 1/3, or 2/3 of the series is always smaller than S_k for the whole series. Fundamental fluctuations with 12.5, 24, and 75 hour periods arise in each part of the

whole series. At a 75 h period, the S_k value always increases toward
the end of a series. Fluctuations of the diurnal tidal period are predominant.
At different $\Delta = 0.5$ to 2 h and a constant $\nu = 10$, the tabulated S_k maxima
for long-period (75 h) and diurnal (24 h) fluctuations are the same (470 and
1600 cm^2 sec^{-2} h, respectively), but S_k values for semi-diurnal (12.5 h)
fluctuations decrease by 7 and 11% at $\Delta = 1$ and 2 hr, respectively. For a
given N and Δ, the absolute S_k values decrease with increase in ν from 10
to 19. At both ν values, three main periods of current fluctuations are
evident. This finding reveals a satisfactory ratio of accuracy to detail of
spectra evaluation.

In summary, the results show that selection of the governing
parameters is of prime methodological importance in any statistical analysis
of long-term series of current observations.

2. Surface Effects

Zagorodnikov, A. A. Using artificial earth satellites to measure waves. FAiO, no. 7, 1974, 791-798.

The possibility is investigated of using artificial earth satellites for measurements of spatial two-dimensional spectra of sea waves.

In satellite-borne measurements of sea state, a radar with high longitudinal and low lateral resolution should be used ($\Delta W_x < \overline{\Lambda}$, $\Delta W_y >> \overline{\Lambda}$, $S_w(v) = \delta(v)$. In such a case the spatial spectra of one-dimensional realizations of full-viewing or side-looking radars are given in the form

$$S_{qx}(K, a) \approx \int_{-\infty}^{\infty} \frac{K^2}{|\cos(\theta-a)|^2} S_z \left[\frac{K}{|\cos(\theta-a)|} ; \theta \right] \times$$

$$\times S_{wx} \left[\frac{K}{|\cos(\theta-a)|} \right] \delta(\theta-a) d\theta = K^2 S_{wx}(K) S_z(K; a), \tag{1}$$

$$S_{qx}(a) \approx \int_{-\infty}^{\infty} a^2 S_z(u, v) S_{wx}(u) \delta(v) dv = a^2 S_{wx}(a) \mathcal{L}_z(a, 0). \tag{2}$$

In the case of sea waves with $\overline{\Lambda} \geq 5 \Delta W_x$, the filtering affect of the radar can be neglected and eqns. (1) and (2) become

$$S_{qx}(K, a) \approx K^2 S_z(K, a), \quad S_{qx}(a) \approx a^2 S_z(a, 0), \tag{3}$$

where $S_z(k, \alpha)$ and $S_z(u, 0)$ are cross-sections of two-dimensional spectra of waves in α and $v = 0$ directions. The structure of eq. (3) shows that the spatial spectrum of a one-dimensional realization at antenna direction α is uniquely related to the cross-section of the two-dimensional spectra of waves in the same direction.

Scanning of sea surface from a polar orbiting satellite at
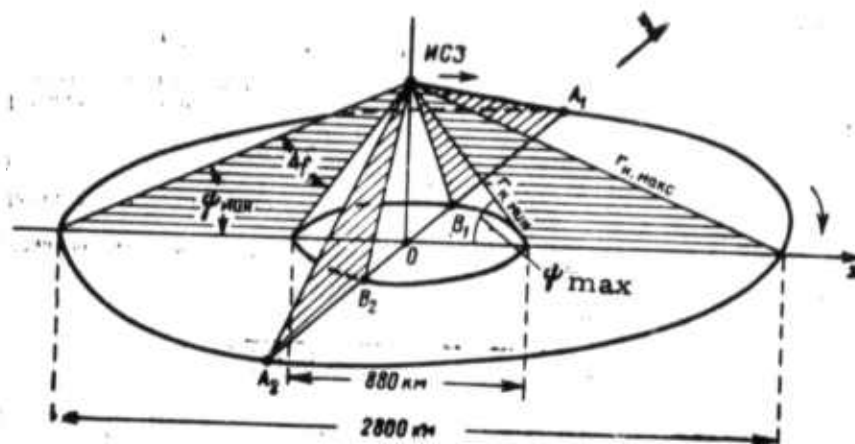a height of 62.5-630 km is illustrated in Fig. 1. Geometrical considerations

Fig. 1. Model for satellite scanning of a sea surface.

show that at $\Delta\alpha = 2^{\circ}$, $T \geq 10^{-2}$ sec and satellite rotation period of ~ 100 min,
each point of the target zone is irradiated numerous times. In order to
reproduce spectral function of sea waves, cross-sections in an angular
sector $\theta = 0 - \pi$ are needed, which can be achieved by a system of three
satellites: one polar orbiter and two orbiting at angles of $+53^{\circ}$ and -53° with the
equatorial plane.

The author concludes that spatial two-dimensional spectra of
sea waves can be measured from satellites, and that the use of aerial
photography is also promising for these measurements. Some sample aerial
photos of sea states are included.

Belousov, P. S., Ye. O. Zhilko, A. A.
Zagorodnikov, V. I. Korniyenko, V. S.
Loshilov, and K. B. Chelyshev. Results of
studying sea turbulence using SLAR. IN:
Sb. Predvarit. rezul'taty ekspeditsii "Bei ing",
Leningrad, 1973, 84-94. (RZhGeofiz, 4/74,
no. 4V66). (Translation)

Results are reported of radar ocean mapping in the Bering Sea
during February-March 1973. The following was observed: (1) radar image
characteristics remain unchanged when radar illumination direction is
changed; also the spectral component series do not shift from their position
on the wave number plane, but images and spectra of the wave systems with
beam direction close to the illumination direction become more prominent;
(2)   the two-dimensional spectrum of radar images reflects foam bands, and
(3) analysis of a two-dimensional spectrum makes it possible to determine the
number of wave systems, the positions of the spectral density peaks on the
wave number plane, beam and average wave length of each move system, and
the integral angular spectrum of all wave systems and of each system (if the
spectra do not overlap too much). Also, it is possible to evaluate the narrow
frequency band in the angular spectrum of each wave system, the three-
dimensional frequency spectrum, and the spectrum of a wave series. Wind
direction at the time of mapping can be determined from the foam bands.

Troilin, V. N. Determining the structure of the
scattering matrix in the case of perpendicular
irradiation of a surface. Trudy Taganrog r-t in-ta,
no. 39, 1973, 32-35. (RZhF, 6/74, #6 Zhl51).
(Translation)

It is shown that in the case of perpendicular irradiation of a
perfectly reflecting surface, the scattering matrix is diagonal, while flux
density of the energy carried by the reflected signal does not change in time,

regardless of polarization. In the case of perpendicular irradiation of a rough surface with a finite conductivity, the scattering matrix contains all elements, while the energy flux density has a maximum which depends on the selection of transmitter polarization.

Sosunov, A. S., and V. T. Lobach. Distribution moments of a radio signal reflected from a statistically uneven surface. IN: Trudy Taganrog r-t in-ta, no. 39, 1973, 3-7. (RZhF, 6/74, #6Zh147). (Translation)

The average value and dispersion are considered of the quadrature components of a field reflected from a statistically rough surface.

Timokhin, A. A. Possibility for height measurement of sea waves using phase fluctuations of reflected radio signal. IN: Trudy Taganrog r-t in-ta, no. 39, 1973, 12-15. (RZhF, 6/74, #6Zh149) (Translation)

The possibility is considered of height measurement of sea waves using phase fluctuations of a radar signal reflected from the sea surface. Expressions are obtained for the standard deviation of the phase of reflected signal at different ratios of coherent and incoherent components. It is shown that σ_φ is a function of the relative heights of sea waves when $H_{3\%}/\lambda \leq 0.5$, where $H_{3\%}$ is wave height at 3% tolerable error.

Timonov, V. V., and I. T. Zamkov. Problem
of increasing the accuracy of Doppler true air
speed indicators while flying over the sea. IN:
Trudy Taganrog r-t in-ta, no. 39, 1973, 44-49.
(RZhF, 6/74, no. 6Zh153). (Translation)

The possibility is considered of using current information on
the state of a disturbed sea surface and a priori data on the relative shift of
the spectral peak of a Doppler echo-signal. The purpose is to reduce the
error of true air speed measurements while flying over the sea.

Timokhin, A. A. Profiling of a statistically
nonuniform suface. IN: Trudy Taganrog r-t in-ta,
no. 39, 1973, 23-26 (RZhF, 6/74, no. 6Zh150).
(Translation)

The possibility is considered of designing equipment for height
determination of irregularities of a statistically uneven surface (e. g. a sea
surface) from an aircraft by a noncontact method. A functional diagram of the
equipment is discussed.

Okishev, V. B., S. V. Polozhentsev, and I. A.
Podval'nyy. Depth dependence of the accuracy of
measurement of sea wave height by a radio method.
Trudy Taganrog r-t in-ta, no. 39, 1973, 36-38.
(RZhF, 6/74, #6Zh152). (Translation)

Accuracy in measuring the height of sea waves from an aircraft
is analyzed as a function of water depth for the cases of a deep and a shallow
sea.

Molebnyy, V. V. Remote device for measuring
the orientation of sea surface facets. Otkr. izobr.,
no. 23, #433339, 1974, 100. (Translation)

A remote device for measuring the orientation of sea surface
facets contains a highly directional light source, a unit for polarization control,
a generator of signals for polarization control, photodetector, and a unit for
analysis. The device features a linear-circular polarizer and a phase difference
meter which is connected to the polarization control signal generator and to an
amplitude modulation meter for echo signals. Both additions were introduced
for the purpose of automation.

Lobach, V. T. Possibility of determining the
average length and principal propagation direction
of sea waves by radar. Trudy Taganrog r-t inta,
no. 39, 1973, 16-22. (RZhF, 6/74, #6 Zh418)
(Translation)

The possibility was investigated of determining the average
length of sea waves, from data on scattering of radiowaves in the meter
range by the sea surface. The transmitter/receiver device is assumed to
move uniformly over the surface. The problem was considered in an
approximation of the method of perturbations, for the case in which the
fluctuating component of the field is small relative to the regular one. It is
shown that the average length of sea waves in a given direction correlates
in a simple fashion with the mean number of zero crossings per unit time
of the envelope of the reflected signal. The principal direction of propagation
is determined from the average wave lengths in various directions. The
results of experiments with a radar at a transmitted frequency of 30 MHz and
pulse duration of 1 microsec are given, which corroborate theoretical
conclusions.

Matveyev, D. T., Yu. A. Volkov, A. P. Kestner,
and S. O. Lomadze. Measurement of slope
characteristics of a disturbed sea surface by remote
microwave sounding. IN: Sb. TROPEKS-72.
Leningrad, Gidrometeoizdat 1974, 540-547. (RZhGeofiz.
8/74, #8B73). (Translation)

The results are given of microwave measurements of slope
characteristics of a disturbed sea surface, using a 2.5 cm wavelength.
Measurements were conducted from an elevation-stabilized platform at an
angle of 20° to the horizon, aboard the R/V Akademik Kurchatov. Measure-
ments with a wire-type wave gage were conducted simultaneously. Data were
recorded on magnetic tape and computer processed. Spectra were obtained
of slope projections onto the main and orthogonal directions of sea wave
propagation. Analysis shows that the spectra obtained have rather steep slopes
at high frequencies, which is caused by the limited spatial resolution of the
radiometer. In other respects the results of microwave measurements agree
well with the results of wave-gage measurements as well as with theoretical
considerations.

Lande, B. Sh. On a theory for determining
parameters of sea surface profile from radar
reflections. IN: Tr. Sev. -Zap. zaoch.
politekhn. in-ta, no. 25, 1974, 8-10. (RZhF,
11/74, #11Zh141). (Translation)

An explanation is given for polarization and spectral character-
istics of a scattered field, based on a two-dimensional model of scattering
of microwaves at a sea surface and using the method of small perturbations.
This was accomplished by modeling spectra of capillary waves using finite
functions in a frequency-time domain. Recommendations are given for
determining the volume of data required for reconstruction of the main
parameters of the sea surface.

Garnaker'yan, A. A., A. S. Sosunov, and V. T. Lobach. Coherent and incoherent components of a radio signal reflected from an isotropic sea surface with a quasiharmonic correlation function. Trudy Taganrog r-t in-ta, no. 39, 1973, 3-7. (RZhF, 6/74, #6Zhl48). (Translation)

Expressions are obtained for the power of fluctuating and regular components of a field scattered by an isotropic sea surface. The effect of the length of sea waves upon the power of the scattered signal is analyzed.

Bol'shakov, E. A., and V. I. Saplin. Determining the phasor of a radio signal reflected from a statistically rough surface. Trudy Taganrog radiot. in-ta., no. 39, 1973, 27-31. (RZhF, 8/74, #8Zh212) (Translation)

Expressions were derived for modulus and phase of the polarization ratio (phasor) of a radio signal reflected from a statistically rough surface, having large gently-sloping irregularities whose heights have a normal distribution. Analysis of these expressions shows that polarization characteristics of the reflected signal depend on angle of incidence, as well as on the statistical parameters and electrical properties of the rough surface.

Bespalov, A. A., N. Ye. Kuznetsov, V. V. Naumova, and V. D. Rusin. Recording system for space-time characteristics of surface wave disturbances. VMU, no. 4, 1974, 406-410.

A description is given of a system for simultaneous measurements of height and period of wind waves at eight points, and spatial correlation

at any two of these points. Block diagrams of the measuring system, recording gage channel and correlator are given in Figs. 1-3, respectively.
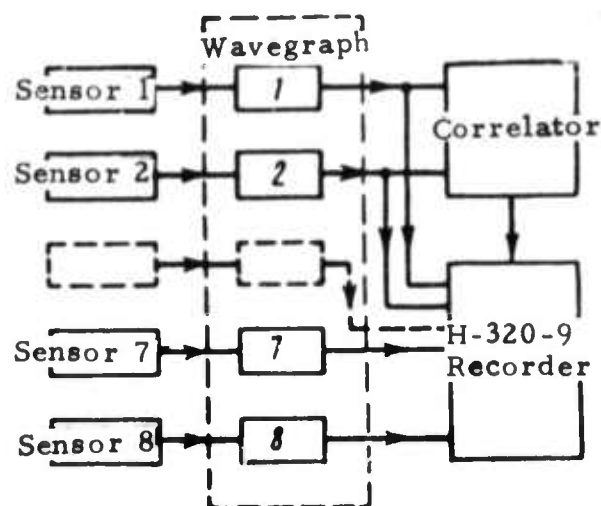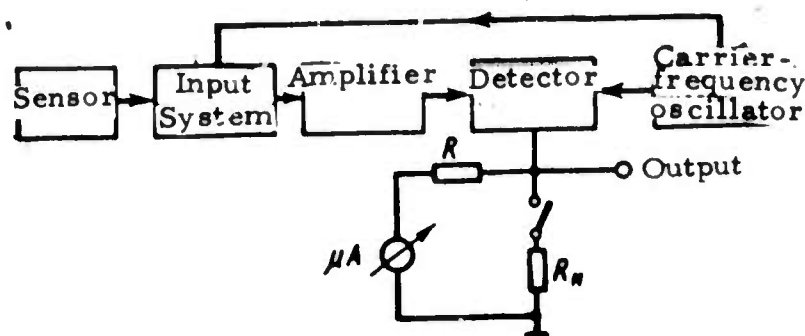

Fig. 1. Measuring system.

Fig. 2. Wavegraph channel

The sensor arrangement of the system is as follows: seven sensors are set along a 2.8 m-long base line with various spacing between them; one sensor is placed to form an equilateral triangle 20 cm distant from either of two sensors set on the base line. The system can be used for dip measurements at $\bar{\lambda} = 1.2 - 1.6$ m. The accuracy of height measurements is $\pm 5\%$.
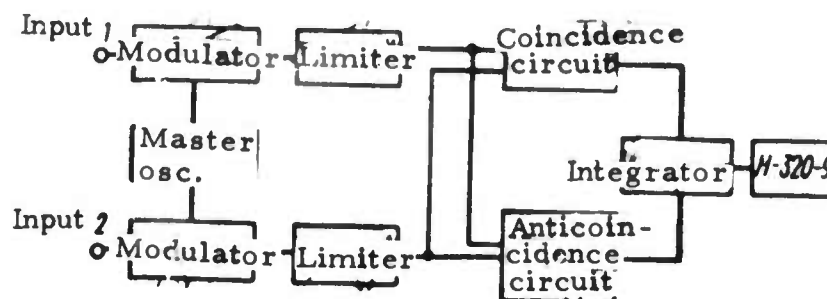
Fig. 3. Correlator

Schematics of the modulator and one stage of the limiter in the correlator are included. This system has been used in the study of surface waves in the near-shore zone of a reservoir.

Vinogradov, V. V., L. V. Mironov, Yu. I. Popov, and V. V. Ukrainskiy. Results of measuring water surface temperature by infrared radiometer in the tropical Atlantic. IN: Sb. TROPEKS-72, Leningrad, Gidrometeoizdat, 1974, 609-619. (RZhGeofiz, 8/74, no. 8B32). (Translation)

Technical specifications are given for a new shipboard IR radiometer, and its accuracy in measuring surface water temperature is evaluated. Systematic errors in the shipboard measurements are discussed. Preliminary results are given of measuring the daily variation in sea surface temperature and of computational methods for mapping it. Questions are treated on using radiation temperature to calculate the heat balance of the sea surface.

Fuks, I. M. Spectral widths of signals scattered
by a wavy sea surface. Akusticheskiy zhurnal, no.
3, 1974, 458-468.

Reasons are analyzed for the spectral broadening of sonic
signals, reflected from a wavy sea surface. Formulas are obtained for
scattered field spectra, and the effect is evaluated of attenuation on spectral
broadening of a signal scattered by small ripples. Criteria are stated
for the applicability of the "two-scale" model of a scattering surface for
the case of developed sea waves. The contribution is considered of Doppler
broadening, caused by ripple motion on large-scale wave components, on
the instantaneous frequency fluctuation and energy spectrum of the scattered
signal. Spectral width is correlated with wave parameters, namely wind
velocity, wave height, and frequency of energy-carrying components.

Korzun, V. A. Technical possibilities of remote
(space) imaging of the ocean. Ekspress informatsiya,
ser. 9, no. 1, 1974, Promyslovaya okeanologiya,
1-28.

This is a review of the modern technical means for oceano-
graphic and surface meteorological studies, with emphasis on possibilities
of remote imaging from space in selected areas of research. The review
is based on ocean data collections published from 1967 through 1973. Technical
means of remote imaging of the ocean include space carriers, on-board
instrumentation, reception, and processing of data.

Selection of technical means is correlated with the purpose,
i. e. forecast or research, of the experiment. The requirements of observation
frequency, accuracy, and volume are summarized for meteorological and
oceanographic purposes. Characteristics of different types of U. S. spacecraft
used for the cited purposes are tabulated. Selection of the optimum system
of data collection by means of satellites is discussed. The advantage is
indicated of using manned space stations, such as Salyut or Skylab, for certain

experiments. Technical potentialities of photographic and TV cameras, IR and microwave radiation meters including side-looking radar, are examined in relation to oceanography and surface meteorology.

The spatial resolution of various cited instruments is discussed as the main problem in data collection. Technical possibilities of remote sensors with respect to their resolution power are illustrated by tabulated data from a Western source. The relatively low detection capability of IR sensors is indicated to be the main cause of the lower resolution power of IR instruments, in relation to TV instruments. The use of scanning and point-locked radiation meters in observation of cloud-free regions is outlined. Potential resolving power of present on-board thermal radiation instruments can be very high, e.g., 5-10 km on board geosynchronous satellites.

Active radar systems and passive microwave radiometers used for ocean imaging are reviewed with respect to their resolving power, weight, and power requirements. It is concluded that only active systems can be used on orbiting space stations. The fundamental deficiency of photographic, TV, IR, and microwave imaging is considered to be ambiguity in interpretation of the collected data. Analysis of the Earth spectral imaging data collected during orbiting of the Soyuz-6, 7, and 8 spacecrafts showed that the spectral brightness coefficient data at a few wavelengths is sufficient to identify a surface from its reflection spectrum.

Methodological problems of data reception, processing, and interpretation are also discussed. A comparison is made between direct transmission of data and transmission from the satellite to Earth via buoy with data recording on magnetic tape or drum. Potentialities are examined of photo-interpretation and digital processing of the data. Specifications of marine meteorological and oceanographic parameters collected from buoys are summarized and discussed; a communications flow chart is given for the satellite-buoy and satellite-ground station systems.

In the near future the author sees data being collected by buoy from geostationary or heliosynchronous observation satellites. Advantages and deficiencies of these two satellite-buoy systems are compared in a table. Examples are cited of the operational and projected U. S. geostationary and heliosynchronous satellites. The author's further views and recommendations are given on future developments of the ocean imaging from space. There are 52 references, of which some 20% are Soviet.

Timofeyev, N. A., and Ye. N. Shutova. Angular structure of the emitted shortwave radiation field over the ocean. IN: Sb. Mor. gidrofiz. issled., Sevastopol', no. 2(61), 1973, 132-141. (RZhGeofiz, 12/73, no. 12B234). (Translation)

The angular structure of the brightness field of the ocean-atmosphere system is investigated, on the basis of actinometric measurements and cloud observations made in October 1969 by the Meteor-1 and Meteor-2 meteorological satellites. A method is introduced for converting the satellite-measured intensity of $0.3-3.0 \mu$ radiations reflected to space into radiation flux into a hemisphere at a nominal upper boundary of the atmosphere.

Kondrat'yev, K. Ya., V. V. Melent'yev, and Yu. I. Rabinovich. The Soviet-American Bering experiment. IN: Sb. Predvarit. rezul'taty ekspeditsii "Bering", Leningrad, 1973, 3-29. (RZhGeofiz, 4/74, no. 4B36). (Translation)

The chief purposes of the joint American-Soviet expedition in the Bering Sea from February 15 to March 7, 1973 were: (1) Airborne measurements

of microwave radiation from an open sea surface and from an area of
rainfall; (2) shipboard measurements of ice parameters, surface temperature,
surface waves, and liquid water content of the atmosphere, and (3) exchange
of comparable microwave and direct measurement data on characteristics
of atmosphere, ice cover, and sea surface.

Martsinkevich, L. M. Preliminary analysis of
results of wave measurements in the Bering
experiment (Bering Sea, Feb.-Mar. 1973). IN:
Sb. Predvarit. rezultaiy ekspeditsii "Bering",
Leningrad, 1973, 95-111. (RZhGeofiz, 4/74,
no. 4V69). (Translation)

The aggregate wave heights and periods measured on radar
maps obey known distribution laws. Ripple components and secondary energy
peaks, which probably are related to nonlinear effects of wave decay, were
revealed by spectral analysis of one sea roughness state. An approximate
correlation was obtained between a foam-covered sea surface area (in %)
and wind velocity. In the absence of an experimental cyclone distribution over
a turbulent sea surface, theoretical studies are required for interpretation of
a mixed sea roughness from radar mapping data. Also, solution of such a
problem requires synchronized measurements of r-f thermal radiation from
a rough sea surface, surface slope, and characteristics of the foam cover.

Bykova, V. Ye., I. V. Kireyev, L. F. Monakhov,
and A. V. Svechnikov. [Radar] measurement of the
true gradients and synchronous measurements of wave
heights, periods, and velocities. IN: Tr. Gos.
okeanograf. inst., no. 117, 1973, 17-24.

Measurement procedures and data are reported and discussed
on the interaction of radar waves with a wavy sea surface. The true instantaneous

wave slope tan α was measured in directions of wave propagation and normal to it. A nine-channel wire-type wave gage synchronously recorded oscilloscope traces of signals from five wire sensors spaced at 50 or 100 cm distances from each other. The oscilloscope data were read out, converted to digital form, and recorded on punched tape by means of an analog-digital converter-recorder. The wave slope values were computed on a Minsk-22 computer.

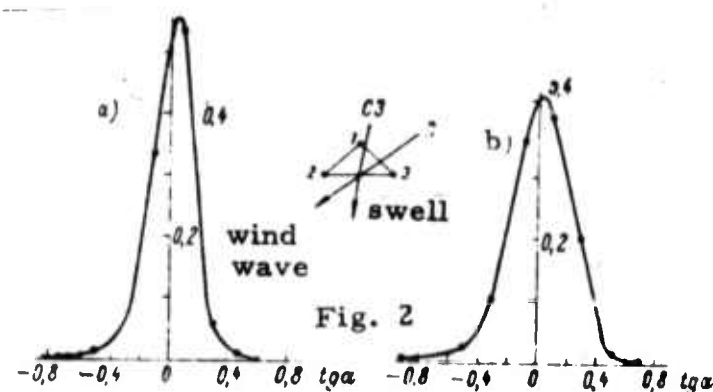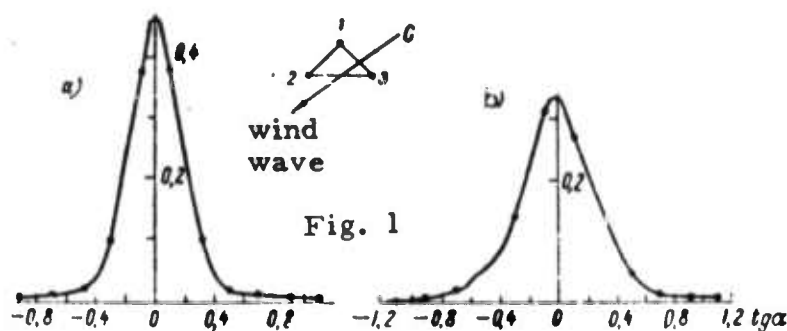The plotted tan α data (Fig. 1 and 2) show that under given

Fig. 1 and 2. Slope distribution density for a simple wave system and a hybrid system:

a- normal to direction of wind wave propagation,
b- in the same direction; 1, 2, and 3- sensor numbers.

hydrometeorological conditions, true wave steepness increases with an increase in wave amplitude, and that tan α distribution is nearly symmetrical for developed wind waves but asymmetric with respect to the ordinate axis for a hybrid wave system. Statistical analysis of the true tan α data was made

using the Kolmogorov test for normality and the chi-square compatibility
test. Both tests verified applicability of the normal distribution hypothesis
to the slopes normal to wave propagation direction, but only for developed
wind waves.

The tabulated $\tan \alpha$ data measured at 0.5 and 1 m. separation
intervals in the direction of wave propagation are found to be in fairly
good agreement, a fact which indicates that statistical distribution of slope
data is practically the same for measurements at the cited intervals.
Comparison of the charts in Fig. 3 shows that the highest $\tan \alpha$ values
correspond to ripples, while the low $\tan \alpha$ values are more characteristic
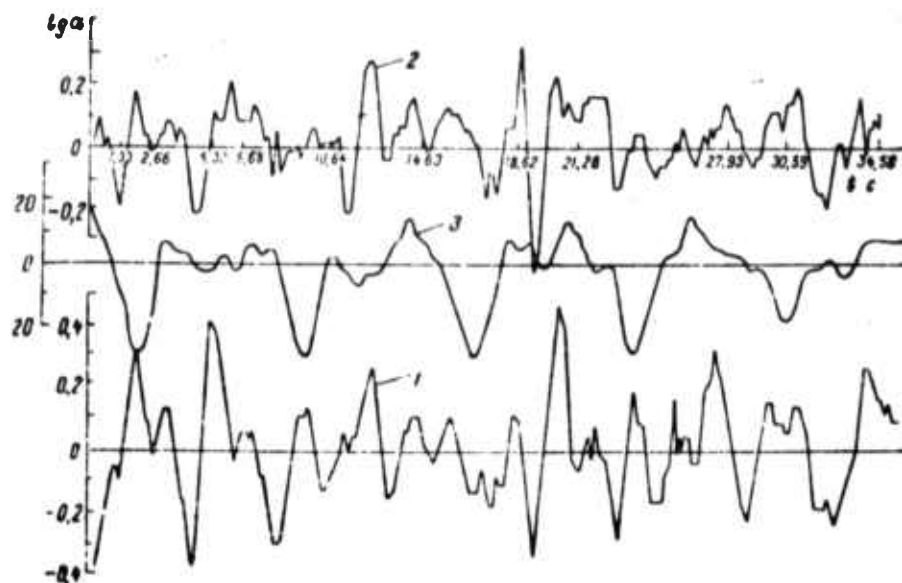of large waves.

Fig. 3. Wave slope vs. time charts:

1 - in direction of wave propagation, 2 - in normal
direction, 3 - wave oscilloscope trace.

Synchronous measurements of wave height, period T, and
sum velocity V_ϵ are also described. A wire type wave recorder with
vertical and horizontal wire sensors was used in the measurements. A
series of the V_ϵ and T data from one oscilloscope trace are tabulated.
Analysis of the data from a horizontal sensor led to the conclusion that
time intervals between adjacent peaks or an adjacent minimum and inflection

point of a wave profile have to be considered as the wave oscillation period,
when correlating sea wave parameters with radar signals. Analysis of the
vertical velocity spectrum revealed that the frequency spectrum is asymmetric
with respect to the frequency of maximum energy, and the corresponding
random processes are concentrated in a narrow band.

3. SOURCE ABBREVIATIONS

AiT	-	Avtomatika i telemekhanika
APP	-	Acta physica polonica
DAN Arm SSR	-	Akademiya nauk Armyanskoy SSR. Doklady
DAN AzSSR	-	Akademiya nauk Azerbaydzhanskoy SSR. Doklady
DAN BSSR	-	Akademiya nauk Belorusskoy SSR. Doklady
DAN SSSR	-	Akademiya nauk SSSR. Doklady
DAN TadSSR	-	Akademiya nauk Tadzhikskoy SSR. Doklady
DAN UkrSSR	-	Akademiya nauk Ukrainskoy SSR. Dopovidi
DAN UzbSSR	-	Akademiya nauk Uzbekskoy SSR. Doklady
DBAN	-	Bulgarska akademiya na naukite. Doklady
EOM	-	Elektronnaya obrabotka materialov
FAiO	-	Akademiya nauk SSSR. Izvestiya. Fizika atmosfery i okeana
FGiV	-	Fizika goreniya i vzryva
FiKhOM	-	Fizika i khimiya obrabotka materialov
F-KhMM	-	Fiziko-khimicheskaya mekhanika materialov
FMiM	-	Fizika metallov i metallovedeniye
FTP	-	Fizika i tekhnika poluprovodnikov
FTT	-	Fizika tverdogo tela
FZh	-	Fiziologicheskiy zhurnal
GiA	-	Geomagnetizm i aeronomiya
GiK	-	Geodeziya i kartografiya
IAN Arm	-	Akademiya nauk Armyanskoy SSR. Izvestiya. Fizika
IAN Az	-	Akademiya nauk Azerbaydzhanskoy SSR. Izvestiya. Seriya fiziko-tekhnicheskikh i matematicheskikh nauk

IAN B	-	Akademiya nauk Belorusskoy SSR. Izvestiya. Seriya fiziko-matematicheskikh nauk
IAN Biol	-	Akademiya nauk SSSR. Izvestiya. Seriya biologicheskaya
IAN Energ	-	Akademiya nauk SSSR. Izvestiya. Energetika i transport
IAN Est	-	Akademiya nauk Estonskoy SSR. Izvestiya. Fizika matematika
IAN Fiz	-	Akademiya nauk SSSR. Izvestiya. Seriya fizicheskaya
IAN Fizika zemli	-	Akademiya nauk SSSR. Izvestiya. Fizika zemli
IAN Kh	-	Akademiya nauk SSSR. Izvestiya. Seriya khimicheskaya
IAN Lat	-	Akademiya nauk Latviyskoy SSR. Izvestiya
IAN Met	-	Akademiya nauk SSSR. Izvestiya. Metally
IAN Mold	-	Akademiya nauk Moldavskoy SSR. Izvestiya. Seriya fiziko-tekhnicheskikh i matematicheskikh nauk
IAN SO SSSR	-	Akademiya nauk SSSR. Sibirskoye otdeleniye. Izvestiya
IAN Tadzh	-	Akademiya nauk Tadzhiksoy SSR. Izvestiya. Otdeleniye fiziko-matematicheskikh i geologo-khimicheskikh nauk
IAN TK	-	Akademiya nauk SSSR. Izvestiya. Tekhnicheskaya kibernetika
IAN Turk	-	Akademiya nauk Turkmenskoy SSR. Izvestiya. Seriya fiziko-tekhnicheskikh, khimicheskikh, i geologicheskikh nauk
IAN Uzb	-	Akademiya nauk Uzbekskoy SSR. Izvestiya. Seriya fiziko-matematicheskikh nauk
IBAN	-	Bulgarska akademiya na naukite. Fizicheski institut. Izvestiya na fizicheskaya institut s ANEB
I-FZh	-	Inzhenerno-fizicheskiy zhurnal

IiR	-	Izobretatel' i ratsionalizator
ILEI	-	Leningradskiy elektrotekhnicheskiy institut. Izvestiya
IT	-	Izmeritel'naya tekhnika
IVUZ Avia	-	Izvestiya vysshikh uchebnykh zavedeniy. Aviatsionnaya tekhnika
IVUZ Cher	-	Izvestiya vysshikh uchebnykh zavedeniy. Chernaya metallurgiya
IVUZ Energ	-	Izvestiya vysshikh uchebnykh zavedeniy. Energetika
IVUZ Fiz	-	Izvestiya vysshikh uchebnykh zavedeniy. Fizika
IVUZ Geod	-	Izvestiya vysshikh uchebnykh zavedeniy. Geodeziya i aerofotos"yemka
IVUZ Geol	-	Izvestiya vysshikh uchebnykh zavedeniy. Geologiya i razvedka
IVUZ Gorn	-	Izvestiya vysshikh uchebnykh zavedeniy. Gornyy zhurnal
IVUZ Mash	-	Izvestiya vysshikh uchebnykh zavedeniy. Mashinostroyeniye
IVUZ Priboro	-	Izvestiya vysshikh uchebnykh zavedeniy. Priborostroyeniye
IVUZ Radioelektr	-	Izvestiya vysshikh uchebnykh zavedeniy. Radioelektronika
IVUZ Radiofiz	-	Izvestiya vysshikh uchebnykh zavedeniy. Radiofizika
IVUZ Stroi	-	Izvestiya vysshikh uchebnykh zavedeniy. Stroitel'stvo i arkhitektura
KhVE	-	Khimiya vysokikh energiy
KiK	-	Kinetika i kataliz
KL	-	Knizhnaya letopis'
Kristall	-	Kristallografiya
KSpF	-	Kratkiye soobshcheniya po fizike

LZhS	-	Letopis' zhurnal'nykh statey
MiTOM	-	Metallovedeniye i termicheskaya obrabotka materialov
MP	-	Mekhanika polimerov
MTT	-	Akademiya nauk SSSR. Izvestiya. Mekhanika tverdogo tela
MZhiG	-	Akademiya nauk SSSR. Izvestiya. Mekhanika zhidkosti i gaza
NK	-	Novyye knigi
NM	-	Akademiya nauk SSSR. Izvestiya. Neorganicheskiye materialy
NTO SSSR	-	Nauchno-tekhnicheskiye obshchestva SSSR
OiS	-	Optika i spektroskopiya
OMP	-	Optiko-mekhanicheskaya promyshlennost'
Otkr izobr	-	Otkrytiya, izobreteniya, promyshlennyye obraztsy, tovarnyye znaki
PF	-	Postepy fizyki
Phys abs	-	Physics abstracts
PM	-	Prikladnaya mekhanika
PMM	-	Prikladnaya matematika i mekhanika
PSS	-	Physica status solidi
PSU	-	Pribory i sistemy upravleniya
PTE	-	Pribory i tekhnika eksperimenta
Radiotekh	-	Radiotekhnika
RiE	-	Radiotekhnika i elektronika
RZhAvtom	-	Referativnyy zhurnal. Avtomatika, tele-mekhanika i vychislitel'naya tekhnika
RZhElektr	-	Referativnyy zhurnal. Elektronika i yeye primeneniye

RZhF	-	Referativnyy zhurnal. Fizika
RZhFoto	-	Referativnyy zhurnal. Fotokinotekhnika
RZhGeod	-	Referativnyy zhurnal. Geodeziya i aeros"-yemka
RZhGeofiz	-	Referativnyy zhurnal. Geofizika
RZhInf	-	Referativnyy zhurnal. Informatics
RZhKh	-	Referativnyy zhurnal. Khimiya
RZhMekh	-	Referativnyy zhurnal. Mekhanika
RZhMetrolog	-	Referativnyy zhurnal. Metrologiya i izmeritel'naya tekhnika
RZhRadiot	-	Referativnyy zhurnal. Radiotekhnika
SovSciRev	-	Soviet science review
TiEKh	-	Teoreticheskaya i eksperimental'naya khimiya
TKiT	-	Tekhnika kino i televideniya
TMF	-	Teoreticheskaya i matematicheskaya fizika
TVT	-	Teplofizika vysokikh temperatur
UFN	-	Uspekhi fizicheskikh nauk
UFZh	-	Ukrainskiy fizicheskiy zhurnal
UMS	-	Ustalost' metallov i splavov
UNF	-	Uspekhi nauchnoy fotografii
VAN	-	Akademiya nauk SSSR. Vestnik
VAN BSSR	-	Akademiya nauk Belorusskoy SSR. Vestnik
VAN KazSSR	-	Akademiya nauk Kazakhskoy SSR. Vestnik
VBU	-	Belorusskiy universitet. Vestnik
VNDKh SSSR	-	VNDKh SSSR. Informatsionnyy byulleten'
VLU	-	Leningradskiy universitet. Vestnik. Fizika, khimiya
VMU	-	Moskovskiy universitet. Vestnik. Seriya fizika, astronomiya

ZhETF	-	Zhurnal eksperimental'noy i teoreticheskoy fiziki
ZhETF P	-	Pis'ma v Zhurnal eksperimental'noy i teoreticheskoy fiziki
ZhFKh	-	Zhurnal fizicheskoy khimii
ZhNiPFiK	-	Zhurnal nauchnoy i prikladnoy fotografii i kinematografii
ZhNKh	-	Zhurnal neorganicheskoy khimii
ZhPK	-	Zhurnal prikladnoy khimii
ZhPMTF	-	Zhurnal prikladnoy mekhaniki i tekhnicheskoy fiziki
ZhPS	-	Zhurnal prikladnoy spektroskopii
ZhTF	-	Zhurnal tekhnicheskoy fiziki
ZhVMMF	-	Zhurnal vychislitel'noy matematiki i matematicheskoy fiziki
ZL	-	Zavodskaya laboratoriya

4. AUTHOR INDEX